Efficient Harvester with Wide Dynamic Input Power Range for 900 MHz Wireless Power Transfer Applications

by

Abdullah Mohammed H. Almohaimeed

A thesis presented to the Ottawa Carleton Institute for Electrical and Computer Engineering in partial fulfillment to the thesis requirement for the degree of

Doctor of Philosophy

in

Electrical and Computer Engineering

uOttawa

University of Ottawa

Ottawa, Ontario, Canada

Abstract

Wireless Power Transfer (WPT), as well as Energy Scavenging and Harvesting, are becoming an active and attractive area of research for scientists and engineers due to the ever-growing need for flexible, sustainable, and unfailing sources of energy. Furthermore, WPT is seen as an environmental solution and a cost-effective approach since it drastically reduces the need to replace and recycle dead batteries.

Among existing WPT techniques, RF electromagnetic (EM) techniques, performed through a rectenna, have been retained because of their benefits in transporting power over long distances. Among the rectenna blocks, the diode-based rectifier configuration is the one that significantly influences the performance of WPT systems in terms of maximum Power Conversion Efficiency (PCE). However, such configurations have noticeable limitations like their inability to operate over wide input power range while maintaining an acceptable PCE level.

So, to efficiently address the above issues in diode rectifiers, an analysis was first performed to highlight the parameters that prevent the rectifier to operate over a wide range of input power while achieving high PCE at 915 MHz, in the Industrial-Scientific-Medical (ISM) band. From that, different approaches have been proposed to operate over wide range of input power including adaptive/reconfigurable topology, active load modulation, and harmonic trapping. In addition, with the aim to further maximize the rectifier PCE, a dual-band rectifier operating at 915 MHz and 2.4 GHz was designed.

The fabricated adaptive rectifier exhibits 40% of PCE over a wide dynamic input range of incident RF power levels from -6 to +25 dBm with a maximum PCE of 66% for an input power of +15 dBm. Note that an average error of 1% was observed between simulated and measured results.

Finally, a printed patch antenna was designed to evaluate the harvester as rectenna. It achieved a gain of 3 dBi, a directivity of 5.3 dBi and a radiation efficiency of 57%.

Acknowledgments

In the Name of Allah, the Most Beneficent, the Most Merciful:

First and foremost, all the praises and thanks be to God Almighty, who has granted me the health, wellness, knowledge, and patience to accomplish this research work.

I am heartily thankful to my supervisors, Prof. Mustapha C.E. Yagoub and Prof. Rony E. Amaya whose encouragements, guidance and support from the initial to the final level, enabled me to successfully complete this research work. I will always be grateful for the time I spent working with them.

I would also to thank Dr. Jose Augusto Lima for his help and support without hesitating all the time.

I would like to convey my gratitude and thankful to my dear parents, Mohammed Almohaimeed and Modi Algahrass. Without their encouragements, prayers and support, it would have been impossible to complete this effort.

I owe to express my gratitude to my wife, Ahlam Alomayrini for her love, moral support, loyalty and patience during my studies. This would not be possible without her understanding and help in managing a good balance between the family and school as well being be away from her family and friends.

I am also deeply thankful to my sweet daughters, Mays and Sama, for all love, joy, power and innocent laughs that forgotten my difficulties in this long journey. I apologize for being be away for several times.

I am also grateful to my kind parents-in-law, Ali Alomayrini and Norah Al-twaijry, for being supportive and helpful to me and my family during my studies.

I would like to thank my brothers, sisters, brothers-in-law and sisters-in-law for their support and encouragement during my journey.

I would like to express a special thanks to The Ministry of Higher Education in Saudi Arabia represented by Qassim University and Saudi Culture Bureau in Ottawa to their financial support, scholarship and provide the opportunities to achieve my future studies.

Also, I would like to thank my colleagues who have helped me in my thesis and course work.

Lastly but not least, I will always be appreciative to all of these extraordinary people.

I dedicate this thesis to my daughters, Mays and Sama

Table of Contents

List of Figures

List of Tables

List of Acronyms

Acronym	Definition
ADS	Advanced Design System
AMC	Artificial Magnetic Conductor
CSA	Canadian Standards Association
DC	Direct Current
EC	European Commission
EIRP	Effective Isotropic Radiated Power
EM	Electromagnetic
ESH	Energy Scavenging and Harvesting
FCC	Federal Communication Commission
FET	Field-Effect Transistor
FSPL	Free Space Path Loss
HB	Harmonic Balance
IoT	Internet of Things
ISM	Industrial-Scientific-Medical
MPE	Maximum Permissible Exposure
PCE	Power Conversion Efficiency
pHEMT	pseudomorphic High-Electron-Mobility Transistor
POW	Power Optimized Waveforms
RF	Radio Wave
RFID	Radio Frequency Identification
SAR	Specific Absorption Rate
SHM	Structural Health Monitoring
SSPS	Solar Space Power Satellite
TD	Time Domain
WIMD	Wearable and Implantable Medical Devices
WSN	Wireless Sensor Networks
WPT	Wireless Power Transfer

List of Symbols

Variables	Definition
C_j	Junction Capacitor
C_p	Parallel Capacitor
G_r	Received Antenna Gain
G_t	Transmitted Antenna Gain
I_s	Saturation Current
L_s	Series Inductance
P_t	Transmitted Power
P_{DC}	DC Output Power
R_j	Junction Resistance
R_s	Series Resistance
R_L	Output Load
V_{br}	Voltage Breakdown.
V_{out}	DC Output Voltage

Chapter 1. Introduction

1.1. Motivations

Nowadays, WPT and energy scavenging have been attracting researchers and industrials due to the ever-growing need for flexible, sustainable, and unfailing sources of energy. In addition, with recent advances in Wireless Sensor Networks (WSN), e.g. the Internet of Things (IoT), such intelligent systems are further highlighting this necessity [1][2]. The aim of WPT is to allow devices to operate over an extended period of time without having to charge/replace their batteries, a critical issue because of the inherent costs and difficulties to reach inaccessible areas. Furthermore, WPT is seen as an environmental solution and a cost-effective approach since it drastically reduces the need to recycle dead batteries [2].

WPT techniques can be classified into two main classes (i) inductive and magnetic resonant coupling methods to transfer power over short distances (few centimeters) and (ii) RF electromagnetic techniques to transport the energy over long distances (few meters) [3][4]; the latter being considered in this work due to their benefits in powering miniaturized portable devices over longer distances.

WPT through electromagnetic has been applied in diversities of applications and fields such as Radio Frequency Identification (RFID) [5], WSN, Wearable and Implantable Medical Devices (WIMD) [6], Structural Health Monitoring (SHM) [7], and IoT [8], to name a few. Such applications can involve a wide range of power levels depending on the targeted applications and the distance from the controlled source: RFID (µW to mW), bio-implants (mW to W), wirelessly charging systems for user electronic devices (few W). In this work, we aimed to provide a system to operate over a wide range of input power levels to enlarge its panel of applications. In fact, there are diversities of RF energy sources to power devices through electromagnetic techniques including ambient and dedicated energy sources. Dedicated energy sources have been retained due to their advantages such as consistency, reliability, and the fact that they can be optimized to improve the overall PCE.

Consequently, WPT process is accomplished through a rectenna, which mostly contains an antenna, a rectifier, a matching network, and an output load. Once the RF wave is received by the receiving antenna, it will be converted to DC voltage to either directly power devices or store the energy in batteries.

In recent years, several approaches have been explored to improve the efficiency of WPT systems [9]-[16]. However, optimizing the rectifier's performance remains the most widely used approach to maximize the PCE of a WPT system. The usual procedure to design a rectifier for WPT starts by selecting the appropriate active device, typically a diode [17]-[20]. Based on their biased techniques, diode rectifiers can be classified into two main clusters namely, zero-biased diode configurations and non-zero-biased configurations. The latter requires an external source to operate, which is not appropriate in harvesting energy and WPT applications. Among zero-bias diodes, P-N junction and Schottky barrier devices are the most widely used.

At the circuit level, numerous diode rectifier configurations have been suggested to improve PCE including conventional configurations like series/shunt diodes configurations, voltage doublers, and bridge diode rectifiers. However, all these topologies have noticeable limitations, such as the inability to achieve a high PCE over a wide range of input powers. This is mainly due to restrictions in diode properties including the incapability for a diode to simultaneously exhibit low threshold voltage and high breakdown voltage, resulting into a degradation in power efficiency in RF-DC conversion [4]. The effect of breakdown voltage, identified as early breakdown voltage [21] can be, in fact, one of the significant issues affecting the rectifier's efficiency.

Indeed, the PCE of conventional diode-based rectifiers can be influenced by the internal diode model components such as the junction resistance R_j, the junction capacitor C_j, the diode parasitics (R_s, L_s, and C_p), as well as key internal diode parameters like the saturation current I_s and the voltage breakdown V_{br}. Therefore, it turns out to be critical to outline and understand the effect of such parameters on the Power Conversion Efficiency.

From that, enhanced techniques have been implemented to address such conventional diode-based rectifier issues including adaptive/reconfigurable topology, active

load modulation, and harmonic trapping. Also, to further increase the rectifier input power range, a dual-band circuit was designed.

Finally, with the aim to evaluating the whole rectenna system performance, a patch antenna was implemented making use of metasurface and artificial magnetic conductor (AMC) materials as ground plane as well as printed inks.

1.2. Research Contributions

The aim of this research work was to enhance and overcome the inability of conventional rectifiers to operate over an extensive range of input powers while achieving relatively high PCE. So, to efficiently address such issues in conventional rectifiers, the following contributions can be highlighted:

- A detailed theoretical analysis was performed to investigate the impact of the above mentioned diode model elements and key parameters towards the rectifier PCE. To the best of our knowledge, this is the first time that such theoretical approach was conducted. To achieve so, a generic configuration of a shunt diode rectifier was considered.
- An adaptive reconfigurable rectifier was designed [22][23] to operate within the ISM frequency band at 915 MHz. Starting from a concept described in [24] for devices operating at 100 MHz, the proposed adaptive reconfigurable rectifier uses a transistor FET as switch to combine between low and high input power levels in order to obtain high efficiency over a wide RF input power range. Once fabricated and tested, the rectifier exhibits 40% of PCE over a wide dynamic input range of incident RF power levels from -6 to +25 dBm with a maximum PCE of 66% for an input power of 15 dBm. Note that an average relative error of 1% was observed between simulated and measured results.
- To further enhance the PCE performance, an active load modulation block [25] was designed and added to the adaptive reconfigurable rectifier to prevent the circuit to reach its voltage breakdown by controlling the load value in real-time [26][23]. The design achieved 40% of PCE over a wide dynamic input range of incident RF power

levels from -6 to +32 dBm, i.e., an improvement of 15% compared to the adaptive configuration alone.

- An harmonic trapping technique was implemented to suppress the unwanted harmonics and thus, improve the output DC power [27]. Therefore, an efficiency higher than 40% was achieved over a wide dynamic range of RF input power levels ranging from -9 dBm to +28 dBm while increasing the PCE by 10% at high input powers.
- In addition, a dual-band adaptive rectifier was designed to harvest and collect more power by considering another potential source of power at 2.45 GHz [28]. It achieved an efficiency above 40 % over an extensive-ranging of input power from -11 dBm to 25 dBm and -4 dBm to 21 dBm at 915 MHz and 2.4 GHz, respectively.
- Then, an efficient low-cost metasurface-based printed patch antenna was used to evaluate the system as a rectenna (rectifying antenna) [29][30], with a gain of 3 dBi, a directivity of 5.3 dBi and a radiation efficiency of 57%.

Finally, the designed adaptive/reconfigurable rectifier was fabricated, the active load, harmonic trapping, and dual-band configuration implemented, and the obtained results successfully compared to existing designs found in the literature.

1.3. Thesis Outlines

This thesis is divided into five chapters. After this introductory Chapter, Chapter 2 presents an overview of the WPT concept. In addition, design considerations are discussed and the basic rectifier operation in WPT systems described. In addition, the issues of conventional diode-based rectifiers to operate over a wide input power range while achieving high PCE are investigated; besides, existing solutions proposed in the literature to improve the PCE limitations are reviewed.

In the third chapter, the theoretical analysis of diode-based rectifiers operation and their efficiency limitations are investigated to understand the critical components that affect the overall PCE of the circuit and, thus, how to enhance it. To do so, different parameters are varied and their impact evaluated.

Chapter 4 introduces different approaches used to overcome the inability of conventional rectifiers to operate over an extensive range of input power levels and improve their overall power conversion efficiency. In addition, the design and implementation of proposed rectifier configurations are presented, and their results successfully compared to existing designs found in the literature.

Chapter 5 summarizes the thesis, clarifies the major contributions and points to potential future works.

1.4. Publications

1- **A. M. Almohaimeed**, R. E. Amaya, J. A. Lima, and M. C. E. Yagoub, "Adaptive power harvester with active load modulation for highly efficient short/long range RF WPT applications," *Electronics Journal,* Special Issue on RFID, WPT and Harvesting Energy, vol. 7 (125), 2018.

2- **A. M. Almohaimeed**, M. C. E. Yagoub, J. A. Lima, R. E. Amaya, G. Xiao, and Y. Tao, "UHF metasurface-based antenna for WPT RFID applications" *IEEE Radio Frequency Identification (RFID 2018),* Florida, USA, 2018, pp. 1-2.

3- **A. M. Almohaimeed**, M. C. E. Yagoub J. A. Lima and R. E. Amaya, G. Xiao and Y. Tao, "Metasurface-based WPT Rectenna with extensive input power range in the 900 MHz" *IEEE Canadian Conference on Electrical and Computer Engineering (CCECE)*, Quebec, Canada, 2018, pp. 1-4.

4- **A. M. Almohaimeed,** R. E. Amaya, and M. C. E. Yagoub, "Dual-band harvester with wide range input power for WPT applications" *IEEE PELS Workshop on Emerging Technologies: Wireless Power (WoW)*, Montreal, Canada, 2018, pp. 1-4.

5- **A. M. Almohaimeed**, M. C. E. Yagoub, and R. E. Amaya, "Efficient harvester with active load modulation and wide dynamic input power range for wireless power transfer applications," *Annual IEEE International Systems Conference (SysCon)*, Montreal, Canada, 2017, pp. 1-4

6- **A. M. Almohaimeed**, M. C. E. Yagoub, and R. E. Amaya, "A highly efficient power harvester with wide dynamic input power range for 900 MHz wireless power transfer applications," *IEEE Mediterranean Microwave Symp. (MMS)*, Abu Dhabi, Abu Dhabi, 2016, pp. 1-4.

7- **A. M. Almohaimeed**, M. C. E. Yagoub, and R. E. Amaya, "Efficient rectenna with wide dynamic input power range for 900 MHz wireless power transfer applications," *IEEE Electrical Power and Energy Conference (EPEC)*, Ottawa, Canada, 2016, pp. 1-4.

8- **A. M. Almohaimeed**, M. C. E. Yagoub, and R. E. Amaya “Theoretical approach to the rigorous design of diode-based rectifiers operating over wide dynamic range of input powers” To be submitted.

Chapter 2. Wireless Power Transfer Overview

In this chapter, an overview of WPT is presented and the existing transport power techniques reviewed, highlighting the electromagnetic (EM) technique as the approach to select due to its advantages for transporting power over long distances. Thus, diverse RF energy sources are described including the ambient and dedicated energy sources, the latter being preferred in this work. Possible applications are then explored. In addition, design considerations and RF power transmission parameters are considered including power range and operating frequency. Furthermore, a link budget set to estimate the power level that can be transmitted, received, harvested, and the maximum distance to be reached.

Then, the WPT RF system is introduced including the transmitter and the rectenna. In a rectenna system, the rectifier block is considered as the key element to improve and maximize the overall PCE for WPT and harvesting energy. Therefore, the main rectifier parameters are introduced including efficiency, sensitivity and output load. Note that Schottky barrier devices have been selected due to their high saturation current, low series resistance, and high breakdown voltage. In addition, the limitations of conventional diode-based rectifier configurations are highlighted, i.e., the inability to operate over a wide dynamic input power range with high efficiency, and different alternative rectifier configurations investigated.

2.1. Wireless Power Transfer Principle

The concept of WPT is to wirelessly transfer power. WPT, as well as Energy Scavenging and Harvesting (ESH), are becoming an active and attractive area of research for scientists and engineers due to the ever-growing demand for flexible, sustainable, and unfailing sources of energy. In addition, with recent advances in wireless sensor networks, e.g. the Internet of Things, wearable and implantable medical devices and structural health monitoring, such intelligent systems are further highlighting this necessity [1][2]. The aim of WPT is to allow devices to operate for a longer period of time without having to charge/replace their batteries, a critical issue because of the inherent costs and difficulties

to reach inaccessible areas. Furthermore, WPT is seen as an environmental solution and a cost-effective approach since it drastically reduces the need to recycle and dispose of dead batteries [2].

WPT can involve a wide range of power levels depending on the targeted applications: radio frequency identification (μW to mW), bio-implants (mW to W), wirelessly charging systems for using electronic devices (few W) or electrical vehicles (several kW) [31]. Recently, different organizations are working toward the standardisation of WPT technologies including Wireless Power Consortium, Power Matters Alliance, and Alliance for Wireless Power [32]. Following these standards, several products have been commercialized: charging electronic devices such as cellphone station pads [33] or powering home electrical equipment like TVs, lamps, and desktops [34]. Charging electrical vehicles has been also receiving consideration from automobile manufacturers [35]. In addition, independent companies such as Qualcomm, WiTricity, and Energous have developed different WPT techniques to achieve and enhance WPT systems [36][37].

2.2. EM Wireless power classifications

WPT can be classified into two main groups depending on the frequency operation and the distance that can be accomplished: (i) inductive and magnetic resonant coupling techniques to transfer power over short distances (near field) and (ii) RF electromagnetic techniques utilized to transport and harvest the energy over long distances (far-field) [22][3].

2.2.1 Magnetic Inductive Coupling

Magnetic Inductive coupling operates by magnetic field induction and delivers the energy between two coils from the primary coil to the secondary coil without using wires. The primary source of energy generates a variable magnetic field across the secondary coil. Then, the near-field process produces a voltage and current that can be utilized to power devices wirelessly [38][39]. It transfers power in the near field region and short distance range; additionally, it mostly operates at low frequencies. Inductive coupling has been manufactured and applied for different applications such as charging electric toothbrushes,

charging pads for cell phones or laptops (Figure 2.1), or implantable blood analyzer chip for medical applications [40].

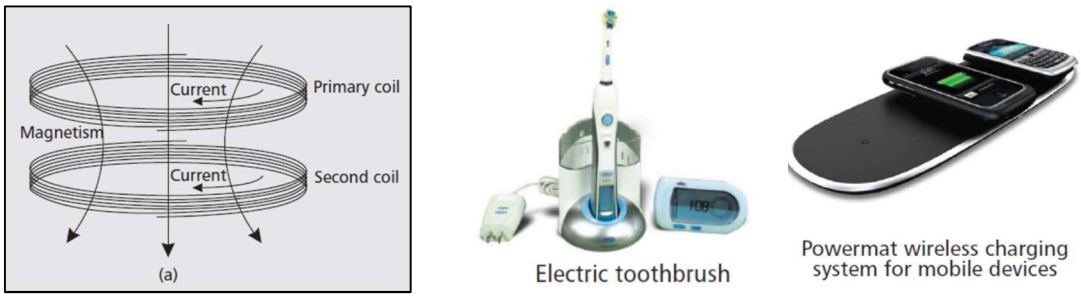

(a) (b)

Figure 2.1 WPT inductive coupling technique: (a) circuits. (b) applications [39][41]

Several factors can affect the inductive coupling efficiency including the coils coupling tightness, specified by the alignment and the distance between the two coils. In addition, the quality factor that represents the ratio of energy stored in the capacitor and inductor to the energy dissipated as thermal losses, is an essential parameter to optimize the efficiency by selecting a proper material, choosing the right shape and dimensions and frequency operation [39]. An overview of near-field can be found in [42] along with the drawbacks of both near and far fields in WPT applications. In addition, the misalignment issue has been investigated in [43] for various coil structures. Moreover, the allowed degree of misalignment acceptable for a specific application has been examined as well. In [44], a WPT system was designed to charge electric vehicles overnight.

2.2.2 Magnetic Resonant Coupling

Magnetic resonant coupling is based on the concept of coils operating at the same resonant frequency and coupled through non-radiative magnetic resonance coupling. Apart from the inductive coupling technique, the primary and secondary coils in the resonant coupling are adjusted to have the two coils resonating at the same frequency by adding a capacitor [38][39]. Then, high transfer power efficiency can be accomplished.

This technique has important advantages compared to the inductive coupling such as transferring power over long distances and powering multiple devices at the same time at different levels of powers with a single source power. In addition, the alignment is not essential as in the inductive coupling technique [38][39]. In [45], a strong magnetic resonance coupling has been developed to transfer power using non-radiative technique.

However, the magnetic resonant coupling has a drawback, i.e., it can be utilized to charge home appliances and electric vehicles but not suitable for mobile applications due to short-range charging with limited spatial freedom [46][36]. In fact, magnetic resonant coupling has been manufactured and applied mainly for specific applications such as charging home appliances including TV, lamp and desktop and charging electric vehicle as illustrated in Figure 2.2-b.

Figure 2.2 WPT applications of magnetic resonant technique [39][41].

2.2.3 Electromagnetic or radio wave

The third category of WPT techniques is transferring and harvesting power through RF EM techniques. This power transfer process is typically performed through a rectenna, which generally comprises an antenna, a rectifier, a matching network, and an output load, as shown in Figure 2.3. The antenna receives the RF wave to be transformed and converts it to DC output voltage via a rectifier. This rectenna will then be used to charge batteries or directly power devices. It has the advantage of long effective charging distance, suitable for powering portable and mobile applications.

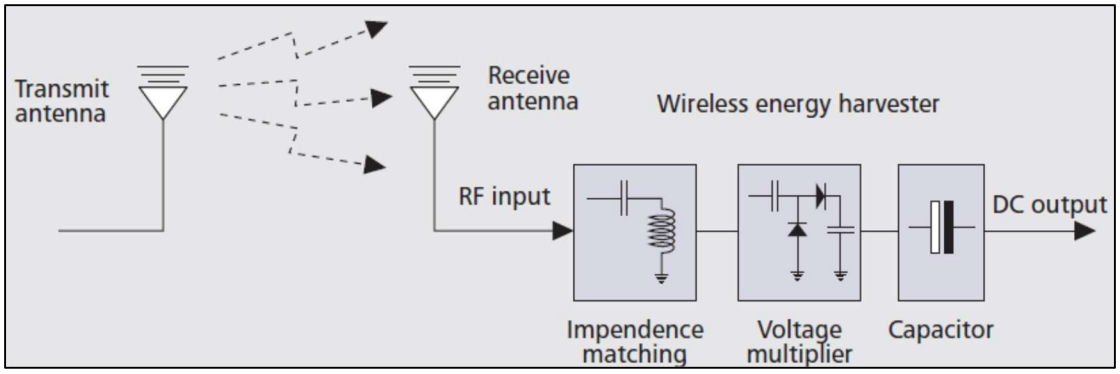

Figure 2.3 RF Electromagnetic Wave technique of WPT [39]

A comparison between the different WPT techniques is summarized in Table 2.1. Among the above WPT techniques, we retained the RF electromagnetic technique for its ability to power devices over long distances.

2.3. WPT history through radio wave

WPT through waves has been already experienced in the 19th century, when H. Hertz attained power transfer by using a spark-gap radio transmitter to generate a high-frequency power and sense it to a receiver, or when N. Tesla conducted WPT experiments at low-frequencies, using a gigantic coil operating at 150 kHz [47][48][49].

In 1963, W.C. Brown introduced and established the WPT concept. He developed the rectifying antenna or "rectenna". After numerous attempts to achieve high RF-DC efficiency, Brown attained in 1970 an efficiency of 26.5% at operating frequency of 2.45 GHz. In 1975, Brown and his team succeeded to demonstrate the largest experiment of wireless power transfer. As shown in Figure 2.4, it contains a parabolic transmitting antenna with a diameter of 26 m and a receiver with a rectenna array of 3.4 × 7.2 m^2.

The rectenna was placed within 1 mile away from the transmitting base station. The experiment was operating at 2.388 GHz with a transmitting power of 450 kW and achieved 30 kW of DC power at 82.5% of rectifier efficiency.

Table 2.1 Comparison between different techniques of WPT [39]

Technique	Advantages	Disadvantages	Effective charging distance	Applications
Inductive coupling	▪Safe for humans ▪Simple implementation	▪Short distance charging ▪Not suitable for mobile applications ▪Tight alignment required	Few millimeters to few centimeters	Smart and tablets (through pads mat), toothbrushes, contactless smart cards …
Magnetic resonator coupling	▪Loose alignment between the charger and charging devices. ▪Simultaneously charging multiple devices at different powers. ▪High charge efficiency	▪Not suitable for mobile applications ▪Limited charging distance	Few centimeters to around a meter	TV, lamp, desktop, charging electrical vehicles …
EM wave	▪Long effective charging distance ▪Suitable for mobile application	▪Not safe when the RF power exposure is high. ▪Low charging efficiency.	Several meters to hundreds of meters	RFID, wireless sensors, implantable medical devices.

Based on Brown's work, the Solar Space Power Satellite (SSPS) was introduced by Glaser in 1968. SSPS's concept is to gather the sun energy in the space through photovoltaic solar sources and send it to the earth as RF wave to a receiving station (rectenna) as illustrated in Figure 2.4-b. However, its large antenna size made the SSPS difficult to transfer power for commercial applications. From that time, many studies have been involved to use this new source of energy. Mainly, the U.S. National Aeronautics and Space Administration (NASA) and Department of Energy (DOE) evaluated its technical possibility and economic feasibility. Then, different SSPS systems have been proposed but not built yet, mainly due to their inherent cost [50][51].

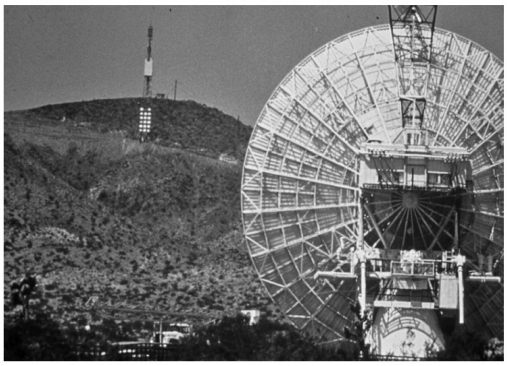

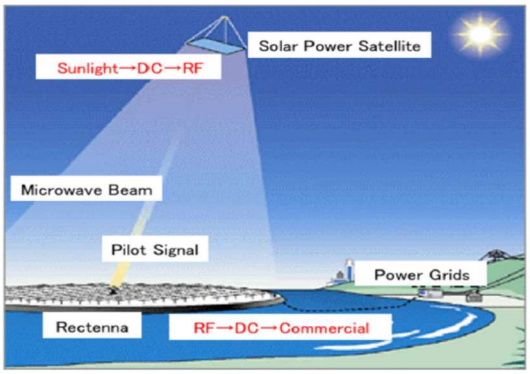

(a) (b)

Figure 2.4 (a) First succeeded experiment of WPT through rectenna in 1975 [49] (b) Configuration of the SSPS system, consisting of ‘‘solar power satellite’’ and ‘‘rectenna’’ [50].

2.4. WPT Applications through radio wave

WPT through EM waves has been applied in various fields including RFID [5][52], wireless sensor networks [38][53], wearable and implantable medical devices [6][54], structural health monitoring [7][55], Internet of Things [8], and Internet of Everything (IoE) [56][57][58][59][60]. In such applications, the major challenge is the limited lifetime of the devices. Therefore, WPT and harvesting energy can be a suitable solution to charge the device's batteries.

As seen, the applications of harvesting energy and WPT are various, leading to a large panel of WPT system designs. Enhancement of a specific design parameter may be destructive for others: sacrificing distance for efficiency, size for robustness, complexity for cost. In this work, we focused on designing a system able to operate over a wide range of input power levels to enlarge its panel of applications with true spatial freedom and insensitivity to location.

2.5. RF Energy sources

There is anticipation that transferring power through RF/microwave bands will be a suitable solution due to the fact that wireless RF/microwave sources are extensively spread in our daily environment. Therefore, a pair of techniques can be referred to provide energy namely, Energy Harvesting (EH) from ambient RF energy and WPT on demand from dedicated RF sources. In both cases, careful design of RF power transfer systems is essential to maximize the system performance for a given scenario.

2.5.1 Ambient RF energy source

The Energy Harvesting (EH) scenario in Figure 2.5 shows a number of devices in a specific surrounding environment that harvest RF energy from different RF sources operating at different frequencies. A radio wave is ubiquitous in our daily lives; it can be found in the form of signals from radios, wireless LANs, mobile phones, etc. [61].

The permissible and available spectrum for harvesting energy can range from few MHz up to few GHz [62]. The available EH power from ambient RF sources is time-varying and unpredictable. In addition, the transmitter specifications such as output power, antenna radiation, and polarization are unknown. Therefore, the transmitter performance should be first estimated to deduce the power link budget of the WPT system. Consequently, at the receiver side, the rectenna should be designed to cover such unknown specifications and its antenna to operate over broadband/multiband frequency range to harvest and scavenge most of the RF surrounding power [63]. The harvesting rectenna design is therefore challenging while trade-offs between system size and performance should be considered due to the EH system necessity to be combined with miniaturized devices [64].

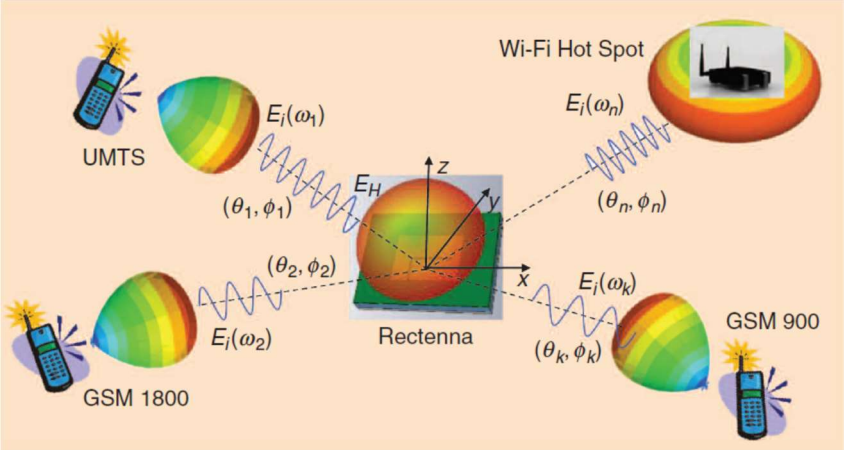

Figure 2.5 An EH scenario with multiple, randomly distributed RF sources [64].

2.5.2 Dedicated RF energy source

WPT with dedicated RF source is represented in Figure 2.6. Compared to the ambient source (Table 2.2), this technique on the receiver side has advantages of knowing the RF source parameters such as the operation frequency and polarization of the incident power. In the WPT system, having a multiband or broadband receiver antenna coherent with the RF source antenna leads to enhance and maximize the overall efficiency [47][64][63].

Dedicating RF energy source should be able to deliver the needed power to the system when requested. Moreover, this power should follow the transmitting and receiving power regulations in the targeted frequency band. Accordingly, implementing a dedicated RF source is considered as a proficient technique for WPT system. It allows to know about the energy availability and provides the ability to enhance the rectenna overall efficiency.

To conclude, harvesting energy from an ambient source is not reliable due to the unidentified design specifications already mentioned. On the other hand, transferring power from a dedicated energy source is consistent and can be optimized to improve the overall PCE. We have then retained this option in our work.

2.6. RF Power Transmission and Design Considerations

Setting the specifications is the first step in any system design. It can include the transmission range, operation frequency, transmission power or link budget and design trade-offs [65][66]. In addition, health and safety considerations of the radiating system should be considered [67]. These rules restrictions and metrics should be then discussed.

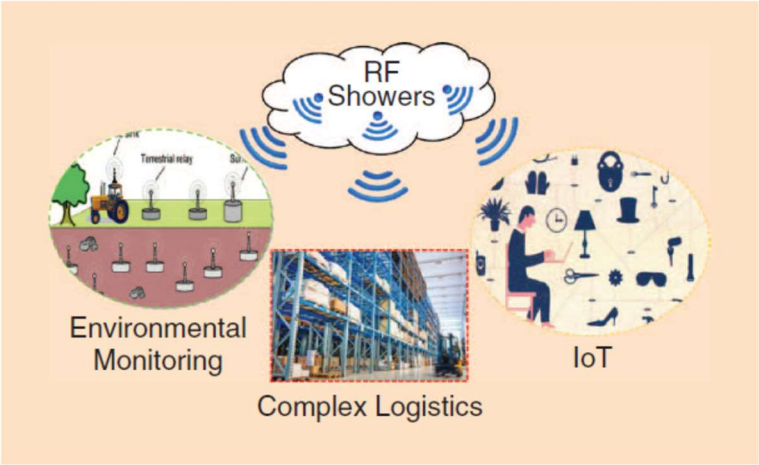

Figure 2.6 A WPT scenario with dedicated known RF source [64].

2.7. RF Power Transmission and Design Considerations

Setting the specifications is the first step in any system design. It can include the transmission range, operation frequency, transmission power or link budget, and design trade-offs [65][66]. In addition, health and safety considerations of the radiating system should be considered [67]. These rules restrictions and metrics should be then discussed.

Table 2.2 WPT system characteristics of RF energy sources [64]

Section	*Parameters*	*Dedicated Energy source*	*Ambient RF energy*
Transmitter side	Power generator	▪ High-efficiency power amplifier ▪ Optimized signal waveform	▪ Not controllable ▪ Multi-tone
	DC- to RF efficiency	▪ Can be optimized	▪ Cannot be optimized
	Antenna specifications	▪ Directive ▪ Defined polarization and positions ▪ Smart beaming is possible	▪ Directivity unknown ▪ Polarization and positions unknown ▪ Multiband source
Radio channel	RF-RF efficiency	▪ Known ▪ Optimized	▪ Unknown ▪ Worst case estimate
Receiver side	Antenna specifications	▪ Directive ▪ Defined polarization and position ▪ Single band	▪ Nondirective ▪ Circular or dual polarization ▪ Multiband resonator
	Rectifier	▪ Design for a specific power density and RF frequencies	▪ Design for a broad range of power and frequencies
	RF-to-DC efficiency	▪ Can be optimized	▪ Can be optimized

2.7.1 Transmission distance range

Based on the distance *R* between the transmitter and the receiver, the EM field region can be classified either as near-field inductive, near-field radiative or far-field radiative (Figure 2.7). They are a function of the wavelength, λ, as seen in (2.1). The most significant parameter in this equation is $\frac{\lambda}{2\pi}$ which determines the field region [65][68] .

$$\boldsymbol{\lambda = \frac{c}{f}} \Rightarrow \begin{cases} R \leq \frac{\lambda}{2\pi} & \text{Near Field Reactive} \\ \frac{\lambda}{2\pi} > R \leq 2\lambda & \text{Near Field Radiative} \\ R > 2\lambda & \text{Far Field Radiative} \end{cases} \tag{2.1}$$

where c $(3 \times 10^8 m/s)$ is the speed of light in free space and f the operating frequency.

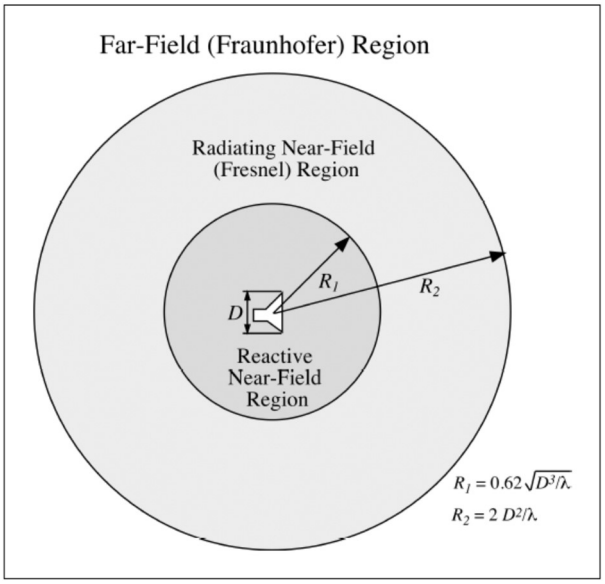

Figure 2.7 EM field regions [69]

2.7.2 Operating frequency

There is a wide selection of frequencies that can be utilized in harvesting energy and WPT in both near and far fields regions. For instance, low-frequency bands are highly valued and suitable for inductive coupling and coupling resonance operating in the near-field region, e.g., 125-134 kHz to wirelessly charge laptops and cellphones or 13.56 MHz to power smart/RFID cards. As for far-field, it ranges from few kHz to around 30 GHz. UHF band is commonly used for harvesting energy due to its flexibility and relatively low interference.

Wavelength is a significant characteristic in WPT systems, which conditions the antenna size, attenuation level, and receiver element parameters. Low frequencies lead to a larger antenna but lower attenuation to nearby objects. In addition, they do not require high-quality circuit elements. In contrast, higher frequencies have the advantage of smaller size; however, the attenuation is higher and components' sensitivity to parasitics is vastly increased. WPT systems can be operated at the ISM bands, i.e., 915 MHz, 2.4 GHz and 5.8 GHz.

2.7.3 Transmission power and safety considerations

To harvest or power devices wirelessly, the energy should be collected from a dedicated power source or an ambient source. There exist certain regulations for such sources in terms of maximum power that can be transmitted. These regulations, built to assure health and safety conditions while operating at ISM bands, are controlled by different associations such as the US Federal Communication Commission (FCC), the Canadian Standards Association (CSA), and the European Commission (CE). FCC, for example, allows transmitting in ISM bands a maximum power of 30 dBm (1W) while Maximum Effective Isotropic Radiated Power (EIRP) is 36 dBm (4W) [65][70].

In addition to safety and health considerations, Maximum Permissible Exposure (MPE) limit and Specific Absorption Rate (SAR) restrictions should be taken into account, particularly in implantable and wearable devices design as discussed in [6][71][70][72]. Also, RF and microwave radiation are considered as nonionizing. A study of biological effects of the radiofrequency electromagnetic field can be found in [73].

2.7.4 Link budget

In order to estimate the power levels that can be transmitted, received, and harvested as well as the maximum distance that can be reached, a power link budget is essential. The propagation in free space between the transmitter and receiver can be expressed via the well-known Friis equation where the received available power can be estimated as in (2.2) [27][74].

$$P_r = P_t G_t G_r \left(\frac{\lambda}{4\pi R}\right)^2 \tag{2.2}$$

where (P_t, G_t) and (P_r, G_r) state respectively for the transmitted and received power and antenna gain. R is the distance between the transmitter and the rectenna.

Most of the power loss while transmitting is the free space path loss (FSPL) [75].

$$FSPL = 10\ log\left(\frac{4\pi Rf}{c}\right)^2 \tag{2.3}$$

Therefore, the maximum received power between two antennas that spreads over a distance R and operating at a specific frequency f can be calculated in dB as in (2.4)

$$P_r\ [dBm] = P_t\ [dBm] - FSPL[dB] + G_t\ [dB] + G_r\ [dB] \tag{2.4}$$

Based on the FCC rules that restrain the maximum transmitter output power to 30 dBm for ISM frequency bands, the following section is allocated to the RF system power link budget. The Friis equation was applied to estimate the power levels that can be received, as well as the distance that can be reached. In Figure 2.8-a, the power link budget was calculated for different operating ISM bands including 915 MHz, 2.4 GHz, and 5.8 GHz for fixed transmitting power (30 dBm), transmitting (6dBi) and receiving antenna gain (6 dBi) while the distance was swept up to 8m.

From that figure, we can conclude that, amongst the ISM bands, 915 MHz is the most promised band due to its ease of accessibility, less attenuation, less sensitivity to circuit parasitics and ease of fabrication [76][70]. As for the others bands (2.4 GHz and 5.8 GHz), even if they exhibit the advantage of size reduction and higher antenna gain, it is at the expense of higher attenuation, which is a key issue in WPT systems. Therefore, in this work, 915 MHz frequency band has been retained for far-field operation.

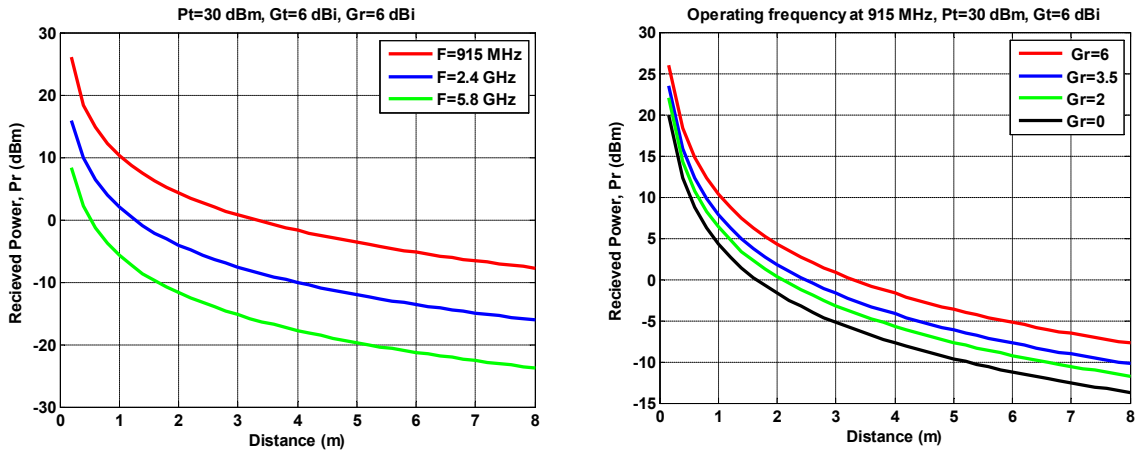

(a) (b)

Figure 2.8 Power link budget vs distance of RF system operation: (a) at different frequencies (b) at different receiver antenna gains at 915 MHz.

As highlighted in Figure 2.8-b, at 915 MHz, there is a trade-off between the received antenna gain and the distance needed to be reached beside the desired level of power. In these calculations, the applied transmitted power was the maximum allowed (30 dBm) and the transmitter antenna gain was set to 6 dBi to get a Maximum Effective Isotropic Radiated Power (EIRP). Note that higher received antenna gains can provide higher levels of power for a given distance as illustrated in the received power link budget in Table 2.3.

2.8. RF System overview

A generic WPT system is shown in Figure 2.9. It contains a transmitter and a rectenna. In the following, a brief explanation of the different RF blocks is presented.

Table 2.3 RF system power link budget

Received power link budget						
Frequency operation	915 MHz				2.4 GHz	5.8 GHz
Wavelength (m)	0.328				0.125	0.0517
Received antenna gain (dBi)	6	3.5	2	0	6 dBi	6 dBi
Transmitted antenna gain	6 dBi				6 dBi	6 dBi
Transmitted power (dBm)	30 dBm				30 dBm	30 dBm
Distance (m)	8				8	8
Received Power (dBm)	-7	-10	-11	-14	-16	-24

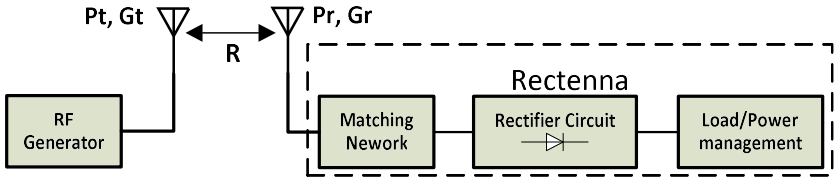

Figure 2.9. Diagram illustration of a WPT system.

2.8.1 Transmitter

In a WPT system, the transmitter design is separated from the rectenna design even though the overall efficiency starts from the transmitter by transmitting power under restrictions of legal regulations and physical transmission properties of the environment. The transmitter hardware enhancement will not add improvement to the rectenna part; however, the transmitted power waveforms possibly will expand the rectification efficiency by increasing the antenna maximum voltage through Power Optimized Waveforms (POW), utilized to deliver and achieve a maximum voltage, leading to a higher overall efficiency of the rectenna.

POW uses periodic amplitude fluctuations to increase the input voltage of the rectenna; subsequently, the efficiency is increasing [65].

2.8.2 Rectenna

Transfer power process is achieved through a rectenna, which mostly contains an antenna, a rectifier, a matching network, and an output load, as illustrated in Figure 2.9. Once the RF wave is received by the receiving antenna, it will be converted to DC voltage through a rectifier circuit to either power devices directly or store the energy in batteries. Therefore, in recent years, research thrusts have been devoted to improve and develop WPT systems like rectennas for specific applications. The rectenna efficiency can be improved and developed at different levels: antenna, matching network, and rectifier.

Therefore, the receiver antenna is an important element to transfer and harvest power through electromagnetic signals. It is responsible for capturing the incident RF signal from either a dedicating RF energy for a specific operating frequency or an ambient RF energy from multiple potential operating frequencies.

The matching impedance circuit is also an important element since it reduces the loss between the antenna and the rectifier by transferring the highest possible amount of power. In WPT and harvesting energy, designing a matching network will be more challenging since the input impedance of the rectifier needs to be matched for a particular frequency operation while the rectifier input impedance is varying as the input power level changes due to the nonlinear components in the circuit.

Finally, the rectifier circuit is a critical block in WPT and harvesting energy systems. In fact, most of the approaches that have been explored to improve the PCE of WPT systems have been dedicated to optimize the rectifier performance.

2.9. Rectifier

The rectifier converts the RF wave into DC power. Because it is a key block in WPT systems, it is worth to first examine the parameters that limit its efficiency and thus, review the techniques that have been proposed to enhance this latter.

2.9.1 Rectifier design parameters

Rectifier performance can be characterized and evaluated by various design parameters [65] as summarized below.

❖ **Power Conversion Efficiency (PCE)**

The RF-DC PCE is a crucial parameter to evaluate and characterize the rectifier's performance. PCE is defined in (2.5) as the ratio of DC output power (P_{DC}) over the RF incident power at the rectifier input (P_t) [77]. The P_{DC} is the dc voltage, V_{out}, across the load resistance R_L. The concept is illustrated in Figure 2.10. Note that the causes of efficiency degradation and approaches to improve it will be discussed in Chapter 3.

$$\eta = \frac{P_{DC}}{P_t} \times 100 \quad \text{with:} \quad P_{DC} = \frac{(V_{out})^2}{R_L} \tag{2.5}$$

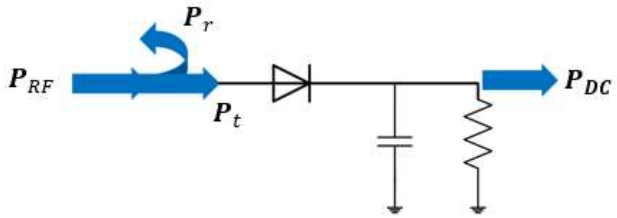

Figure 2.10 Rectifier structure illustrating the concept of efficiency. Here P_{RF} and P_r state for the input radio frequency power and input reflected power, respectively.

❖ **Sensitivity**

Sensitivity is an important metric for evaluating WPT and harvesting energy systems. It is indeed a suitable indicator to determine the Minimum Desired Signal (MDS) or the weakest signal that can be handled. High sensitivity means the circuit is able to cover and capture low input power levels. The rectifier sensitivity depends on the active device threshold voltage: lower the threshold voltage, higher the sensitivity [78]. The relationship between sensitivity and PCE is complex because this latter depends on the input power level. Operating at the lowest possible power level (highest sensitivity) leads to reduced efficiency [65][21].

❖ **Output Load**

The rectifier is an AC/DC converter. The output voltage will drive the load for specified applications such as charging batteries or supplying devices. Consequently, the load resistance plays a critical role in the overall performance. As seen in (2.5), the load resistance, R_L, highly affects the overall PCE and output voltage. Therefore, an optimal value of R_L should be determined to assure maximum power conversion efficiency [79].

❖ **Load Voltage and Current**

The digital subsection of the RF circuit is fed by the output DC voltage, V_{DD}, and the current I_{DD}. The specifications of most ICs need a minimum voltage to operate properly, usually 1V. Therefore, V_{DD} is a control limitation for sensitivity and lower values of input power result in an inadequate voltage to power the digital subsection. Higher voltages can be managed by using limiters or regulators to avoid damaging circuit components [21].

❖ **Overall Efficiency**

The RF-DC PCE is an essential parameter to assess the rectenna performance. In the aim of evaluating the rectenna "efficiency", and not only the rectifier performance, the PCE of the rectenna system is defined in (2.6) as the ratio of DC output power (P_{DC}) delivered to the load over the RF incident power at the antenna input (P_{RF}), which includes the impedance mismatch and reflective scattering (P_r) at the antenna plan [27].

$$\eta_{rectenna}(\%) = \frac{P_{DC}}{P_{RF}} \times 100 \tag{2.6}$$

2.9.2 Transistor vs. Diode

The rectification process can be achieved by using active devices such as transistors, connected as diodes, or diodes. CMOS, GaAs, or GaN transistors can be utilized to achieve the rectification process [80][81][82]. The CMOS technology is suitable for certain low powers due to its low threshold voltage and can be maximized at narrow input power levels while GaAs- and GaN-based transistors can be applied for rectification at high input power levels due to their inherent capability and high threshold and breakdown voltages [83]. In WPT and harvesting energy, having a rectifier working at low power is required. Therefore, among these transistors varieties, the CMOS-based rectifier proven the ability to handle

most of the requirements to accomplish the WPT process. It is compact, of small size, and cost-effective. However, fabrication difficulties, design constraints, and transistor threshold voltage drop need to be taken into account particularly where the power is requisite as in WPT. Therefore, diodes are preferred in conversion efficiency and power managing [66]-[78], mainly because of their low threshold voltage, high saturation current, low series resistance, and high breakdown voltage. As a result, in this thesis, diodes have been selected to design the rectifier for WPT and harvesting system applications.

2.10. Diode Characterization

As the diodes have been retained to design the rectifier, the concept of diode operation as rectifier should be detailed.

2.10.1 Operation concept

Knowing and determining a specific bias (DC) point is an important step for analyzing and designing an active component in order to operate at its optimal point.

Basically, the power dissipation and voltage/current specifications can be extracted from the device I-V curve. In reverse bias ($V_D < 0\ V$) the current across the diode is very small. Hence, the diode is in its OFF-state.

On the other side, the forward bias happens when $V_D > V_{th} > 0$, V_{th} being the threshold voltage. Hence, the diode is ON. The zero-bias state is considered when $V_D = 0\ V$. The current across the diode can be written as in (2.7).

$$I_D = \begin{cases} I_D = -I_s & Diode\ is\ OFF \\ I_D = I_s\left(e^{\frac{V_D - I_D R_s}{nV_T}} - 1\right) & Diode\ is\ ON \end{cases} \tag{2.7}$$

In the ideal case, the series resistance is set up to zero, leading to

$$I_D = I_s\left(e^{\frac{V_D}{nV_T}} - 1\right) \tag{2.8}$$

where:

I_D	is the current through the diode (A)	V_D	is the voltage across the diode (V)
I_s	is the saturation current (A)	V_T	is the thermal voltage $= kT/q$ (V)
R_s	is the diode series resistance (Ω)	q	is the electron charge $(1.60 \times 10^{-19}\, C)$
n	is the ideality factor.	k	is the Boltzmann's constant $(1.38 \times 10^{-23}\, J/K)$

2.10.2 Diode selection

Diodes rectifiers can be classified into two main clusters namely, zero-biased diode configurations and non-zero-biased configurations [83]. The latter requires an external source to operate, which is not appropriate for harvesting energy and WPT applications. Among zero-bias diodes, P-N junction and Schottky barrier devices are the most widely used. Schottky barrier (SB) diodes have faster switching capabilities and a much higher saturation current [83][84]. Consequently, in this thesis, the zero-bias Schottky barrier diode was retained.

2.10.3 Diode Behaviour as Rectifier

When the diode operates as a rectifier, the maximum output DC voltage is restricted by the voltage breakdown, V_{br}, and can be expressed as (2.9)

$$V_{o,DC} = \frac{V_{br}}{2} \tag{2.9}$$

Note that, due to output DC signal saturation, the input AC signal amplitude is limited. So, the diode breakdown voltage determines the maximum peak voltage of the input waveform and thus, having a diode with high breakdown voltage is desirable to operate at high power. For a given load R_L, the maximum output DC power is determined as [85]

$$P_{DC,max} = \frac{{V_{br}}^2}{4R_L} \tag{2.10}$$

2.11. Diode-Based Rectifier Topologies

In microwave diode rectifiers, various topologies have been proposed including simple structures such as series and/or shunt diodes, voltage doublers (charge pump) and bridge diode rectifiers [19].

The most common configuration is a zero-bias single diode because it is simple, easy to fabricate, and cost-effective. The full-wave rectifier has a better performance than the half-wave; however, it needs a transformer, which makes it improper to utilize. The voltage doubler is a decent candidate because the output voltage will increase at a certain point as the number of stages increases, but at the expense of size and cost. In WPT and harvesting energy systems, it is significant to obtain and select a proper configuration to operate a system with high efficiency over a wide dynamic range of input power levels.

In fact, conventional diode-based rectifier configurations have known limitations due to their inability to operate over a wide dynamic input power range, mainly due to constraints in the semiconductor breakdown voltage and by operating out of the optimum power range, thus leading to a radical drop in the RF-DC efficiency. This effect is known as early breakdown voltage and can be seen in Figure 2.11 [21].

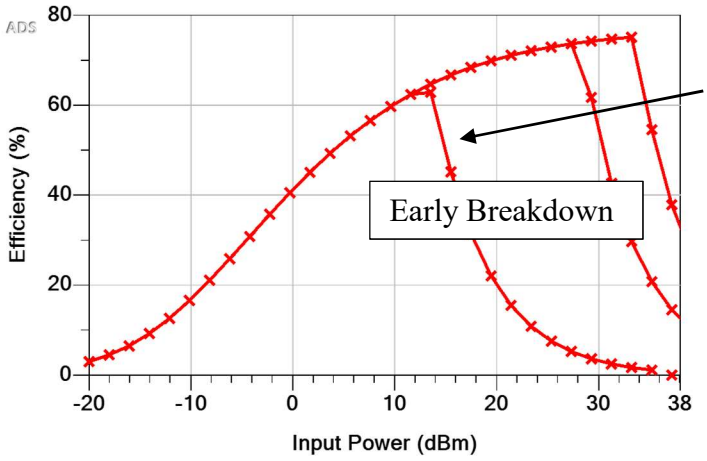

Figure 2.11 Early breakdown voltage illustration

Therefore, several works have been reported to improve the performance of rectifiers and address their device restrictions. Also, varieties of frequency bands rectifiers

have been proposed, including single-band, multi-band, and broad-band rectifiers [9][10][20][86][87][88].

A solution to the sensitivity of the input impedance rectifier versus the input power level and output load has been firstly proposed in [11] by introducing the resistance compression network (RCN) concept to improve the overall rectifier efficiency (by attaining a small variation of the input impedance while changing the input power level and output load); however, the targeted input power range is still narrow. The proposed RCN has been implemented for a single frequency as in [12][89] as well as for dual-band operation to further maximize and enhance the overall system efficiency [1][90].

In [3] and [19], a tunable architecture rectifier was designed to operate over a wide dynamic range of input power levels, but at the expense of complicated and bulky designs. Different rectifiers have been designed at different operating power level capabilities and combined with a single-pole four-throw (SP4T) RF switch structure to extend the operation over a wide range of input powers. Also, the rectifier optimized in [13] at different incident power levels can be connected in parallel to extend its operating range. Furthermore, maximum power point tracking (MPPT) approaches have been utilized to improve the rectifier PCE over a wide range of input powers [14][91][92][93].

Additionally, to solve the breakdown voltage issue of zero-bias Schottky diodes, two types of transformers have been proposed for impedance matching: series-divider-transformer (SDT) and parallel-divider-transformer (PDT) [15].

Correspondingly, an extended power range topology was suggested in [21] and [16] by using a simple configuration of a diode connected in series with a pHEMT transistor to extend the breakdown voltage. However, it needs to be improved to cover wider input power levels. Furthermore, to still improve the rectifier overall PCE, harmonics terminations have been proposed to reject unwanted generated harmonics [94][95][96]. In [97], a nonlinear model has been proposed to rectify and recycle the harmonics with the aim of increasing the RF-DC power conversion efficiency. Moreover, an automatic load control has been proposed in [98] to improve the PCE by changing the load according to the input power variation. Furthermore, a rectifier array has been presented to extend the range of

rectification process as in [99]. Also, to extend the power range of the rectifier, an asymmetric power divider has been proposed in [100].

Moreover, an adaptive reconfigurable rectifier working at 100 MHz has been proposed in [24] to solve the failure of conventional rectifiers to operate over a wide range of input power levels. Likewise, an adaptive load block proposed for the bridge rectifier configuration to improve the overall efficiency has been discussed briefly in [25]. Moreover, an automatic load control has been proposed in [98] to improve the PCE by changing the load according to the input power variation.

Indeed, the efficiency of conventional diode rectifiers can be optimized by adjusting various parameters including frequency operation, input power, saturation current, voltage breakdown, series resistance, device parasitics, capacitor and inductor quality factors, matching network and output load.

Therefore, it turns out to be critical to outline and understand the effect of such parameters and their impact limitations on the circuit performance, which will be highlighted in Chapter 3.

2.12. Summaries and Conclusion

In this chapter, WPT concept was introduced, following by its powering classifications techniques (i) near-field magnetic inductive coupling and magnetic resonant coupling for short range and (ii) far-field EM wave for long range. This work focused on the EM wave technique due to its advantages of long distance charging and powering devices. From that, different RF energy sources were described such as the ambient and dedicated energy sources. The dedicated source was chosen for this work due to mentioned benefits over ambient RF source. In addition, possible applications were explored within the scope of EM-based WPT. The aim application of this work is to have a system operating for a wide range of input power levels to broaden its panel of applications.

In addition, design considerations and RF power transmission parameters were discussed including the transmission range, operation frequency, and safety considerations.

Moreover, a link budget was set to estimate the power level that can be transmitted, received, harvested and the maximum distance to be reached.

Moreover, the RF system was briefly introduced including the transmitter and the rectenna, where the rectifier is one of its fundamental components. Then, the main rectifier parameters were introduced including efficiency, sensitivity and output load. Thus, the diodes, and particularly the Schottky barrier devices, have been selected to achieve WPT due to their low threshold voltage, high saturation current, low series resistance, and high breakdown voltage.

In addition, the issue of conventional diode-based rectifier configurations was raised, i.e., the inability to operate over a wide dynamic input power range with high efficiency. From that, several existing rectifier configurations were discussed to improve the overall PCE of the WPT system while operating with a wide range of input power levels.

To summarize, the following conclusions have been raised:

- EM Wave through a rectenna has been retained with dedicated RF energy source for energy transfer.
- 915 MHz has been retained as operating frequency due to its ease of accessibility, less attenuation, less sensitivity to circuit parasitics and ease of fabrication.
- The diode-based rectifier configuration has been selected as a result of its advantages of operating for low threshold voltage and high voltage breakdown.
- The inability of conventional diode-based configurations to operate over wide range of input powers was highlighted, raising the issue of proposing enhanced solutions to overcome this limitation.

Therefore, in the flowing chapter, different approaches have been proposed and implemented with the aim of improving the PCE while operating over wide range of input powers.

Chapter 3. Rectifier Analysis and Limitations

3.1. Introduction

Designing a rectifier with high PCE and capable of operating over extensive dynamic input power levels, is crucial for WPT and harvesting energy. Therefore, it is important to, first, determine the parameters that can affect the overall performance of a diode-based rectifier, and then to investigate their impact on its Power Conversion Efficiency. In fact, since trade-offs should be made, it is essential to understand how the above parameters govern the rectifier performance in order to optimize its operation over a wide input power range.

3.2. Diode Model

We first started by considering a generic configuration of a rectifier as shown in Figure 3.1. In this figure, the well-known diode Spice model [101] highlights the diode elements that affect the circuit performance such as the junction resistance R_j, the junction capacitor C_j, the diode parasitic, (R_s, L_s, and C_p), as well as key internal diode parameters like the saturation current I_s and voltage breakdown V_{br}. The output load (assumed to be R_2) should be also considered [85], while R_1 has been included to control the current flowing through the diode.

Therefore, in this study, we had to sweep these parameters within a predefined range to determine their influence on the circuit PCE. To do so, we had to review the most widely used commercial Schottky barrier diodes in WPT applications as reported in Table 3.1 [101][102]. From the datasheets of these diodes, we, then, came up with a practical range of values of their parameters for operation in the 915 MHz ISM band (Table 3.2); the objective being to have a diode with high saturation current (I_s), and high breakdown voltage (V_{br}).

In fact, these two parameters are considered as the most significant parameters affecting the rectifier efficiency. When the rectifier active device is driven in reverse bias,

the electric field near the junction can reach its maximum allowable value. Once the breakdown occurs, the current will suddenly increase while the dc output voltage remains almost constant, producing a major loss in the output dc power [85][84].

As for the saturation current, it controls the threshold voltage, V_{th}, which can be defined as the voltage value from where an active device can operate and detect the signal at low input power level. In fact, the threshold voltage is inversely proportional to the saturation current [83][85].

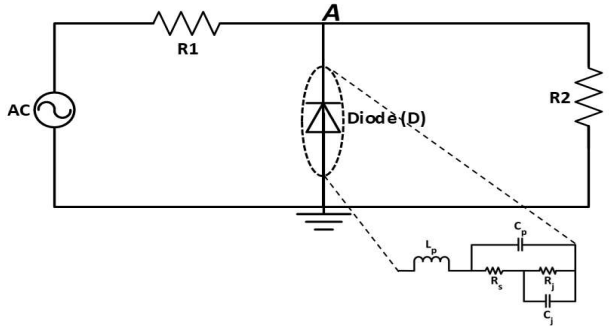

Figure 3.1 Half-Wave rectifier configuration and its equivalent circuit (Spice model) [101]

Table 3.1 WPT Diode Parameters (SPICE model)

Diode Parameters	**Diode Type**					
	HSMS280x	HSMS281x	HSMS282x	HSMS285x	HSMS286x	SMS7360
V_{th}**(V)**	0.38	0.45	0.42	0.15	0.35	0.14
R_s**(Ω)**	30	10	6	25	5	20
V_{br}**(V)**	75	25	15	3.8	7	2
I_s**(A)**	3E-8	4.8E-9	2.2E-8	3E-6	5E-8	5E-6
C_{jo}**(pF)**	1.6	1.1	0.7	0.18	0.18	0.14
R_j**(Ω)**	**	**	**	**	**	**
L_s**(nH)**	N/A	N/A	N/A	2	2	1.5
C_p**(pF)**	N/A	N/A	N/A	0.1	0.1	N/A

** These values depend on the saturation current and bias current as in equation (3.1)

In the above table, each diode has a different set of characteristics and its optimal power operating range. For instance, HSMS-280x from Avago Technologies has the highest voltage breakdown, but at the expense of higher resistance. In applications that did not require high voltage, the HSMS2860 and HSMS282x with low series resistance can provide higher current. In WPT, having a system able to capture and sense low level of power is crucial; therefore, the HSMS2850 and SMS7360, from Skyworks Solutions, Inc, with high saturation current are good candidates for operating at low level of input power. Since the junction capacitance controls the cut-off frequency and the diode switching, diodes with small C_j is preferable as in the HSMS2850, HSMS2860 and SMS7630. Therefore, by selecting the proper diodes to operate at low and high input power levels, low threshold voltage and high breakdown voltage can be accomplished.

3.3. Preliminary Simulations

In this first set of simulations, some parameters were not considered (Table 3.2). In fact, since we had to develop a code in Matlab [103] to solve numerically the equations governing the circuit, the purpose of these preliminary simulations was to validate our code.

Table 3.2 Range of the Parameters Considered in the First Set of Simulations

Diode Parameters	Range of value	Default value
$\boldsymbol{R_s}$(Ω)	0 - 50	0
$\boldsymbol{V_{br}}$(V)	2 - 75	∞
$\boldsymbol{I_s}$(A)	5E-11 - 3E-6	5E-6
$\boldsymbol{C_{jo}}$(pF)	0.1 - 2	0

From that, we assumed, for simplification, that the diode is operating in linear mode. In this case, R_j is directly related to the diode saturation current as [101].

$$R_j = \frac{8.33 \times 10^{-5}\, nT}{I_s + I_b} \tag{3.1}$$

where I_s and I_b are the saturation current and external applied bias current (in A). So, to avoid redundancy, we only considered I_s. As for the parasitics L_s and C_p, we can see from Table 3.1 that their values remain quite close (around 2nH and 0.1 pF, respectively). Consequently, they have been considered, at first approximation, as constant. Finally, we fixed the load to 50 ohms ($R_L(\Omega) = 50\ \Omega$).

Then, we analyzed the circuit in both DC, time-domain (TD) and harmonic balance (HB) to determine how these parameters can affect the circuit performance and thus, the overall PCE of the rectifier.

3.3.1 Initial simulations

From (2.7), the equation governing the circuit in Figure 3.1 can be expressed as:

$$\frac{V_{in}}{R_1} = -I_s\left(e^{\frac{V_D - I_D R_s}{nV_T}} - 1\right) + V\left(\frac{1}{R_1} + \frac{1}{R_L}\right) \tag{3.2}$$

with nV_T = 26 mV at 300º K. In order to validate our approach, the above equation was solved in Matlab [103] for a frequency of 915 MHz, with $R_L = 100\ \Omega$ and $R_1 = 50\ \Omega$. Note that the input voltage V_{in} was set to 5 V.

3.3.2 List of simulations

In order to study the parameters listed above, we summarized in Table 3.3 the different analyses we performed. In fact:

- Analyses #1 and #2 were set to examine the effect of the series resistance on the time domain and the I-V DC characteristics, respectively.
- The purpose of the analyses #3 and #4 was to explore the impact of the voltage breakdown toward the response of the output voltage in time-domain and the I-V characteristics in the DC analysis.
- Analyses #5 and #6 were preformed to show the effect of the saturation current on the time domain and DC characteristics.

- Finally, the analysis #7 was set to evaluate the PCE as function of the input power for different voltage breakdown values.

Table 3.3 Lists of implemented TD, DC and HB analyses

Analysis No	Parameters swept	Parameters kept fixed (default value)	Simulation type (DC, TD, HB)	Expected conclusion based on Matlab simulations
1	R_s	V_{br}, C_{jo}, I_s, R_L	TD	As $R_s \uparrow \Longrightarrow V_{DC} \downarrow$
2	V_{br}	R_s,C_{jo}, I_s, R_L	TD	As $V_{br} \uparrow \Longrightarrow V_{DC} \uparrow$
3	I_s	R_s,C_{jo},V_{br} , R_L	TD	As $I_s \uparrow \Longrightarrow V_{DC} \uparrow$
4	R_s	V_{br}, C_{jo}, I_s, R_L	DC	As $R_s \uparrow \Longrightarrow I_D \downarrow$
5	V_{br}	R_s,C_{jo}, I_s, R_L	DC	As $V_{br} \uparrow \Longrightarrow V_{DC} \uparrow$
6	I_s	R_s,C_{jo},V_{br} , R_L	DC	As $I_s \uparrow \Longrightarrow V_{th} \downarrow$
7	V_{br}	R_s,C_{jo}, I_s, R_L	HB	As $V_{br} \uparrow \Longrightarrow V_{DC} \uparrow$

3.3.3 Time Domain and DC Analysis

Time-domain voltage waveforms and diode I-V DC characteristics provide a good knowledge to understand the rectifier operation and analyze the effect of such parameters on the output voltage and the I-V DC characteristics.

To do so, (3.2) was implemented in Matlab to study the influence of the diode's series resistance, R_s, voltage breakdown, V_{br}, and saturation current, I_s on the output voltage in time-domain. Then, the numerical results data were successfully compared to the responses from the Keysight's Advanced Design System (ADS) simulator (Figure 3.2).

With the aim of analyzing the I-V DC characteristics numerically, we therefore considered the well-known current diode equation (2.7) as an implicit equation; implemented in Matlab, it was successfully compared to the results extracted from ADS (Figure 3.3).

From the obtained results (Figure 3.2 and Figure 3.3), we can see that:

a) Analyses #1 and #4:

A lower series resistance, R_s, provides a higher output DC voltage, leading to a higher PCE (see section (3.4.1)).

b) Analysis #2 and #5:

A higher voltage breakdown, V_{br}, allows to handle more output voltage at high input power levels which helps increasing the DC output. Moreover, as V_{br} increases, the PCE becomes border to operate over a wide range of input powers, as discussed in section (3.4.2).

c) Analysis #3 and #6:

The saturation current, I_s, directly controls the diode's threshold voltage (V_{th}) or turn-on state. A higher I_s allows detecting signals with low input power, thus leading to higher PCE, as discussed in section (3.4.3).

3.3.4 Harmonic Balance Analysis

In this section, the behaviour of the rectifier was investigated using the harmonic balance (HB) simulation tool, with the aim of evaluating the effects of the retained parameters on the overall PCE. Let the input voltage, V_{in}, in Figure 3.1 be expressed as:

$$V_{in} = V_p \sin \omega_0 t \tag{3.3}$$

In case of an input voltage magnitude, $V_p < V_{th}$, the diode is OFF, and the output voltage can be expressed as

$$Vout = V_p \sin \omega_0 t = V_{in} \qquad \Rightarrow \qquad V_{DC} = 0 \tag{3.4}$$

In case of $V_p > V_{th}$ and $V_p < V_{br}$, the diode is ON and the output voltage displayed in Figure 3.4. In order to calculate the DC output voltage, the waveforms have been divided into four parts (I_1, I_2, I_3, I_4) to perform the integral and find the output DC voltage (more details can be found in Appendix A).

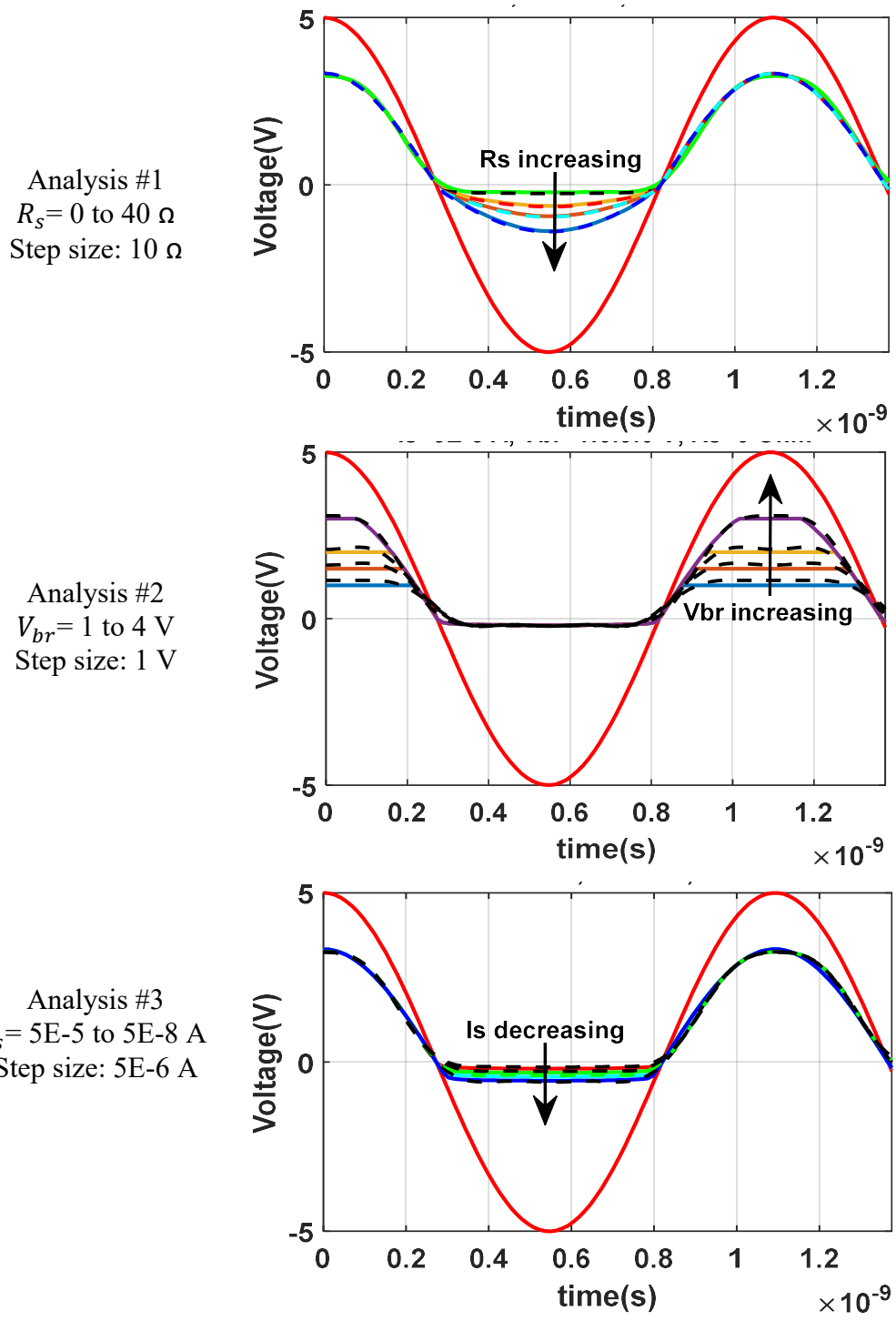

Figure 3.2 Time domain input vs. output voltage: analyzing the shunt rectifier for different series resistance, R_s, voltage breakdown, V_{br} and saturation current, I_s. (the dash lines represent the ADS simulation and the solid lines the numerical results obtained through Matlab).

Analysis #4
R_s= 10 to 50 Ω
Step size: 5 Ω

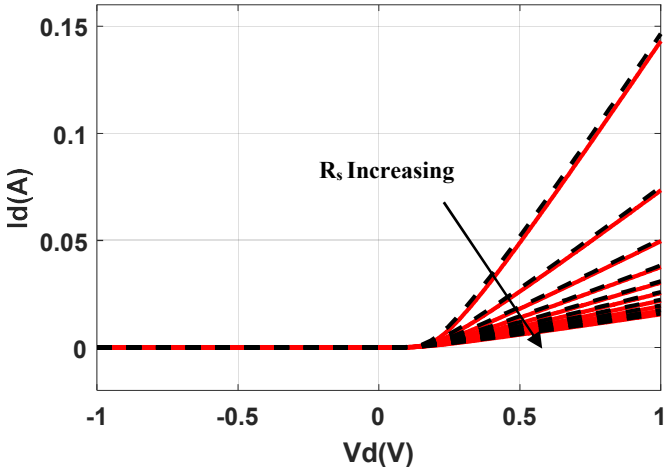

Analysis #5
V_{br}= 4 to 24 V
Step size: 5 V

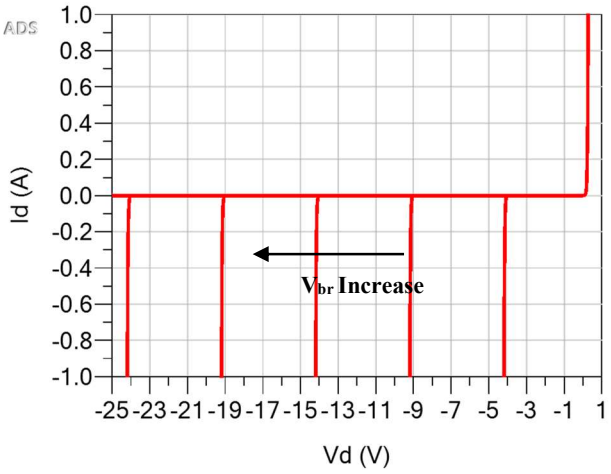

Analysis #6
I_s= 5E-5, 5E-6, 5E-7, 5E-11 A

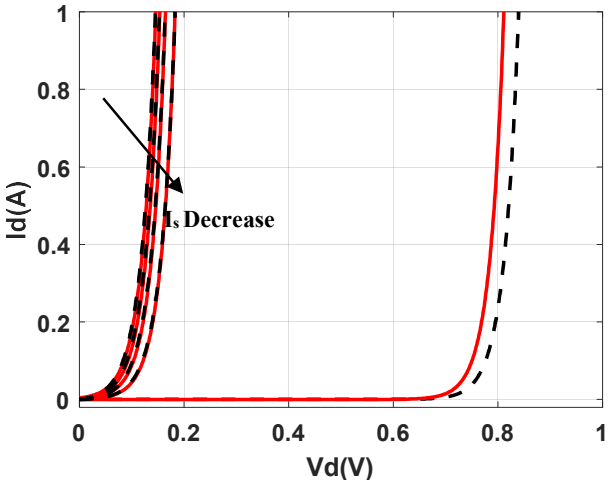

Figure 3.3 I-V curve characteristics: analyzing the shunt rectifier for different series resistance, R_s, voltage breakdown,V_{br}, and saturation current, I_s. (the dash lines represent the ADS simulation and the solid lines the numerical results obtained through Matlab).

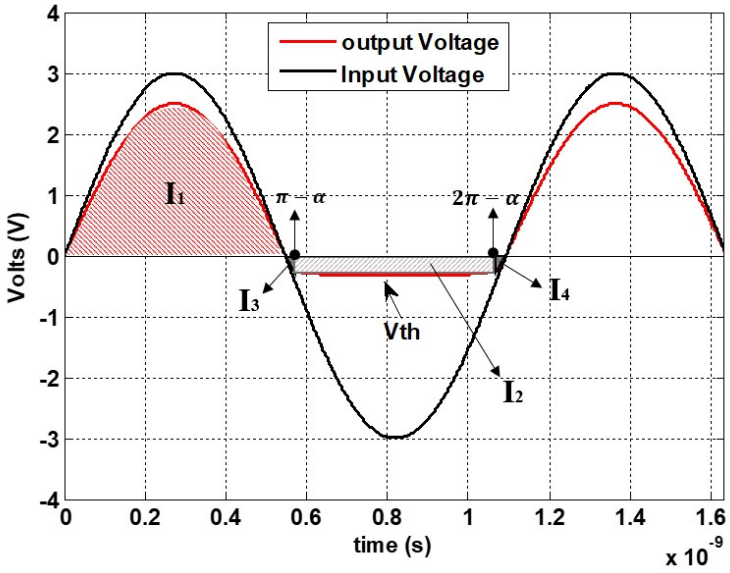

Figure 3.4 Output voltage of the half wave rectifier at $V_p > V_{th}$ and $V_p < V_{br}$

Therefore, the total output DC voltage can be written as

$$V_{T_{dc}} = \frac{V_p}{\pi} + V_{th}(\pi - 2\alpha) + \frac{V_p}{\pi}(1 - \cos\alpha) \tag{3.5}$$

with

$$\alpha = \sin^{-1}\left(\frac{-V_{th}}{V_{in}}\right) \tag{3.6}$$

In case of $V_p > V_{th}$ and $V_p > V_{br,}$ the diode is ON and the output voltage is limited by the voltage breakdown as illustrated in Figure 3.5.

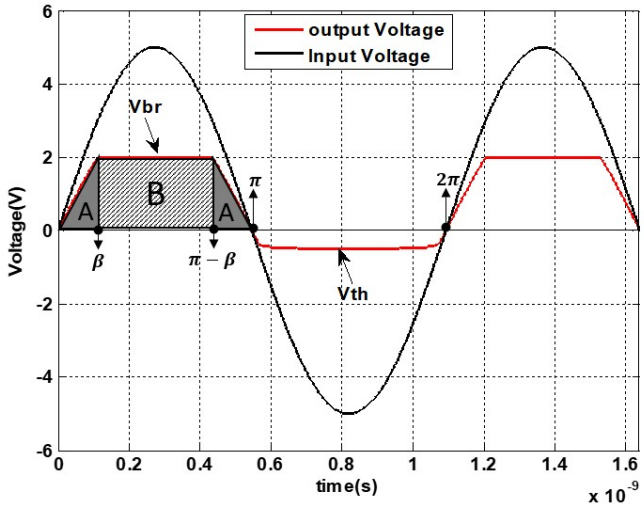

Figure 3.5 Output voltage of half wave rectifier at $V_p > V_{th}$ and $V_p > V_{br,}$

In order to calculate the DC output voltage, the waveforms have been divided into four parts (A, B, I_2, I_3, I_4) to integrate and obtain the DC voltage. The total output DC voltage can be written as

$$V_{T_{dc}} = \frac{V_p}{\pi}(1-\cos\beta) + V_{br}(\pi - 2\beta) + V_{th}(\pi - 2\alpha) + \frac{V_p}{\pi}(1-\cos\alpha) \tag{3.7}$$

with

$$\beta = \sin^{-1}\left(\frac{V_{br}}{V_{in}}\right) \tag{3.8}$$

d) Analysis #7:

In order to verify its Power Conversion Efficiency, the circuit configuration was simulated in the Keysight's Advanced Design System simulator for different voltage breakdown values and the results effectively compared to the numerical data obtained by solving (3.5) and (3.7) in Matlab, as shown in Figure 3.6.

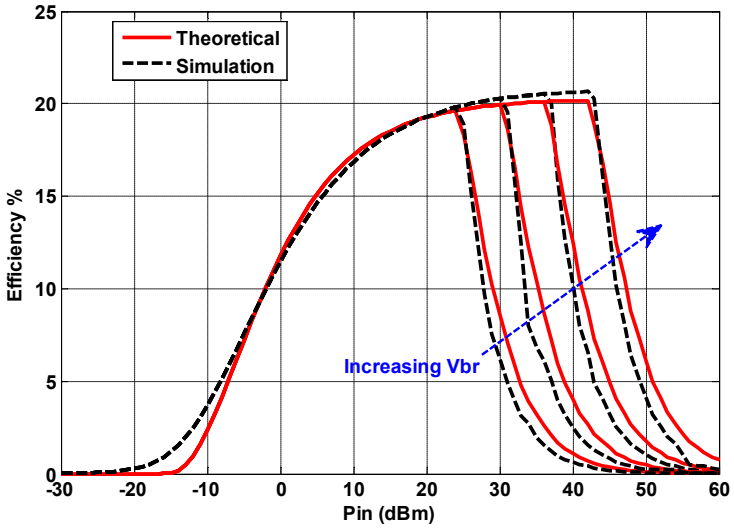

Figure 3.6 Half wave rectifier efficiency as a function of input power for different voltage breakdown values, V_{br} = 20 to 60 V; step size:10 V (the dash lines represent the ADS simulation and the solid lines the numerical results obtained through Matlab)

Because the above numerical results of the time domain (TD), DC analysis and the harmonic balance (HB) agree with the extracted simulation data with an average error less than 1%, we can conclude that the code we implemented in Matlab is now validated.

3.4. Rectifier PCE Limitations and Effects

For this new set of simulations, once our approach was validated, we have then to consider the diode junction capacitance C_j, junction resistance R_j, and the output load R_L along with the previous parameters. Indeed, the junction capacitance, C_j, affects the total efficiency due to its nonlinearity effect and adds a loss to the system resulting into efficiency degradation [85][104]. The nonlinear junction capacitance can be modeled and specified as in (3.9) by using the spice parameters including zero-bias junction capacitance C_{jo}, junction potential V_j and grading coefficient M.

$$C_j = \frac{C_{j0}}{\left(1 - \frac{V_D}{V_j}\right)^M} \tag{3.9}$$

As for the nonlinear junction resistance, R_j, its behaviour can be extracted from the scattering parameters and the DC-current-voltage [83][85][101]. Finally, the output load or load resistance was also varied to allow a thorough set of trade-offs among these parameters.

Therefore, the impacts of these parameters on the circuit performance need to be investigated as they are related to each other as in (3.10).

$$\eta(\%) = \frac{P_{DC}}{P_t} = \eta\left(R_s, V_{br}, I_s, C_{jo}, R_j, R_L\right) \tag{3.10}$$

Figure 3.7 shows the PCE of a rectifier at different input power levels; the efficiency at low input power increases monotonically until reaching its maximum then it drops dramatically as the input power became higher due to the rectifier voltage breakdown [85][105][106]. Consequently, the schematic view of the half wave rectifier in Figure 3.8 is utilized to measure and evaluate the overall PCE.

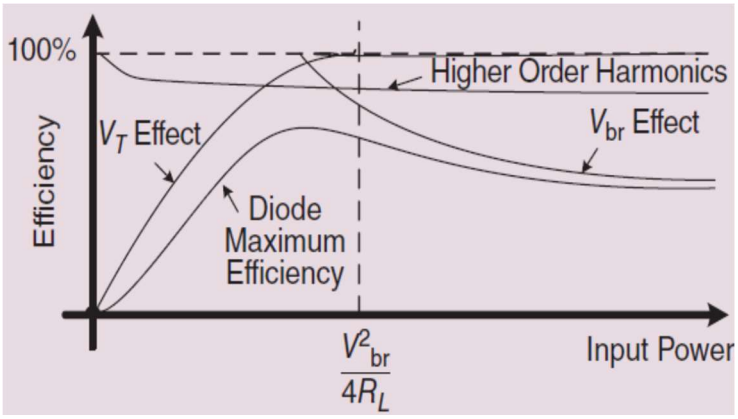

Figure 3.7 Relationship between efficiency and different limitation parameters [85]

To avoid potential power loss in the harmonics, the harmonics generated from the nonlinearity components are first assumed to be negligible. Therefore, we summarized in Table 3.4 the different analyses we performed and their predictable conclusions.

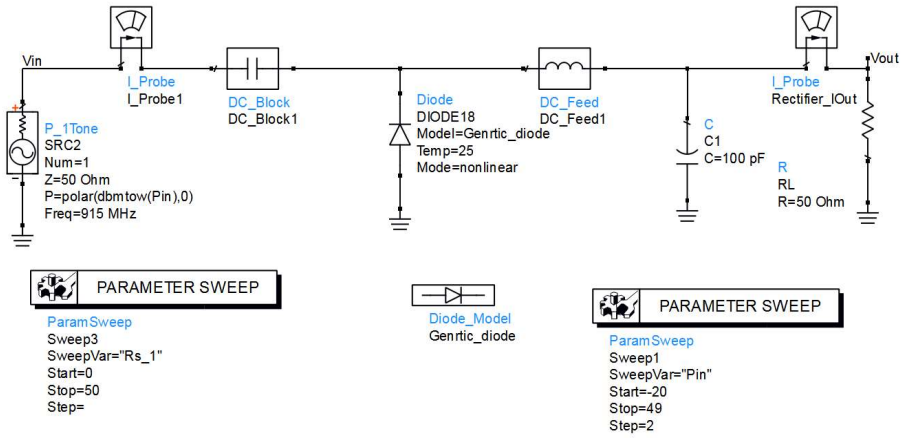

Figure 3.8 Harmonic balance setup of the half wave rectifier (ADS view)

Table 3.4 Lists of implemented HB analyses for PCE

Analysis No	Parameters swept	Parameters kept fixed	Expected conclusion on PCE
1	R_s	$V_{br}, I_s, C_{jo}, R_j\ R_L$	As $R_s \uparrow \Longrightarrow$ PCE degraded
2	V_{br}	R_s,C_{jo}, I_s, R_j, R_L	As $V_{br} \uparrow \Longrightarrow$ wider range of input power
3	I_s	R_s,C_{jo},$V_{br}, R_j\ , R_L$	As $I_s \uparrow \Longrightarrow$ low signal can be detected
4	C_{jo}	R_s,V_{br}, R_j, R_L	As $C_{j0} \uparrow \Longrightarrow$ PCE degraded due to cut-off frequency
5	R_j	R_s,C_{jo},V_{br}, R_j, R_L	As $R_j \uparrow \Longrightarrow P_{DC}$ reduced
6	R_L	R_s,V_{br}, C_{jo}, I_s, R_j	As $R_L \uparrow\downarrow \Longrightarrow$ PCE optimized

3.4.1 Analysis #1: Series resistance (Rs)

In this analysis, the effect of series resistance towards the PCE is studied as in Figure 3.9-a and Figure 3.9-b. As noticeable, as R_s increases, the overall efficiency degrades since the current flowing through the diode is reduced as shown in the I-V DC characteristics and the produced DC power as in (3.11) is reduced as well. Moreover, the overall efficiency as a function of series resistance and input power, P_{in} , is shown in Figure 3.10 [83].

$$P_{DC} = \frac{{V_{DC}}^2}{R_L + R_v} = \frac{{V_{DC}}^2}{R_L + R_j + R_s} \tag{3.11}$$

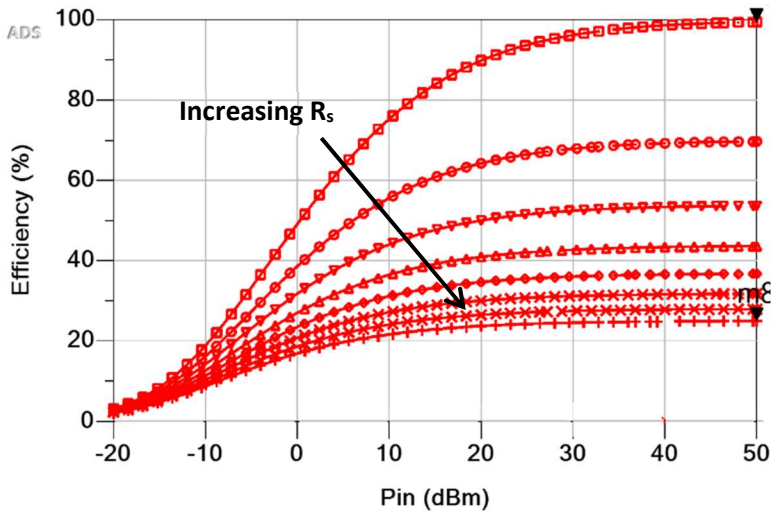

(a)

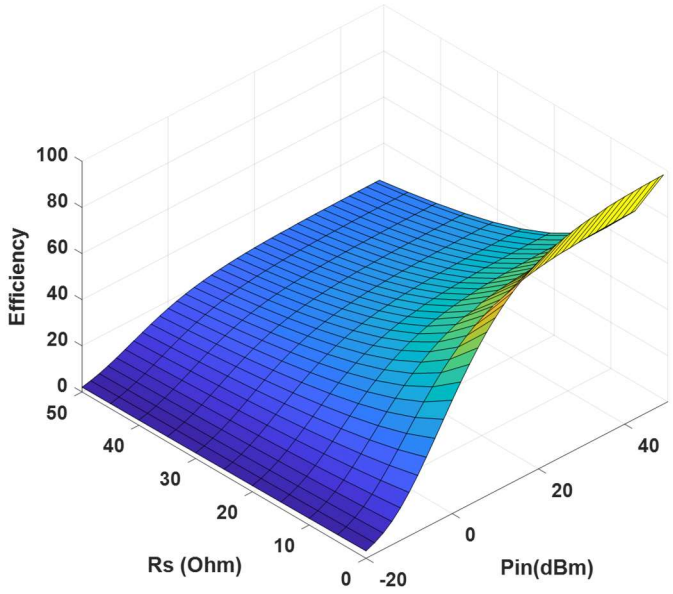

(b)

Figure 3.9 Series resistance effect on the overall PCE (a) two-dimensions (2D). (b) three-dimensions (3D); (R_s= 0 to 48 Ω. Step: 6 Ω).

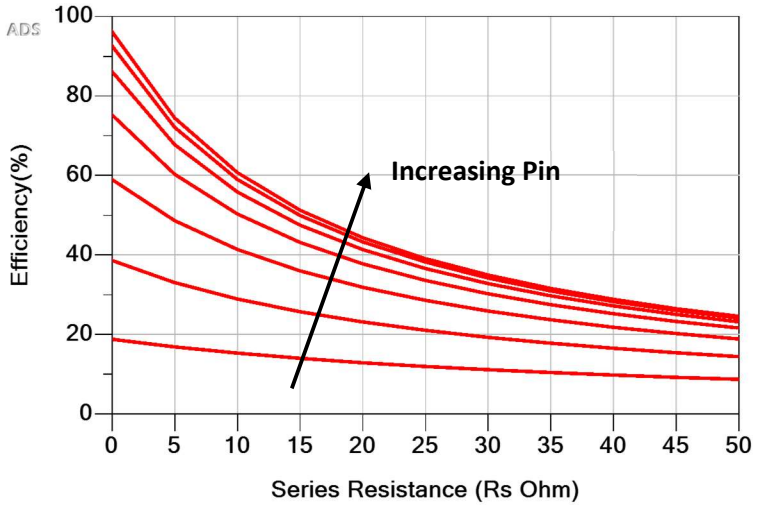

Figure 3.10 Overall PCE as a function of series resistance and input power (Pin =-20 to 49 dBm step size: 7 dBm)

3.4.2 Analysis #2: Breakdown voltage (V_{br})

In this analysis, having a rectifier with high breakdown voltage is required to achieve high efficiency. The effect of the voltage breakdown on the overall PCE is shown in Figure 3.11-a and Figure 3.11-b. As noticed, as the voltage breakdown increases, the overall efficiency becomes broader and able to handle a wider input power range, thus achieving higher efficiency.

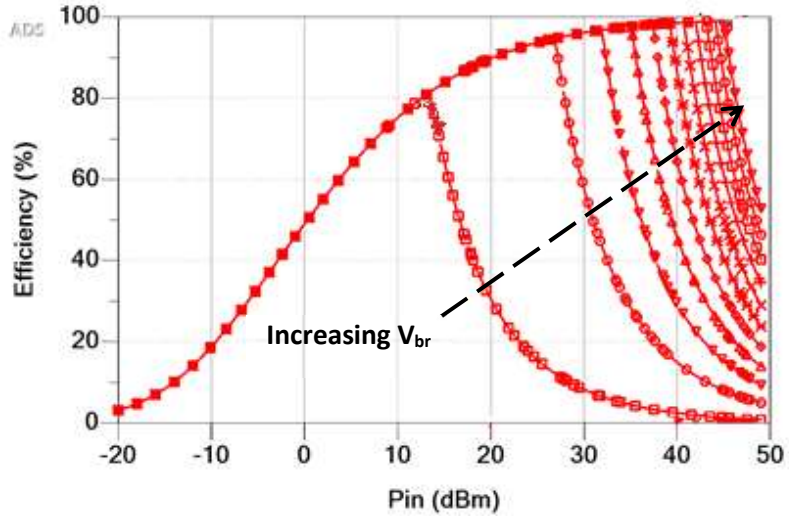

(a)

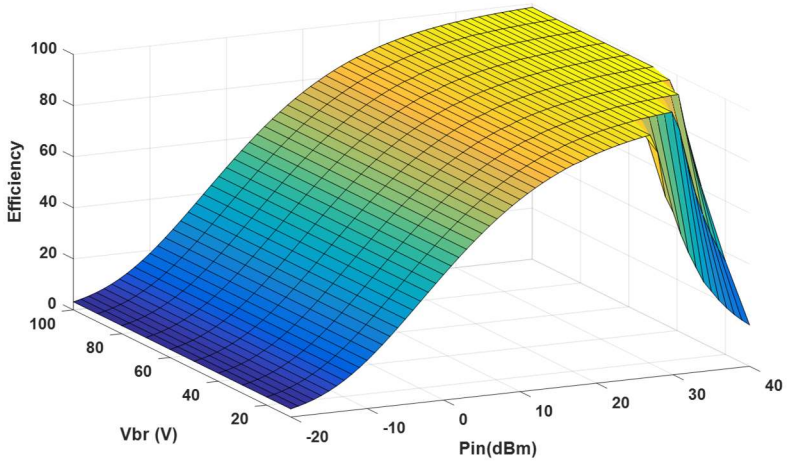

(b)

Figure 3.11 Voltage breakdown effect on the overall PCE (a) two-dimensions (2D). (b) three-dimensions (3D). (V_{br} = 20 to 100 V. Step size: 10 V)

3.4.3 Analysis #3: Saturation current I_s

Figure 3.12 shows that a diode with high saturation current is desirable in WPT applications to manage low signals [84]. In addition, the effect of the saturation current on the overall PCE is illustrated in Figure 3.13-a and Figure 3.13-b showing that loss at low input power is due to lower saturation current and vice-versa. Moreover, the overall efficiency as a function of saturation current and input power, P_{in}, is shown in Figure 3.14.

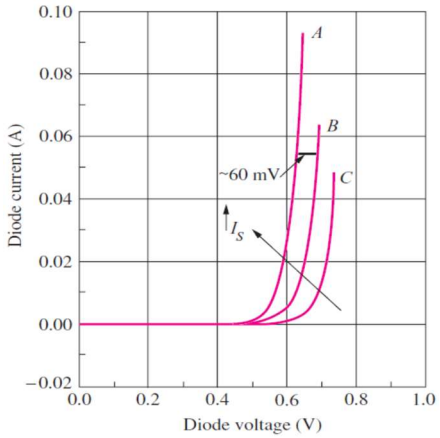

Figure 3.12 Diode characteristics for three different reverse saturation currents [84]

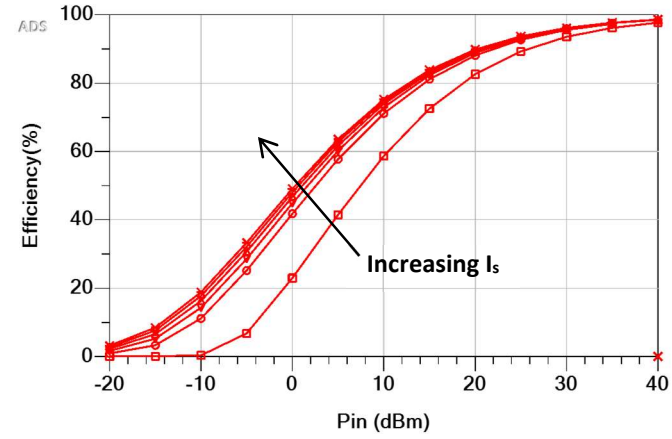

(a)

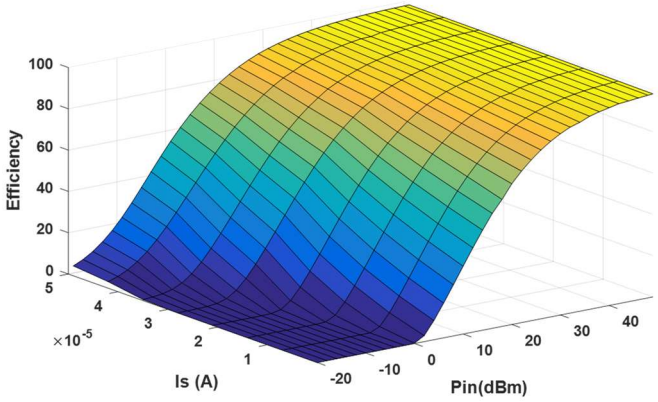

(b)

Figure 3.13 Saturation current effect on the overall PCE (a) two-dimensions (2D). (b) three-dimensions (3D) (I_s= 5E-10 to 5E-5 A Step size: 1E-5 A).

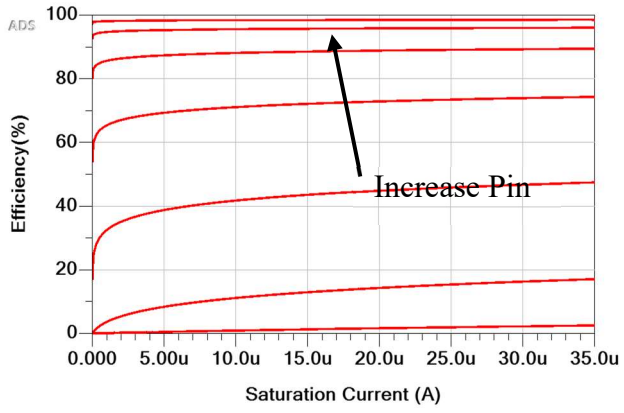

Figure 3.14 Overall PCE as a function of saturation current and input power (Pin =-20 to 49 dBm step size: 7 dBm).

We can conclude from analyses # 1, #2, and #3, that the series resistance helps maximizing the PCE while the voltage breakdown affects the input power range. As for the saturation current, it plays a role in selecting the minimum detectable input power. Consequently, in order to operate for a wide range of input powers while achieving high PCE, a high saturation current is desirable to operate at low input power, a low series resistance is required for achieving high PCE and a high voltage breakdown is needed to handle wider input power range.

3.4.4 Analysis #4: junction Capacitance

Since the junction capacitance controls the cut-off frequency of the diode as illustrated in (3.12) [85][104], the effect of the junction capacitance on the PCE for different frequencies is shown in Figure 3.15, with C_{j0}= 1 pF, R_s = 25 Ω. As in Figure 3.15, as the frequency increases, the overall efficiency degrades due to the cut-off frequency.

$$f_c = \frac{1}{2\pi R_s C_j} \tag{3.12}$$

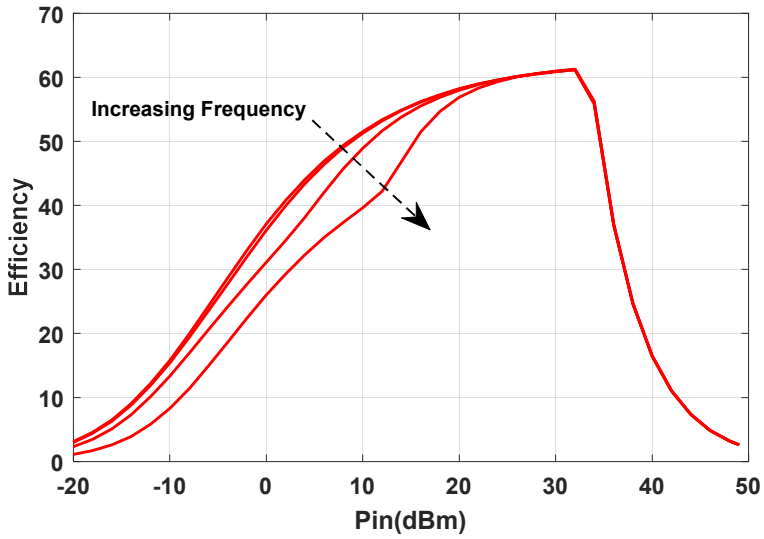

Figure 3.15 Junction capacitance (C_j) effects on the overall efficiency (frequency varied from 915 MHz, 2 GHz, 3.5 GHz and 5 GHz).

3.4.5 Analysis #5: Junction resistance

Due to its nonlinearity, the junction resistance behaviour should include harmonics. In order to assess the effect of harmonics towards the overall efficiency, the harmonics level was swept from 10 to 30 dBm below the fundamental. As noticed in Figure 3.16, as the levels of the 2nd and 3rd harmonics are far below the fundamental frequency, the overall efficiency is improved. However, when they start increasing, the output DC power degrades as in (3.11). Then, as the 2nd and 3rd harmonics are terminated by a circuit trapping, a noticeable improvement in the PCE can be shown as in Figure 3.16-g.

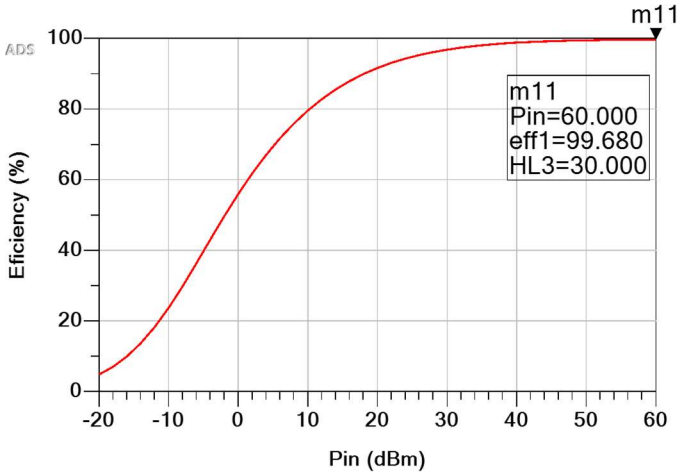

(a) PCE: ideal case with no harmonics

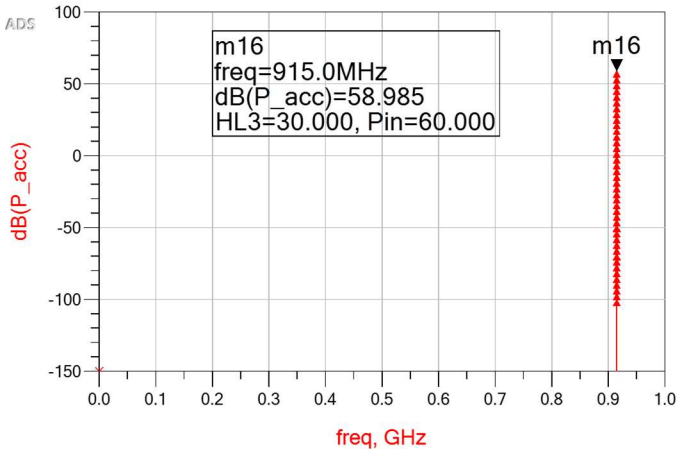

(b) Frequency spectrum of the ideal case

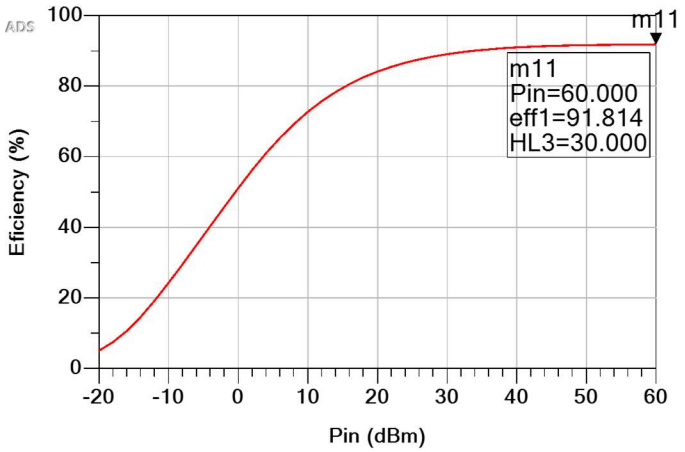

(c) PCE: effect of the 2nd harmonic

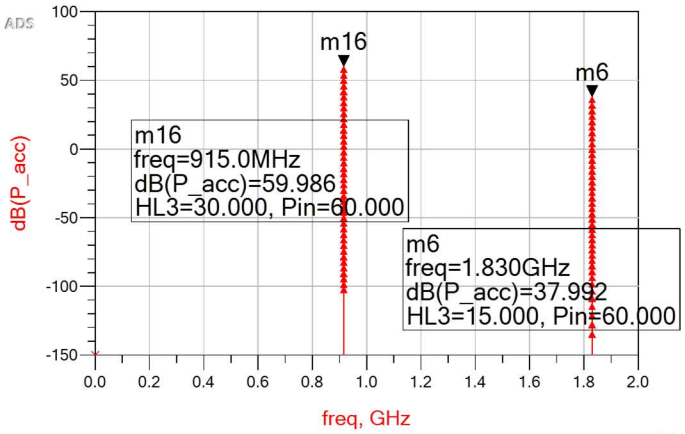

(d) Corresponding frequency spectrum of case (c) with the fundamental and 2nd harmonic.

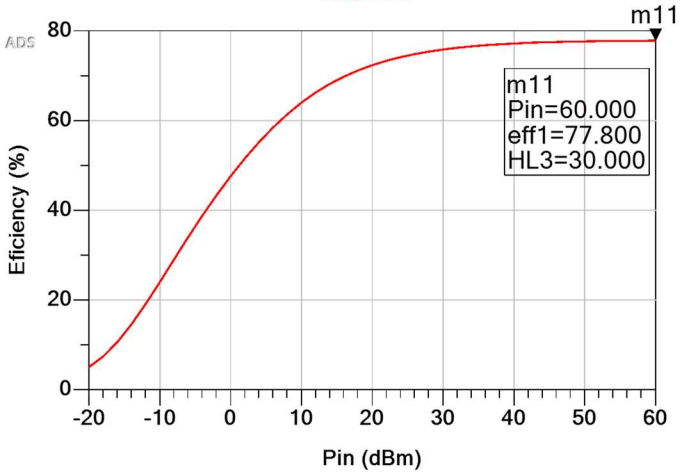

(e) PCE: effect of the 3nd harmonic

(f) Corresponding frequency spectrum of case (e) with the fundamental, 2nd and 3rd harmonics.

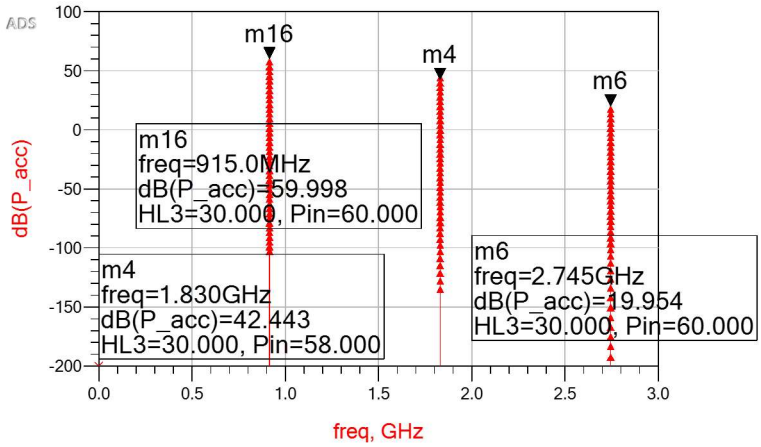

(g) PCE: with trapping the harmonics

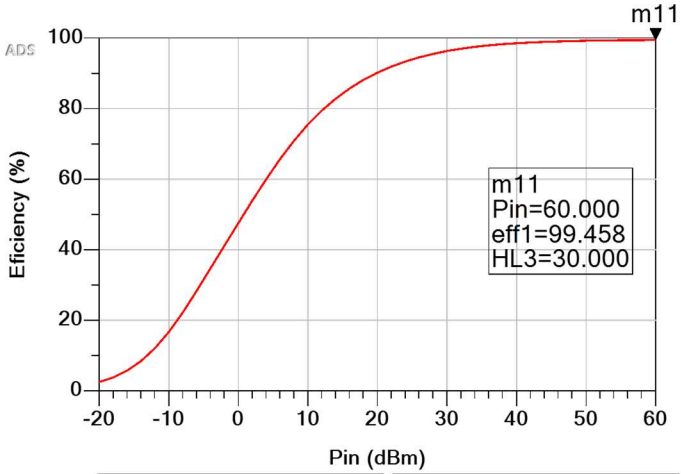

(h) Corresponding frequency spectrum of case (g) with the fundamental, 2nd and 3rd harmonics.

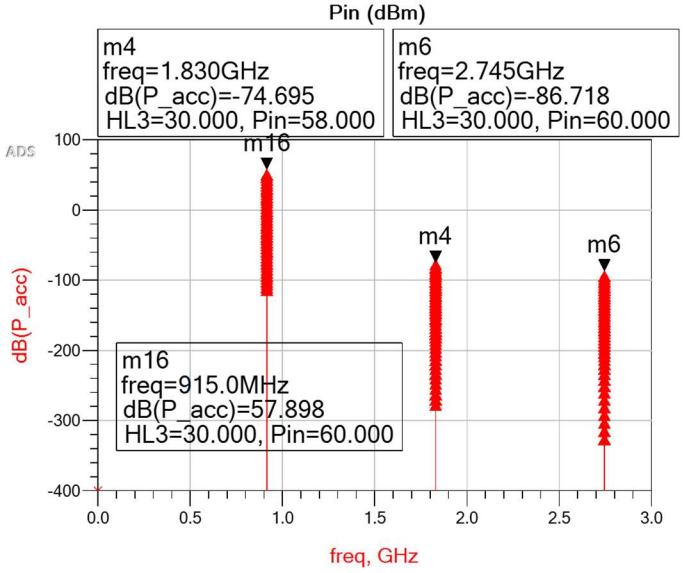

Figure 3.16 Efficiency of the 2nd and 3rd harmonic as a function of the harmonic level for different input powers (a)-(b) the ideal case with no harmonics. (c)-(d) the effect of the 2nd harmonic. (e)-(f) the effect of the 2nd and 3rd harmonics. (g)-(h) the effect of trapping the 2nd and 3rd harmonics.

3.4.6 Analysis #6: Output load

Once the RF wave is rectified, the output DC power is used by the load [83]. Let $R_v = R_j + R_s$ be the diode video resistance (i.e., the small-signal low frequency dynamic resistance of the diode). The maximum dc power transfer efficiency is obtained for low video resistance as in (3.13). Therefore, an optimal output load, R_L should be applied to achieve maximum power conversion efficiency. Using a maximum power point tracking (MPPT) circuit that will show an optimum load to the rectifier, the dc power transfer losses can be strongly reduced (Figure 3.17).

$$\eta_{DC} = \frac{1}{1 + \frac{R_v}{R_L}} \tag{3.13}$$

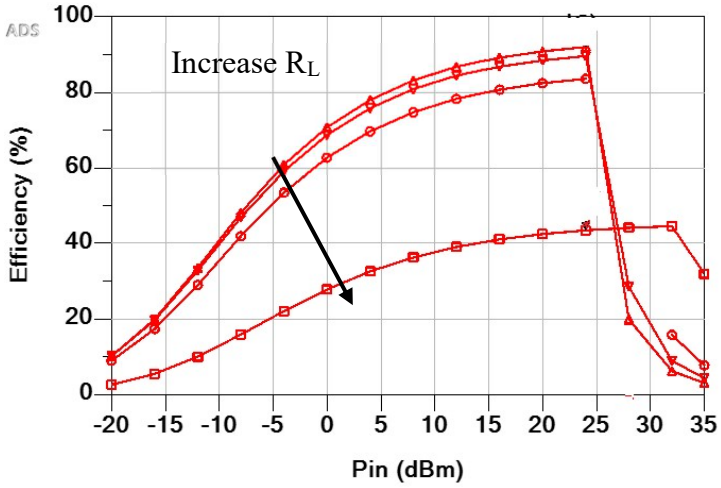

Figure 3.17 Rectifier efficiency vs power for different loads. (R_L = 50 to 200 Ω. Step size: 50 Ω)

3.5. Discussions

Figure 3.18 summarizes the limitations of conventional diode-based rectifiers in terms of efficiency. In this figure, different parameters were varied for a shunt rectifier diode. From Figure 3.18-a, we can notice that the series resistance is inversely proportional to the overall efficiency while in Figure 3.18–b, a high voltage breakdown is important to operate at high power levels. In Figure 3.18-c, a high saturation current is required to operate

at low power levels. Figure 3.18-d shows that the operating frequency is limited by the junction capacitance while Figure 3.18-e shows the effect of the harmonics. Finally, Figure 3.18-f shows that the PCE is quite sensitive to the output load.

Accordingly, a low series resistance is required for achieving high PCE, a high voltage breakdown is needed to handle wide range of input powers and a high saturation current is desirable to operate at low input power levels. Besides, trapping harmonics can significantly improve the overall PCE. Finally, an optimum load is desired to maximize the rectifier PCE. Therefore, in the next chapter, various approaches (i.e., adaptive reconfigurable configuration, active load modulation, harmonic trapping) will be implemented to design a rectifier of high PCE capable of operating over a wide range of input power levels.

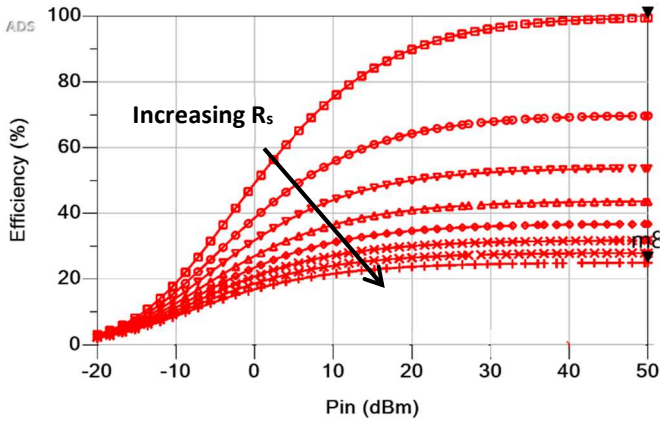

(a)

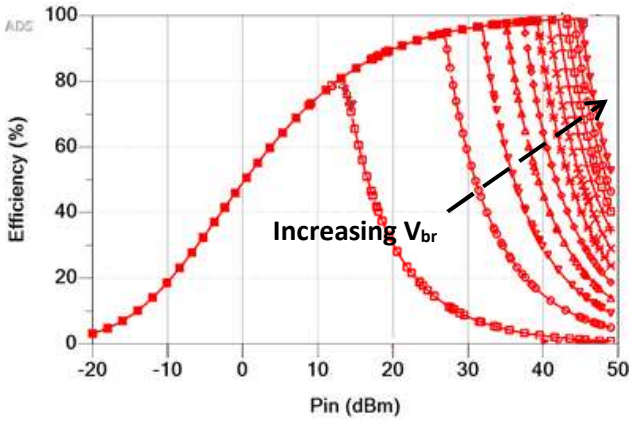

(b)

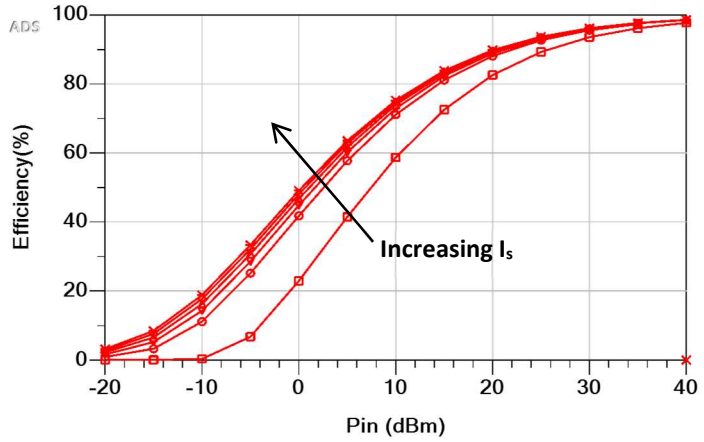
ADS
Efficiency(%)
Pin (dBm)
Increasing I_s

(c)

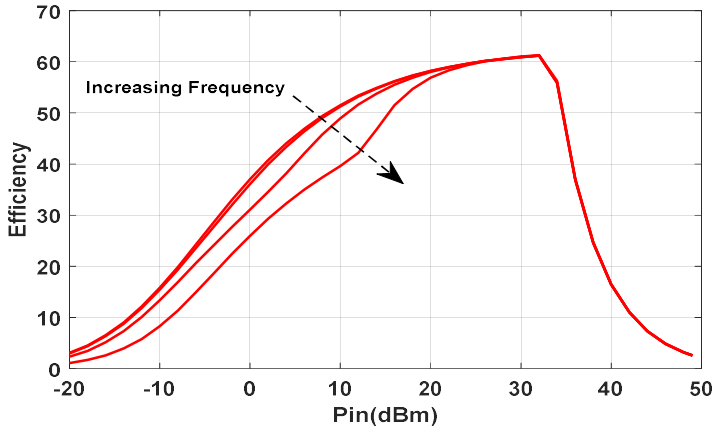
Efficiency
Pin(dBm)
Increasing Frequency

(d)

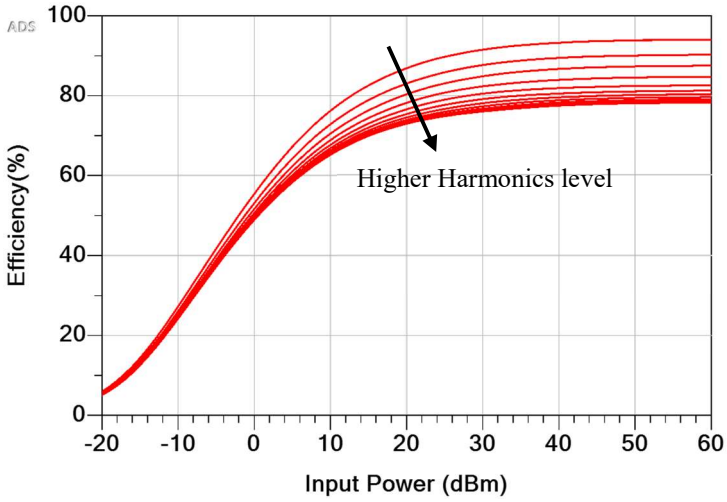
ADS
Efficiency(%)
Input Power (dBm)
Higher Harmonics level

(e)

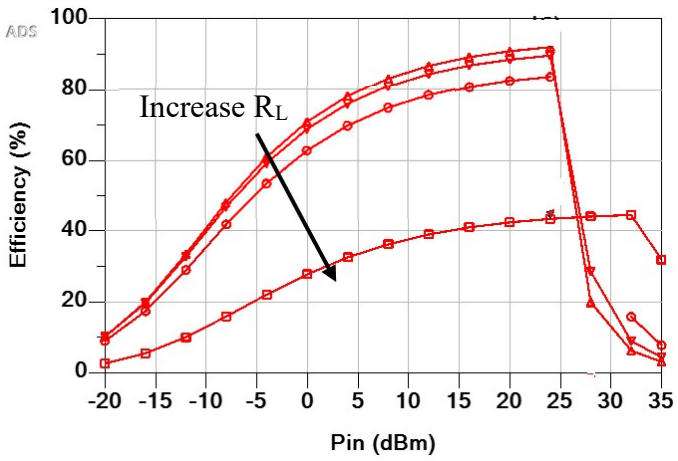

(f)

Figure 3.18 Efficiency performance effect for different diode parameters on shunt rectifier configuration: (a) varying series resistance. (b) varying breakdown. (c) varying the saturation current (d) varying frequency operation. (e) varying harmonics level. (f) varying load resistance.

3.6. Conclusion

In this chapter, the analysis of diode-based rectifiers operation and their efficiency limitations were investigated to understand the critical components that affect the overall PCE of the circuit and, thus, how to enhance it. To do so, different parameters were varied, including the diode's junction resistance, junction capacitor, and series resistance as well as its key internal parameters like its saturation current and voltage breakdown.

To perform this study, we first implemented a code in Matlab and validated it with simulation data from a commercial circuit simulator (i.e., ADS).

Then, we swept the above listed parameters to give us suitable trade-offs to efficiently design an enhanced rectifier, which we will present in the next chapter.

The following remarks can be made:

- The most important diode parameters that allow high PCE while operating over wide range of input powers are high voltage breakdown, $V_{br,}$ and high saturation current, I_s.

- The diode parameters that maximize the PCE are low series resistance, $R_{s,}$ and junction resistance, R_j.

Therefore, trade-offs should be made between the above parameters to optimize the design of a rectifier that can operate over a wide range of input powers while maintaining relatively high PCE.

Accordingly, different approaches to overcome the inability of conventional rectifiers to operate over an extensive range of input powers and improve their overall power conversion efficiency have been proposed and will be implemented in the following chapter.

Chapter 4. Harvester Enhancement: Approaches and Results

4.1. Introduction

After investigating the parameters that affect conventional diode-based rectifier operation, we propose in this chapter different approaches to overcome the inability of conventional rectifiers to operate over an extensive range of input power levels and improve their overall power conversion efficiency.

Therefore, an adaptive reconfigurable rectifier was designed and implemented [22][27] to operate within the ISM frequency band at 915 MHz. Starting from a concept described in [24] for devices operating at 100 MHz, the proposed adaptive reconfigurable rectifier uses a Field Effect Transistor (FET) as switch to combine between the low and high input power regions in order to obtain high efficiency over a wide range of RF input power levels by operating at both low threshold voltage and high voltage breakdown point.

To enhance efficiency and prevent the circuit to reach its voltage breakdown in the adaptive/reconfigurable rectifier, an active load modulation block [25] was then added [26] and a harmonic trapping technique utilized to enhance the PCE at high input powers. Additionally, with the aim of further increasing the output DC voltage, a dual-band adaptive rectifier was designed to harvest and collect power from different energy sources at both 915 MHz and 2.45 GHz.

Finally, to evaluate the harvester system (rectenna), a patch antenna, making use of metasurfaces and artificial magnetic conductor (AMC) materials as ground plane and printed inks for WPT harvesters, was introduced.

4.2. The Adaptive/Reconfigurable Rectifier

Since a single diode cannot cover the entire desired power range for WPT applications (-20 dBm to +30 dBm), different diodes with both low threshold voltage and

high breakdown voltage should be combined. The proposed adaptive reconfigurable rectifier is depicted in Figure 4.1. It uses three shunt Schottky diodes and one n-channel depletion-mode hetero-junction FET transistor, which aims the rectifier to work as a switch among both low and high input power levels for each diode proficiencies. Note that the transistor is connected in parallel with the shunt diodes D2 and D3.

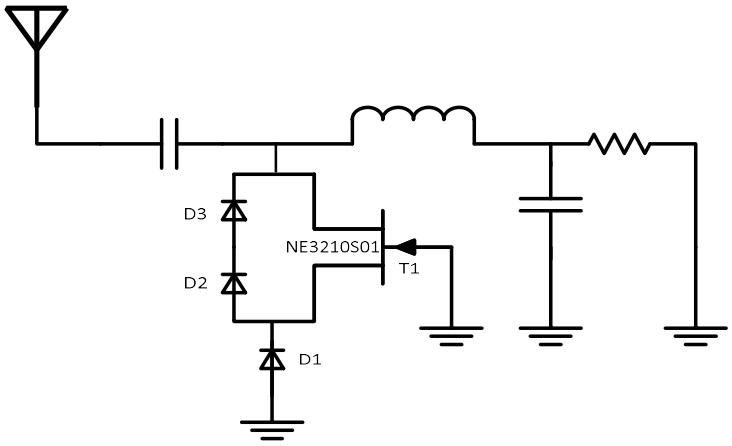

Figure 4.1 The proposed adaptive rectifier circuit.

When the input power level is low, the voltage V_{gs} across the transistor is close to zero, thus turning the transistor ON and allowing the current to pass through the channel, hence short-circuiting D2 and D3 (high power diodes). In this case, the current path goes through T1 and D1 (low power diode). As the input power rises, the transistor is turning OFF and D2 and D3 are working along with D1. Therefore, by selecting the proper diodes to operate at low and high input power levels, low threshold voltage and high breakdown voltage can be achieved simultaneously [22][19]. At low input power,

$$V_{Gs} > V_{th,T},\ \begin{cases} T_1\ is\ ON\ ,\ V_{D1} < V_{th,D1} \\ D_2, D_3 \text{ are shorted} \end{cases} \text{, the current is OFF} \tag{4.1}$$

$$V_{Gs} > V_{th,T},\ \begin{cases} T_1\ is\ ON\ ,\ V_{D1} > V_{th,D1} \\ D_2, D_3 \text{ are OFF} \end{cases} \text{, the current is ON} \tag{4.2}$$

$$V_{out} = Vin - (V_{D1} + V_{DS,T})$$

As the power increases, the voltage increases and T_1 turns OFF

$$V_{out} = Vin - (V_{D1} + V_{D2} + V_{D3}) \tag{4.3}$$

The adaptive rectifier operation can be also explained by using the I-V diode characteristics and the PCE starting from Figure 4.2.

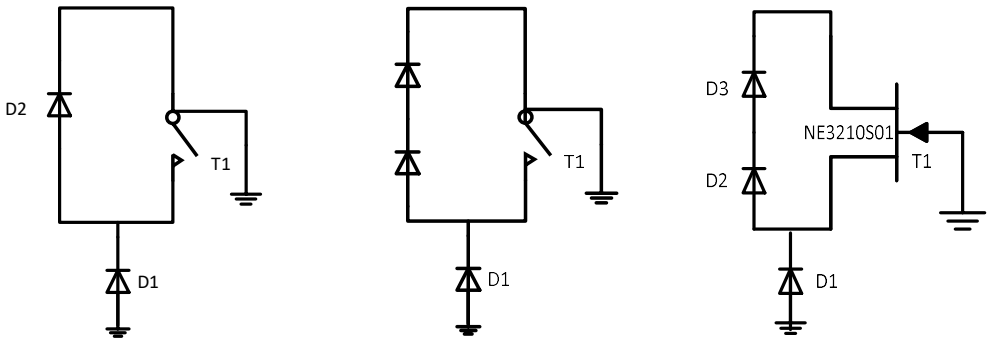

(a) Stack two Diodes (b) Stack three Diodes (c) Adaptive System

Figure 4.2 Outlines of an adaptive rectifier circuit.

In fact, as shown in Figure 4.3 and Figure 4.4, stacking two or three diodes will provide the ability to increase the breakdown voltage compared to a single diode; however, as observed, the threshold voltage will increase as well. Therefore, by applying the adaptive system as in Figure 4.2 -c, low threshold, and high breakdown can be attained.

4.3. Active Load Modulation

To further enhance the ability of the adaptive/reconfigurable rectifier to work over an extensive range of input power levels, an active load modulation has been implemented to actively modulate and vary the output load (Figure 4.5). This is because the output DC power is mainly dependent on the voltage breakdown and the output load as in (2.10).

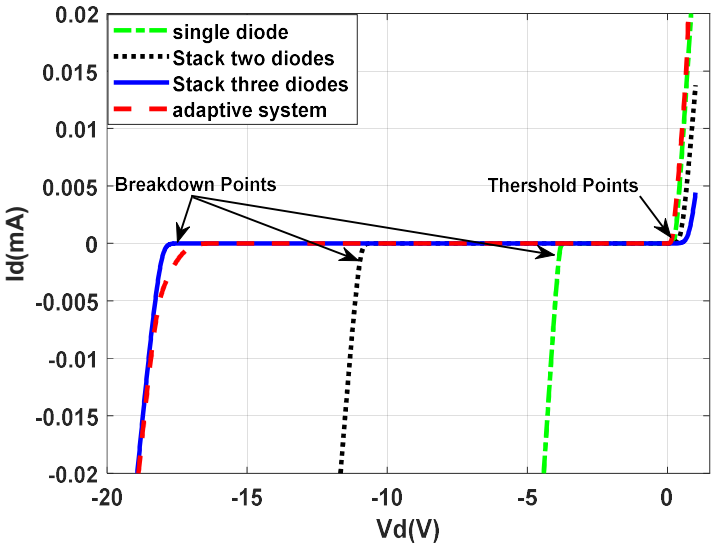

Figure 4.3 I-V curve of the adaptive rectifier technique compared to conventional diode rectifier.

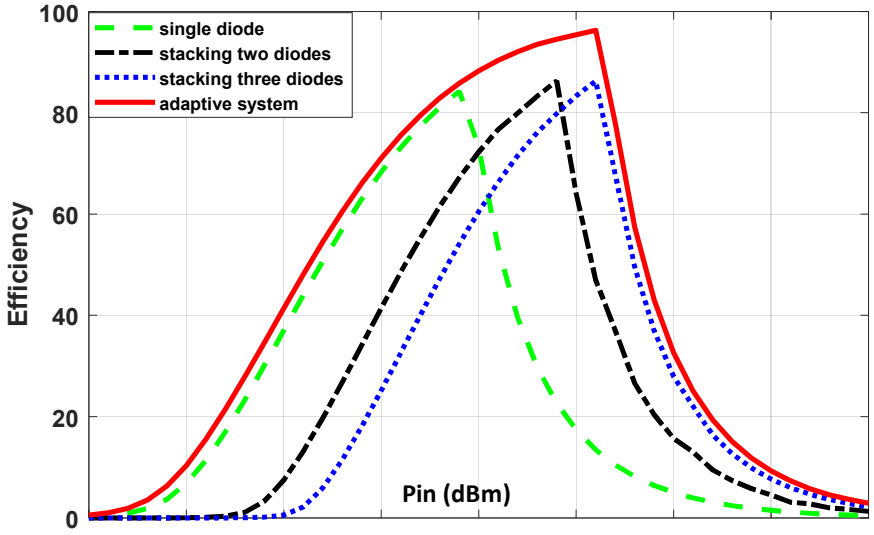

Figure 4.4 PCE of the adaptive rectifier technique compared to conventional diode rectifier.

As shown in Figure 4.6, the efficiency is sensitive to the load. It is indeed one of the crucial parameters that affects the overall power efficiency. Thus, the concept of active load modulation will enable the active component (e.g., transistor) to adjust the circuit load and improve the circuitry efficiency for a predefined input power range.

The design keys for the active load modulation are to achieve high voltage at low input power to maximize the efficiency and reduce the output voltage at high input power to prevent the rectifier's breakdown voltage to occur.

Therefore, an optimal output voltage can be extracted for a certain input power level by selecting the proper output load as in (4.4). At low input powers, large output load is desirable to produce high output voltage and increase the overall PCE. Once the input power increases, it is appropriate to minimize the output load to avoid the rectifier reaching its voltage breakdown, thus maintaining relatively high PCE over a wide range of input power levels [98].

$$V_{out} = \sqrt{P_t \cdot \eta \cdot R_L} \tag{4.4}$$

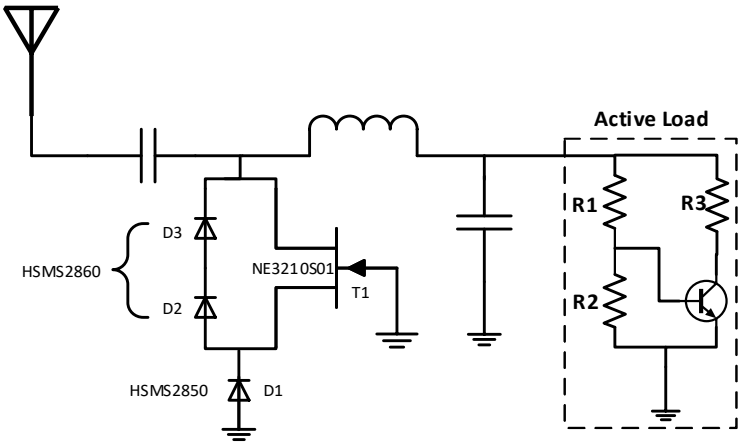

Figure 4.5 Adaptive rectifier circuit with active load configuration.

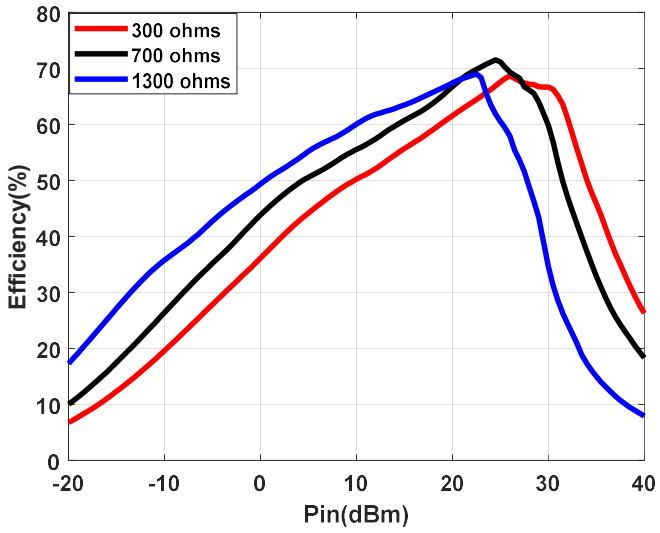

Figure 4.6 Adaptive rectifier efficiency vs power for different loads.

As shown in Figure 4.7-a, the proposed active load circuit contains three resistors (R_1, R_2, and R_3) and a switching transistor. The NPN epitaxial silicon transistor NE68133 [107] has been selected to adjust the load impedance value amongst low and high input powers. It performs the concept of active load as a switch between low and high impedances.

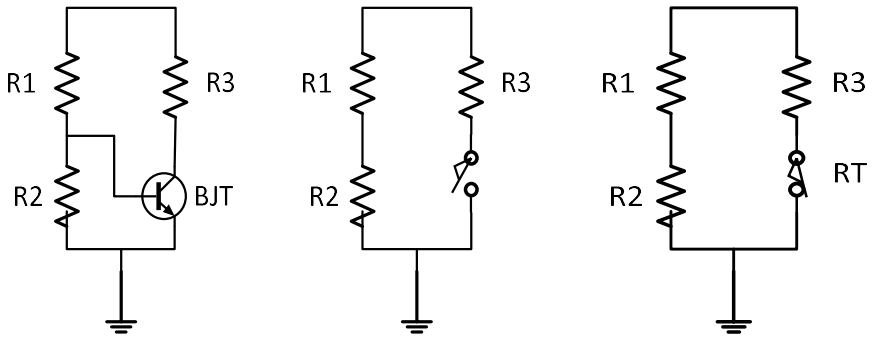

(a) active load circuit (b) OFF-state (c) ON-state

Figure 4.7 Simplified operation of the active load equivalent circuit configuration.

For low power levels, the output voltage is small and the transistor is in OFF-state. Consequently, the load impedance, as depicted in Figure 4.7-b, can be described as in (4.5).

$$R_{eq\ OFF\ state} = R_1 + R_2 \tag{4.5}$$

Once the input power rises, the transistor switches to its ON-state as shown in Figure 4.7-c. The load equivalent impedance changes as

$$R_{eq\ ON\ state} = \frac{(R_1 + R_2)(R_3 + R_T)}{R_1 + R_2 + R_3 + R_T} \tag{4.6}$$

Note that at high driving voltages, the transistor equivalent resistance (R_T) can be neglected compared to R_3 [25], leading to a simplified load equivalent impedance expression

$$R_{eq\ ON\ state} = \frac{R_1R_3 + R_2R_3}{R_1 + R_2 + R_3} \tag{4.7}$$

Therefore, by applying the active load modulation, a high and low load impedance can be achieved to produce high output voltage at low power and prevent the rectifier to reach its voltage breakdown at high input power, thus maintaining high PCE over a wide range of input power levels.

4.4. Trapping the Second Harmonic

Because of their nonlinear transfer function, active components, such as diodes and transistors, can generate harmonics that degrade the rectifier PCE [76]. As discussed in section 3.4.5, supressing harmonics can enhance the rectifier output DC voltage. Thus, a harmonic rejection block was introduced by adding an LC circuit trapping.

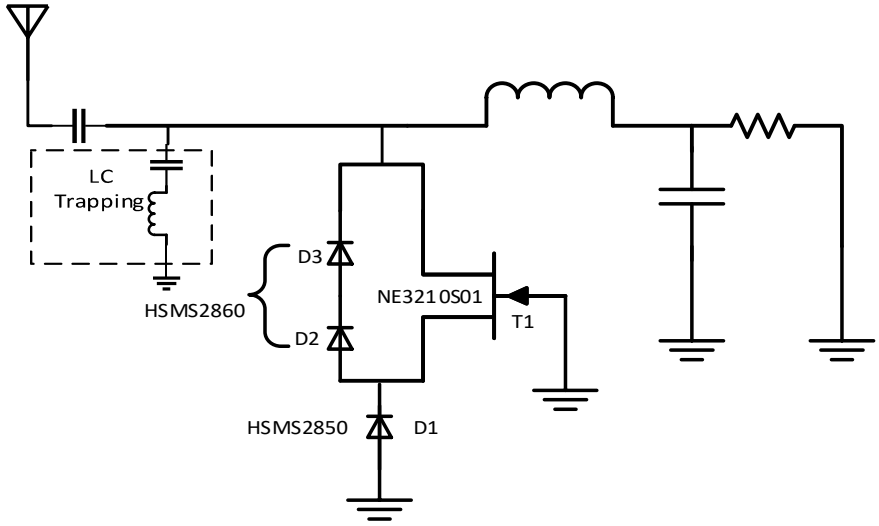

Figure 4.8 An adaptive rectifier circuit with a trapped second harmonic network.

4.5. Dual-band harvester

With the aim of further increasing the output DC voltage, a dual-band matching network was then designed (Figure 4.9) to collect more RF energy from RF sources operating at two different ISM bands, the aim being to attain a high-PCE in each band.

The dual-band network (C_1, C_2, C_3, L_1, and L_2) is based on an L-C impedance matching network to allow 50Ω to operate as an input impedance matching amongst the receiver antenna and the rectifier at both 915 MHz and 2.4 GHz. In fact, the resonant circuit (C_1, C_2, and L_1) is intended for 915 MHz while the circuit with C_3 and L_2 was designed to resonate at 2.4 GHz.

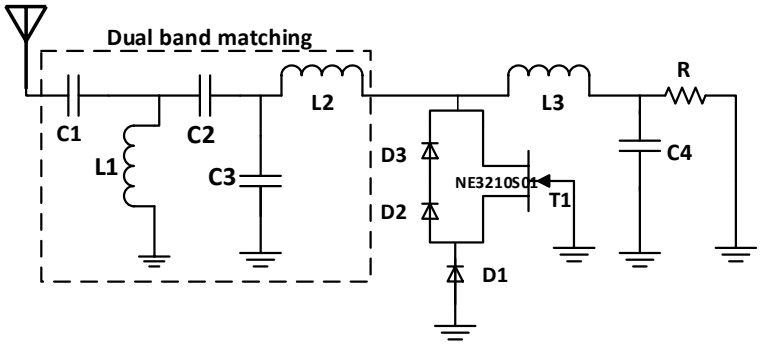

Figure 4.9 Configuration of a dual-band adaptive rectifier circuit.

4.6. Adaptive RF WPT Harvester Design Considerations

After completing the circuit configuration, the next step is to select the appropriate Schottky barrier diodes. As discussed in Chapter 3 (section 3.2), to simultaneously operate for both low threshold voltage and high voltage breakdown while minimizing the series resistance loss, the HSMS2850 and HSMS2860 diodes have been selected [12][13]. Also, to improve efficiency, an impedance matching circuit was included between the antenna and the rectifier (Figure 4.10). Figure 4.11 shows the optimum value of the load resistance, i.e., R_L = 1 kΩ, that maximizes efficiency while maintaining a wide input power range.

As for the input, a matching impedance network should be also designed to ensure the highest transfer of power from the source of impedance (Z_s) to the circuit of impedance (Z_{in}). In our case, the input impedance was found to be $55 + j360\ \Omega$.

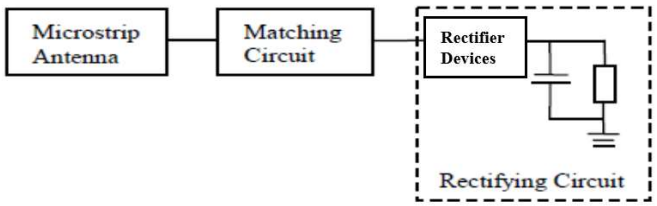

Figure 4.10 Bloc diagram of the WPT system

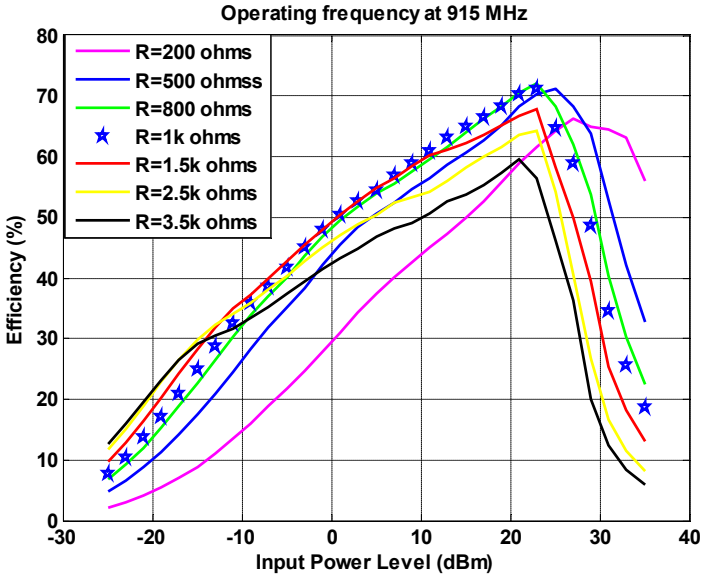

Figure 4.11 Optimum load vs input power level.

4.7. Experimental Validation

Next, the adaptive reconfigurable rectifier with active load modulation trapping was optimized at 915 MHz for high conversion efficiency over the desired range of RF input power. The circuit was implemented by using the Keysight's Advanced Design System (ADS 2017) commercial circuit simulator [108]. A layout co-simulation was performed on a 31 mil-thick Rogers 5880 substrate and transistors NE3210S1 and NE68133 from California Eastern Laboratories (CEL) used [107]. In addition, the diode SPICE models (for HSMS2850 and HSMS2860) were extracted from Avago Technologies datasheets [101]. The S-parameters of the passive components (capacitors, inductors, and resistors) were taken from the datasheets [109].

As for the tests, the equipment utilized include a network analyzer (E57071C), a signal generator (E4432C) and a digital multimeter (1233A) from Keysight (Figure 4.12). The design specifications are summarized in Table 4.1.

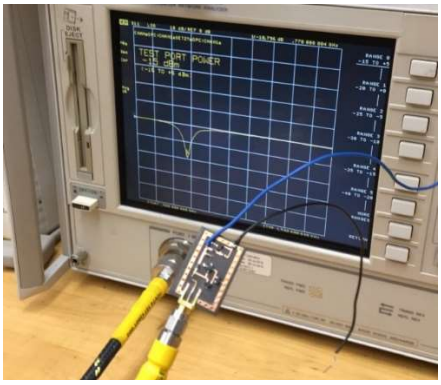

Figure 4.12 Rectifier test bench

Table 4.1 Specifications of the adaptive rectifier with active load modulation

Parameters	Description	
Frequency operation	915 MHz	
Substrate	Rogers 5880 substrate	
Substrate Thickness	31mil	
Diodes	HSMS2850, HSMS2860	
Capacitances C_1, C_{out}	0.4 pF, 100 pF	
Inductance, L_{out}	36 nH	
Rectifier Configuration	Adaptive	Active load
Transistors	NE3210S1	NE3210S1, NE68133
Load	1 kΩ	(0.3 to 1.3 kΩ)

4.7.1 Adaptive/ Reconfigurable rectifier

The adaptive/reconfigurable rectifier circuit (Figure 4.13) achieved a co-simulated maximum power conversion (PCE) of 66 % at +15 dBm input power, as well as a value of about 40% over a wide input dynamic range of RF power levels from -6 to +25 dBm (Figure 4.14).

The simulated results have been successfully compared to the measurements with an average relative error less than 1%. However, due to the test bench limitations, only measurements up to +20 dBm were performed as shown in Figure 4.14.

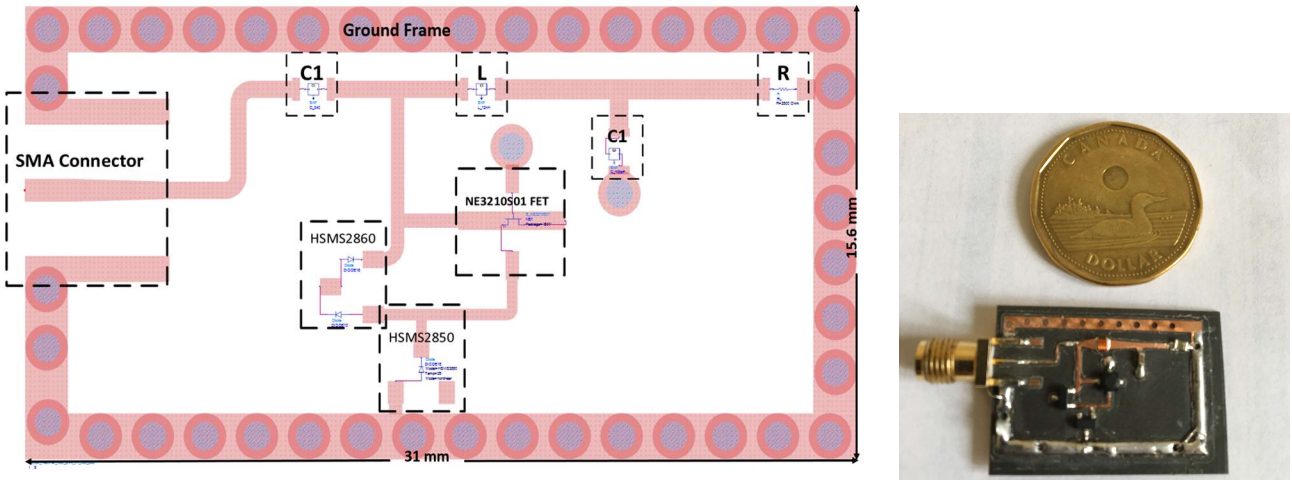

(a) (b)

Figure 4.13 Adaptive rectifier circuit: (a) Co-simulation layout view (without the active load modulation block). (b) Rectifier printed circuit board.

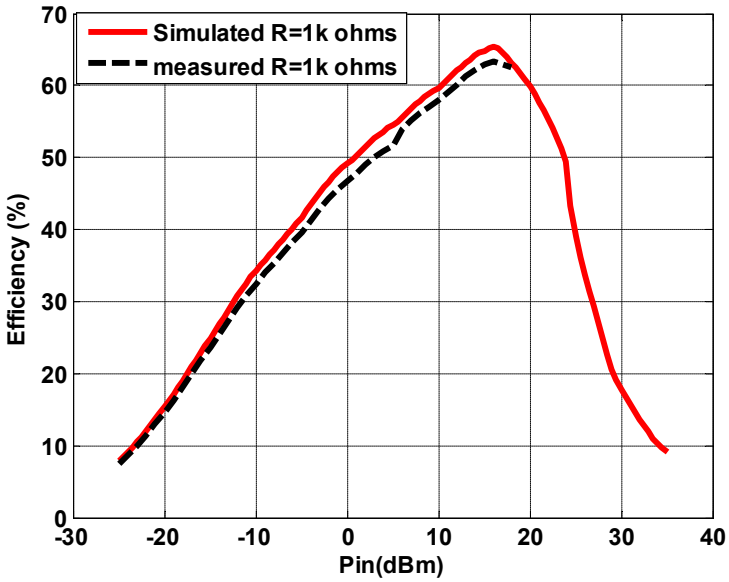

Figure 4.14 Simulated and measured Efficiency parameters at 915MHz for the designed adaptive rectifier with R_L = 1 kΩ

As seen in Figure 4.15, the return loss (S_{11}) of the adaptive rectifier is well matched, over -20 dB, and centered at the designed frequency of 915 MHz. The rectifier achieved 4 V output voltage with an input power of +15 dBm (Figure 4.16).

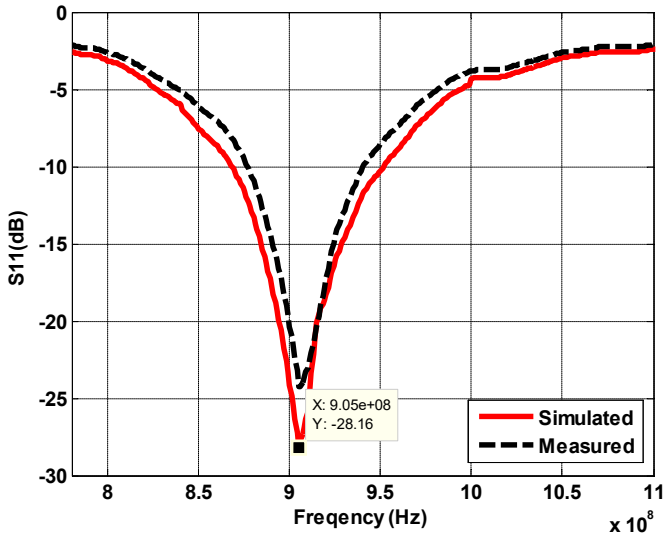

Figure 4.15 Simulated and measured S11(dB) parameters at 915MHz for the designed adaptive rectifier.

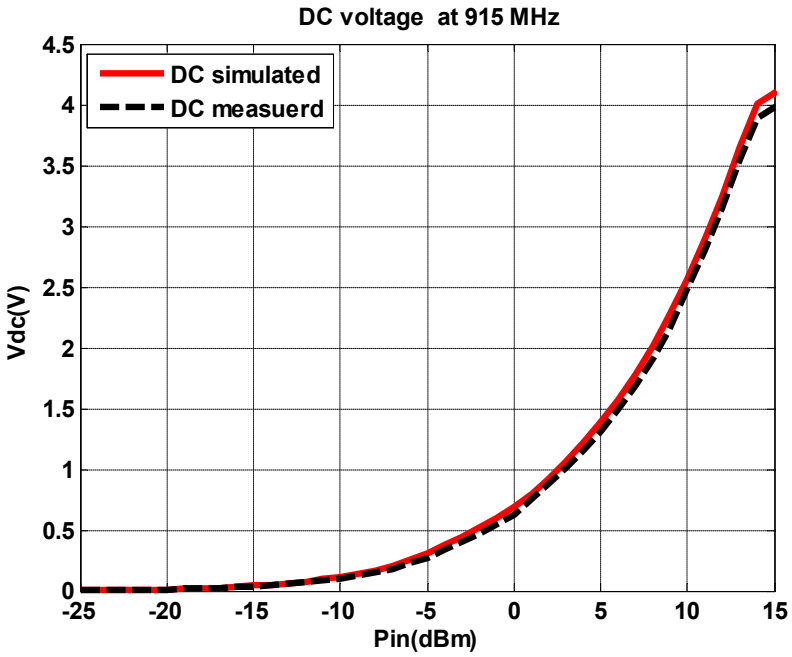

Figure 4.16 Simulated and measured output DC voltage at 915 MHz for the designed adaptive rectifier.

The load resistor, optimized for high efficiency, is of 1 kΩ. The inductor (L_{out}) and capacitor (C_{out}) have been placed after the rectifier circuit to act as low-pass filter for the rectified output. The series capacitor (C_1) has been utilized to match the rectifier circuit to the 50Ω WPT single-ended antenna via the SMA connector. The adaptive/reconfigurable power rectifier uses a layout area of 31×15.6 mm^2, making it suitable for low-cost and compact power WPT harvesters.

4.7.2 Active load modulation

Figure 4.17 shows the adaptive rectifier with the active load modulation layout.

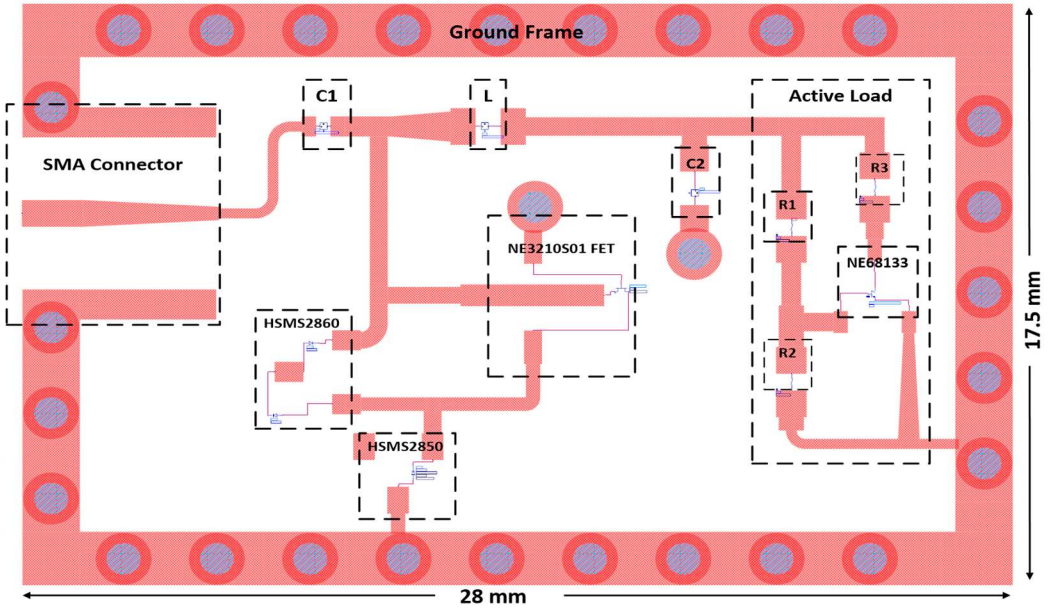

Figure 4.17 Adaptive rectifier circuit with active load configuration: Co-simulation layout view.

In addition, a comparison of the obtained efficiency while using active load modulation vs. fixed load values is presented in Figure 4.18.

As expected, by including the active load, the circuit exhibits a higher co-simulated efficiency, over 40 %, and within a wider dynamic range of input power levels (-7 dBm to +32 dBm) compared to fixed loads. The NPN epitaxial silicon transistor NE68133 allows adjusting the load impedances amongst low and high input powers. Hence, the active load resistors were adjusted to attain high efficiency over the desired wide range RF input power

levels (R_1 = 1 kΩ and $R_2 = R_3$ = 0.3 kΩ). Therefore, the load varies from 0.3 kΩ to 1.3 kΩ. The output DC voltage attained around 3.25 V for an input power of +15 dBm (Figure 4.19). The adaptive active load modulation achieved a return loss of -22 dB at the designed frequency of 915 MHz for an input power of +5 dBm, as depicted in Figure 4.20. The area size of the reconfigurable active load modulation rectifier is 30 × 17 mm^2.

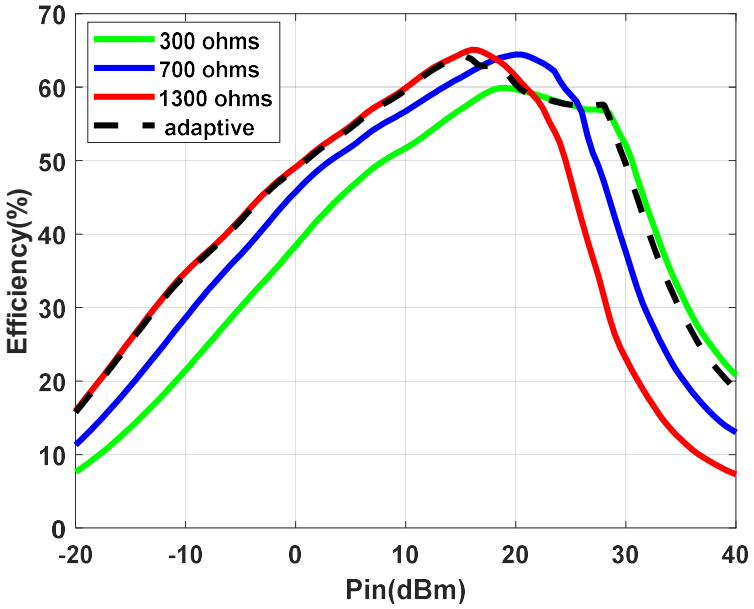

Figure 4.18 Adaptive rectifier circuit with active load configuration: Efficiency with active load and fixed passive load values

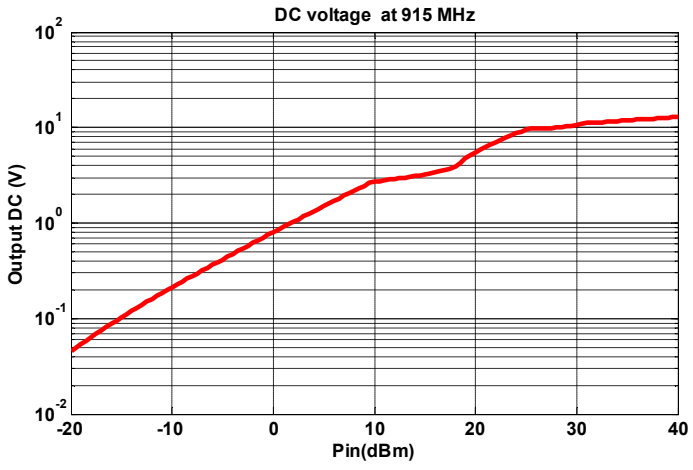

Figure 4.19 Adaptive rectifier circuit with active load configuration: output DC voltage.

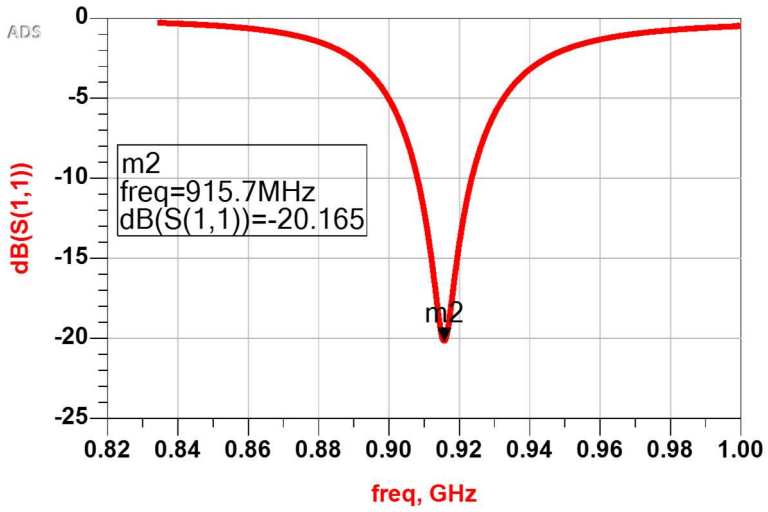

Figure 4.20 Adaptive rectifier circuit with active load configuration: S11(dB).

4.7.3 Trapping harmonics

In order to enhance the adaptive rectifier PCE and output DC voltage as well to decrease the nonlinearity effects of the embedded active devices, a harmonic rejection block was designed by adding an LC trapping circuit, as explained in section 3.4.5.

The achieved RF-DC efficiency (PCE) of the adaptive reconfigurable rectifier is presented in Figure 4.21 with a peak PCE of 72% measured at +9 dBm of input power. In addition, a rectifier's efficiency better than 40% was achieved over a wide dynamic range of RF input power levels ranging from -9 dBm to +28 dBm. As can be seen from Figure 4.21, supressing harmonics will indeed enhance the rectifier overall efficiency.

4.7.4 Dual band adaptive rectifier

With the aim of further optimizing the DC output, a dual-band circuit was designed as shown in Figure 4.9. The dual-band network (C_1=0.4 pF, C_2= 20 pF, C_3=0.6 pF, L_1= 25 nH and L_2=13 nH) was optimized to operate in the ISM bands of 915 MHz and 2.4 GHz. It achieved a maximum efficiency (PCE) of 72 % at 915 MHz and 67% at 2.4 GHz, as shown in Figure 4.22-a. In addition, the load resistor was optimized to achieve an efficiency above 40 % at R = 1 kΩ over an extensive-ranging of input power from -11 dBm to +25 dBm and -4 dBm to +21 dBm at 915 MHz and 2.4 GHz, respectively (Figure 4.22-a).

Furthermore, the power conversion efficiency vs. the operation frequency at an input power of -5 dBm is shown in Figure 4.22-b.

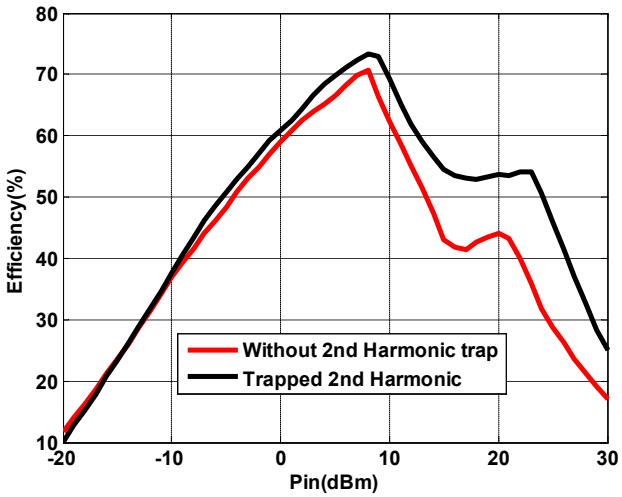

Figure 4.21 Simulated efficiency of the adaptive rectifier versus input power with/without considering the 2nd harmonic rejection.

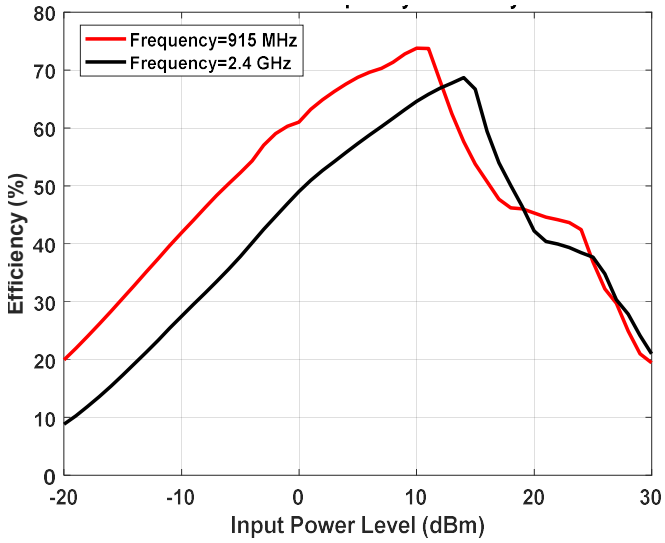

(a)

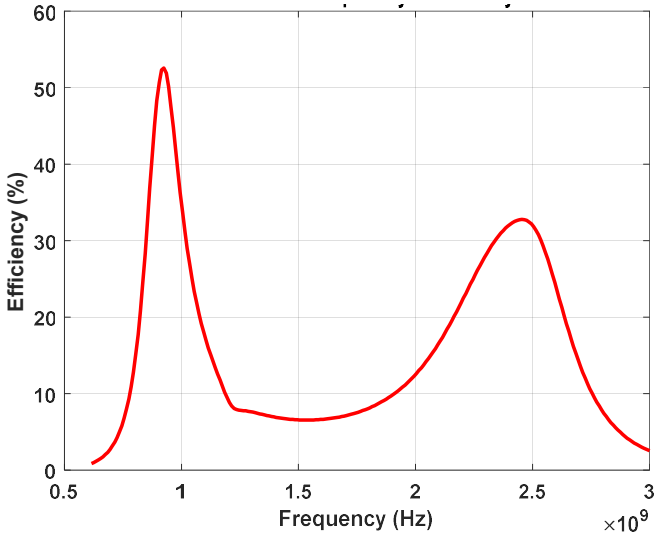

(b)

Figure 4.22 (a) Adaptive rectifier efficiency at 915 MHz and 2.4 GHz. (b) RF-DC conversion efficiency over frequency for R=1 kΩ and Pin= -5 dBm.

The dual-band rectifier accomplished over -15 dB return loss (S_{11}) at both 915 MHz and 2.4 GHz (Figure 4.23-a). It is capable of rectifying 4 V for 15 dBm input power at 915 MHz and 4.5 V for 15 dBm at 2.4 GHz for a load of 1 kΩ (Figure 4.23-b). The output capacitor (C_{out}) and inductor (L_{out}) were retained to operate as output low-pass filter.

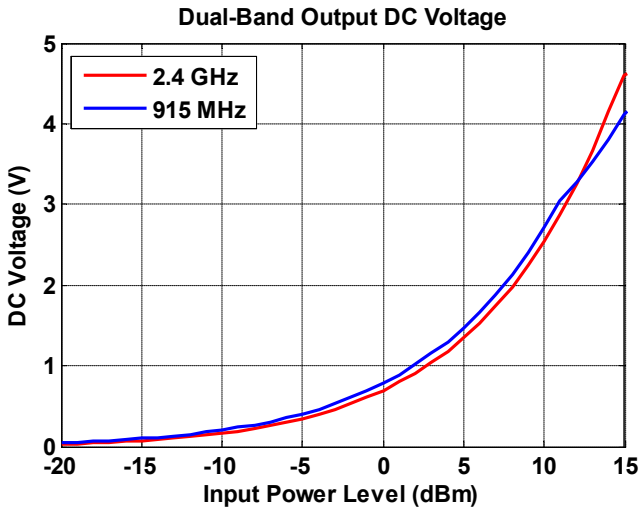

(a)

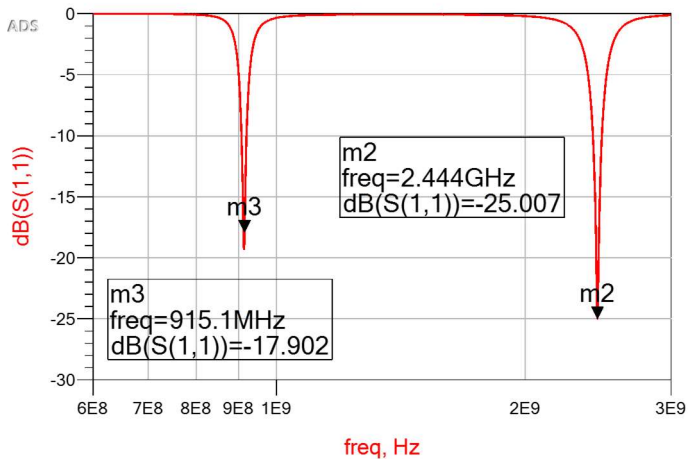

(b)

Figure 4.23 (a) DC output voltage vs. RF input power at 915 MHz and 2.4 GHz. (b) Return loss (S_{11}) for the dual-band rectifier.

To conclude, as reported in Table 4.2, the overall measured rectifier performance was demonstrated through successful comparison with existing published designs. The proposed design demonstrated an extensive range of input power levels to address the issue of conventional rectifiers by simultaneously utilizing the adaptive reconfigurable configuration along with the active load modulation approach.

4.8. Rectenna analysis

After introducing the rectifier, we explore in this section the antenna block to be connected to the rectifier to make it a rectenna for WPT applications.

4.8.1 Antenna

Indeed, the antenna is an important element to transfer and harvest power through electromagnetic signals. It is responsible for capturing the incident RF signal from either a dedicating RF energy for a specific operating frequency or an ambient RF energy from multiple operating frequencies.

Table 4.2 Rectifier Performance Comparison

Ref.	Technology	Frequency (GHz)	Maximum efficiency (%)	Pin (dBm) range for PCE > 40% (Simulated: S, Measured: M)
[1]	Resistance compression networks	0.915 / 2.45	60	-15 to 5 (M)
[9]	Schottky diode	2.4/5.8	65	-6 to 13 (M)
[2]	Proposed multi-stage voltage doubler	0.915	70	-12 to 16 (M)
[21]	Extended power range	0.915 / 1.8	62	-10 to 18 (M)
[98]	Automatic Load Control	2.45	70	3 to 18 (S)
[110]	Shunt diode	2.45	7	-20 to 10 (M)
[111]	Full-wave Greinacher rectifier	2.45	75	-16 to 7 (M)
[112]	Full-wave Greinacher rectifier	1.8-2.5	70	-20 to 5 (M)
This work	**Adaptive shunt diode**	**0.915**	**70**	**-6 to 26 (M)**
	Adaptive shunt diode with active	**0.915**	**66**	**-6 to 32 (S)**
	Dual Band adaptive rectifier	**0.915 / 2.45**	**70 / 62**	**-**

In WPT, the antenna performance depends on the RF energy source from where the receiver antenna captures the signal. Thus, in the ambient RF source, the antenna should be designed with some unknown specifications such as the transmitter power, antenna radiation/polarization, and operation frequency. Consequently, the rectenna antenna should (i) operate over a broadband/multiband frequency range to harvest and scavenge most of the RF surrounding power, (ii) have a polarization suitable for worst-case circumstances, and (iii) exhibit a low Polarization Loss Factor (PLF) [113]. While in a dedicated RF source, the receiver antenna has advantages of knowing the RF source parameters such as the operation frequency and polarization of the incident power. Therefore, the antenna should be designed to be coherent with the transmitter specifications to enhance and maximize the overall efficiency.

In WPT, various parameters need to be considered while designing the antenna such as frequency, polarization, gain, and return loss. In addition, the antenna feeding mechanism (such as probe, aperture, or planar line) plays also a role in improving the overall WPT system. Moreover, the antenna size and substrate materials should be taken into account for possible integration into a chip circuit [64][114].

Different antennas have been proposed for WPT applications, such as linear/circular polarized antennas [115][116][117], multi-band frequency antennas [118][119], harmonic suppression antennas [120][121], electrically small antennas [122][123], and fractal antennas [119] . Because rectennas can receive RF signals operating at different frequencies, multiband or wideband devices can enhance the output voltage [113]. Antenna arrays [121] can be another alternative to increase the rectenna's performance.

In WPT applications, the most important aspect in the receiving stage is the ability of the receiving antenna to maximally collect the incident power per footprint regardless of the wave polarization. Consequently, compared to conventional antennas, metamaterial and metasurface antennas can increase the power harvesting energy efficiency in WPT systems [126]. Therefore, in this work, a metasurface has been utilized and implemented as the ground plane of a patch antenna.

4.8.2 Metamaterials antenna

Metamaterials are synthetic electromagnetic devices engineered to handle the permittivity and permeability of the material through an electromagnetic field [127]. Metasurfaces are considered as the 2D surface of 3D metamaterials. Metamaterials and metasurfaces are backward-wave (BW), negative-index materials (NIM) media. These materials have specific properties, i.e., permeability, permittivity and refractive index with negative values [127].

The elements in metasurface are electrically small, scattered and distributed as a periodic structure. To get the set of desired properties of a given metasurface, its elements should work at their resonant frequency. The resonance frequency of an individual unit cell of a metamaterial or metasurface is primarily indicative of its capability to store energy. The most significant characteristics of a metasurface structure are the thickness and periodicity, and it should be small in comparison to the operating wavelength.

Metasurfaces can be used in various applications, including absorbers, biomedical devices, harvesters, impedance matching surfaces, and detectors. In addition, compared to 3D metamaterial structures, they allow smaller area. Also, metasurfaces provide less-lossy configurations [126].

The ever-higher demand for lightweight, low profile, compact, and low-cost antennas let researchers to consider metasurface antennas. However, even if electrically small antennas have been already proposed, they face certain limitations including gain, bandwidth, and efficiency [127]. Therefore, by introducing a patch antenna making use of metasurfaces and artificial magnetic conductor (AMC) materials as ground plane and printed inks for WPT harvesters is crucial to achieve high performance, low-cost, and flexible substrate.

4.8.3 Metasurfaces as ground plane: design and result

The unit cell of the metasurface structure is shown in Figure 4.24. Its dimensions should be small compared to the operating wavelength in a homogenous medium and should resonate at the desired frequency of 915 MHz, as illustrated in Figure 4.25. The proposed device contains 30 unit cells (5×6 array) as shown in Figure 4.26-a.

The printed patch was designed as an edge-feed rectangular patch antenna and implemented on a 62 mil FR4 substrate, with a silver ink thickness of 25 μm, a ground plane thickness of 35 μm, a silver conductivity of 3.3×10^6 S/m and a permittivity of 4.6 F/m. The patch (76 mm length x 92 mm width) is fed through of a transmission line at 85 mm (Figure 4.26-b). As illustrated in Figure 4.27, two patch antennas with a solid ground plane and a slotted ground plane were also designed to compare their performance with the metasurface patch antenna. They occupy an area of 110 ×170 mm^2 and 120 × 180 mm^2, respectively.

As for the patch antenna with a metasurface ground plane, it exhibits 3 dBi gain, 5.3 dBi directivity and 56% radiation efficiency (Figure 4.28) with a return loss higher than 25 dB at 915 MHz. The solid and slotted ground plane patch antennas achieved a gain of 1.9 dBi and 1.8 dBi, respectively (Figure 4.29), thus showing that the metasurface antenna exhibits a significant gain improvement of 36%.

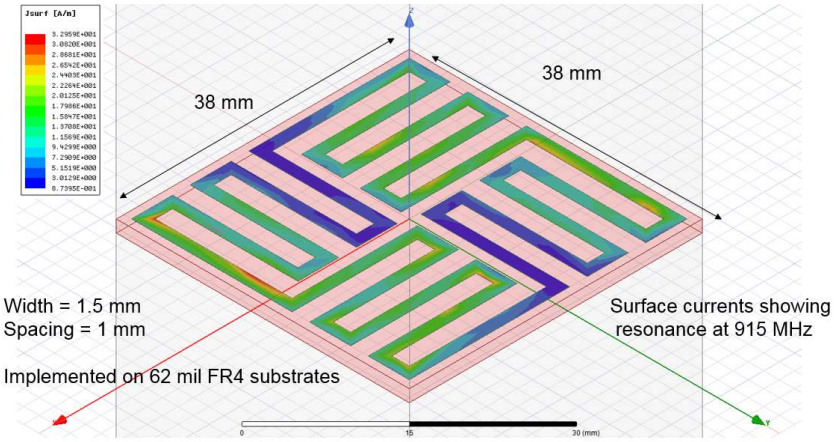

Figure 4.24 The unit cell of a metasurface antenna ground plane.

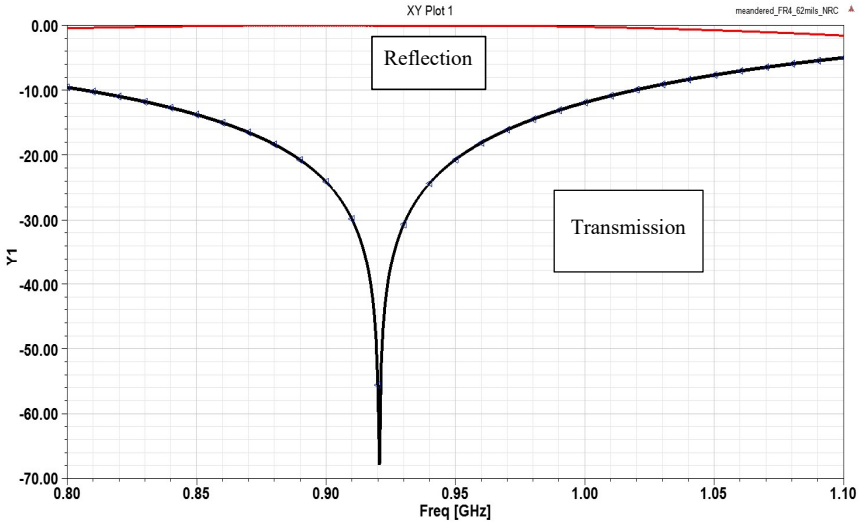

Figure 4.25 The unit cell resonant frequency at 915 MHz.

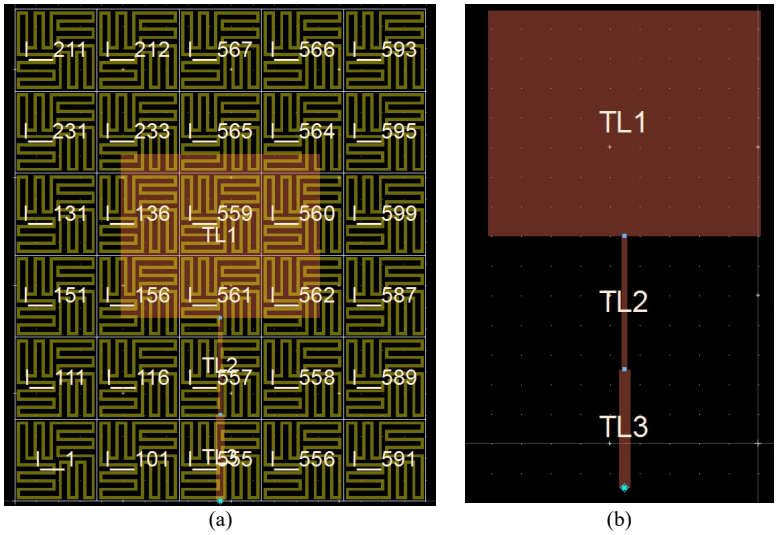

Figure 4.26 Patch antenna and metasurface as a ground plane.

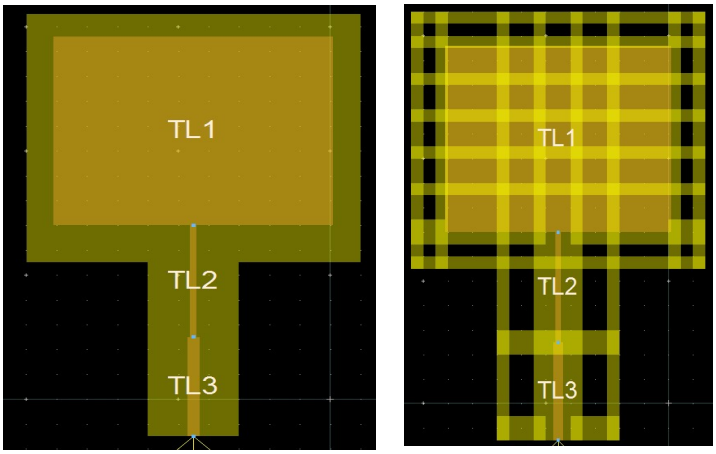

(a) (b)

Figure 4.27 Patch antenna (a) solid; (b) Slotted ground plane.

4.9. System Evaluation

With the aim of further evaluating the harvester (rectenna) performance, a 3-pin coupler was utilized to combine the antenna with the rectifier. As stated in [128] "it is utilized as monotonic frequency depended power to excite the circuit" (Figure 4.30). As expected, the harvester achieved an efficiency greater than 40% over a range of input powers (Figure 4.31) from -5 to +23 dBm. In addition, as shown in Figure 4.32, the achieved return loss is over -20 dB at the center frequency.

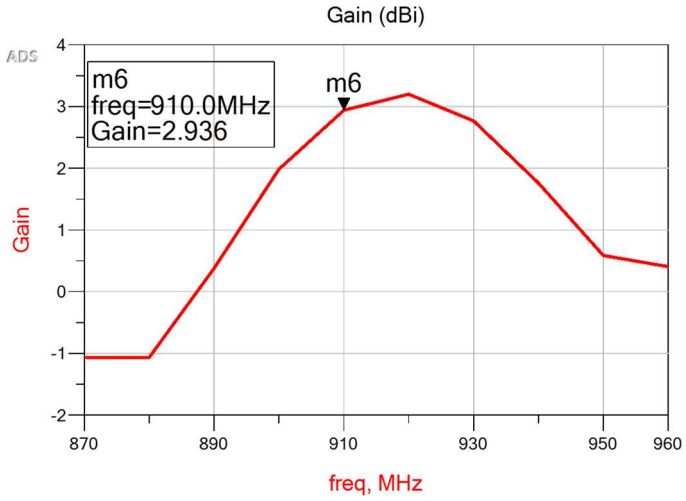

(a)

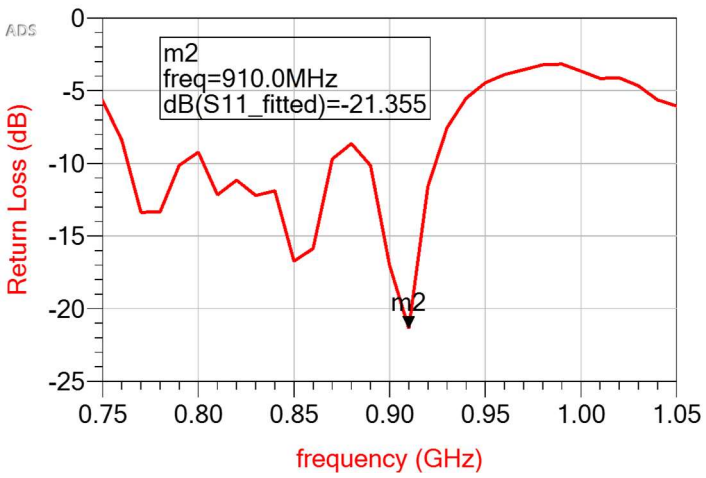

(b)

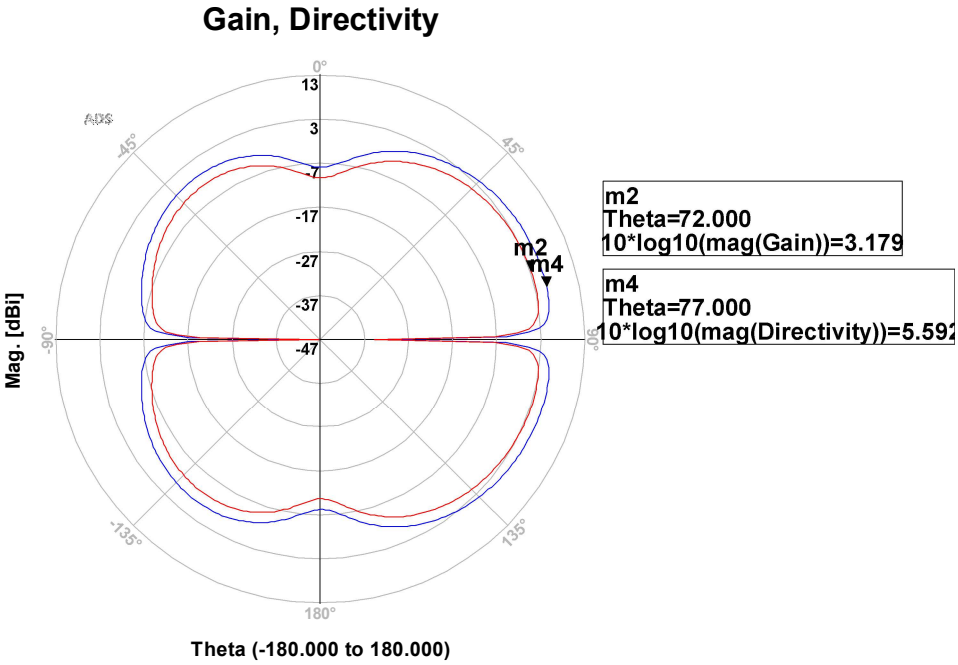

(c)

Figure 4.28 Patch antenna with metasurface ground plane (a) gain vs. frequency. (b) return loss (dB). (c) directivity and gain.

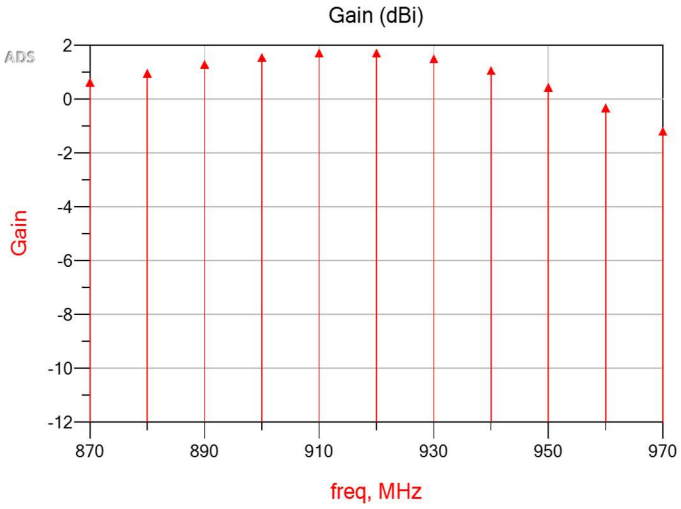

(a)

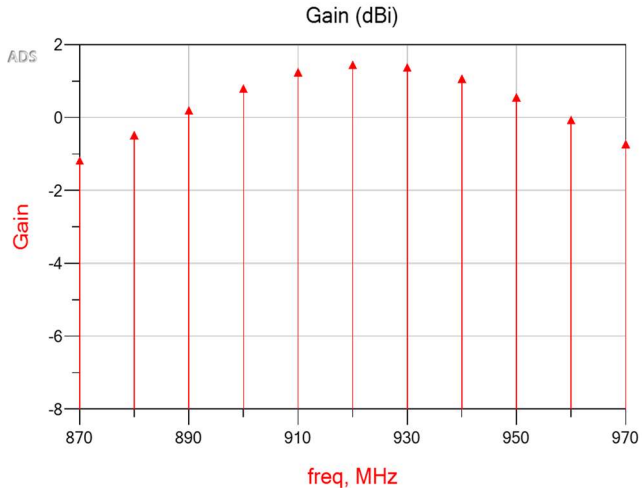

(b)

Figure 4.29 Patch antenna gain vs. frequency: (a) Solid ground plane. (b) Slotted ground plane.

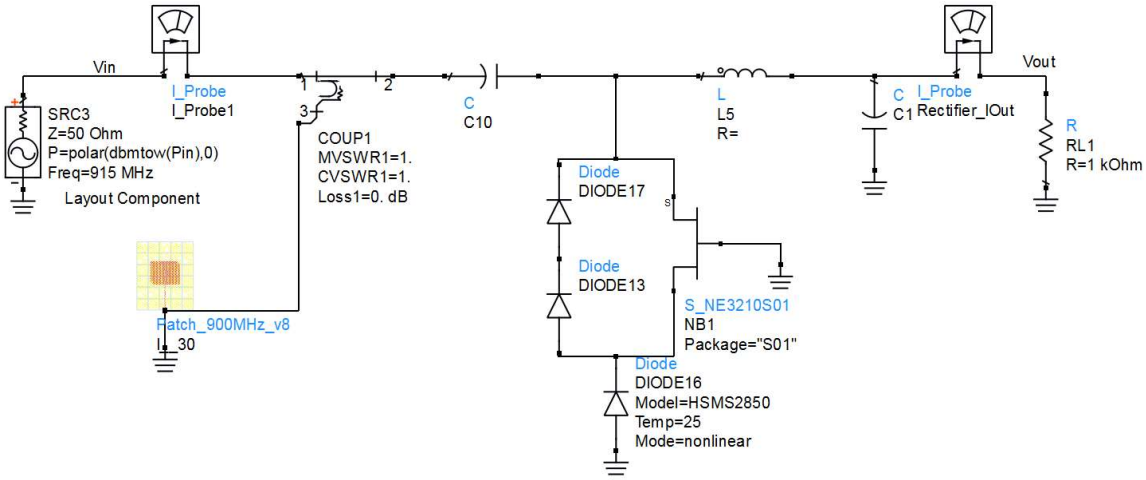

Figure 4.30 Schematic of the harvester (rectenna) circuit.

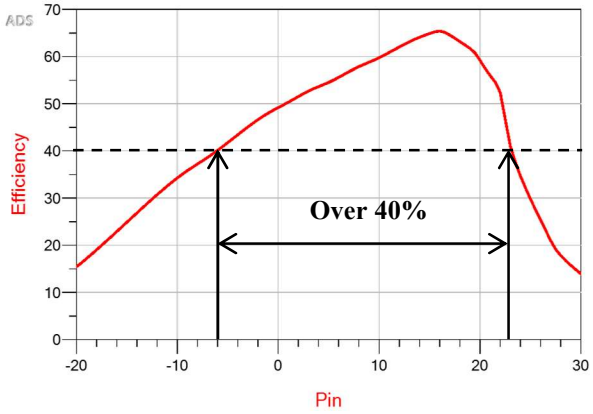

Figure 4.31 Harvester (rectenna) efficiency at output load of 1kΩ.

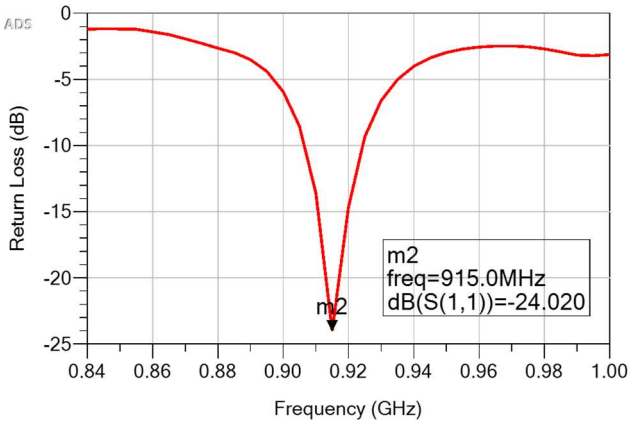

Figure 4.32 Reflection coefficient (S_{11}) of the adaptive energy harvester.

In the calculations, we used the Federal Communication Commission (FCC) regulations with a maximum transmitting power of 30 dBm and an Effective Isotropic Radiated Power (EIRP) of 36 dBm at ISM band. Therefore, the applied transmitted power was set as +23 dBm and the transmitted and received antennas gain were set as 6 dBi and 2 dBi, respectively. Table 4.3 summarizes the received power link budget and the tread-off amongst distance and efficiency of the proposed adaptive rectifier circuits. Note that the system using the concept of adaptive rectifier reaches an efficiency greater than 40% for distances up to 2 meters and 49% of efficiency at 1 meter.

Table 4.3 RF system power link budget

Specifications	**Value**					
Frequency operation	915 MHz					
Received antenna gain	2 dBi					
Transmitted antenna gain	6 dBi					
Transmitted power (dBm)	+23 dBm					
Distance (m)	1	2	3	4	5	6
Received Power (dBm)	0	-6.72	-10.3	-12.7	-14.7	-16.3
Efficiency (%)	49	42	33	28	25	20

4.10. Conclusion

In this chapter, different approaches to overcome the inability of conventional rectifiers to operate over an extensive range of input power levels and improve their overall power conversion efficiency have been proposed, including the adaptive/reconfigurable rectifier and the active load modulation operating in the ISM band at 915 MHz. Then, to further enhance the PCE, trapping harmonic network was implemented. In addition, a dual band adaptive rectifier operating in the ISM bands of 915 MHz and 2.4 GHz has been designed with the aim of increase the output DC voltage while considering more potential RF energy sources.

Furthermore, the proposed rectifier circuit performance was successfully compared to existing designs found in the literature.

Finally, with the intention of evaluating the harvester system as rectenna, a patch antenna making use of the metasurface as ground plane was designed and combined with the adaptive rectifier.

The following remarks can summarize the work achieved in this chapter:

- An adaptive rectifier was designed to operate over a wide range of input powers while maintaining relatively high PCE.
- To further increase the adaptive rectifier performance, an active load modulation block was designed to prevent the circuit to reach its voltage breakdown and expand the input power range.
- A harmonic trap block was added and a dual-band configuration proposed to increase the output DC and enhance the overall PCE.
- These approaches have been implemented and their results demonstrated through successful comparison with existing published designs.
- An efficient low-cost metasurface-based printed patch antenna was designed to evaluate the system as a rectenna (rectifying antenna).

Chapter 5. Conclusions and Future Works

5.1. Summary

In this thesis, a WPT system was introduced and among different approaches of wirelessly transporting power, the RF electromagnetic (EM) option was retained due to its advantages of transferring power over long distances.

WPT through RF EM sources is usually performed by using a rectenna which contains an antenna, a matching network, a rectifier and an output load. The present work focused on improving the PCE of the rectifier. As stated, conventional diode-based rectifier topologies have noticeable limitations, such as the inability to achieve high efficiency over a wide range of input powers due to constraints in diode properties such as the inability for a diode to exhibit both low threshold and high breakdown voltages, thus leading to low RF-DC efficiency.

To identify the diode parameters that can affect the rectifier PCE, a detailed analysis was performed with the aim to operate the circuit over a wide range of input powers while maintaining a high PCE.

From that, different approaches were proposed and implemented in the ISM band at 915 MHz, including the adaptive/reconfigurable rectifier and the active load modulation. Then, to further improve the overall efficiency and increase the DC output, a dual-band adaptive rectifier operating at both 915 MHz and 2.4 GHz was designed.

A successful comparison of the performance of the proposed circuits with those found in the literature demonstrated the above designs.

The fabricated adaptive/reconfigurable rectifier exhibits 40% of PCE over a wide dynamic input range of incident RF power levels from -6 to +25 dBm with a maximum PCE of 66% for an input power of +15 dBm. Note that the simulated results were successfully compared to the measurements with an average relative error of 1%.

By adding the active load modulation, the circuit performance was improved by 15%. Furthermore, the harmonic trapping technique helped maximizing the PCE by 10% at high input powers.

Finally, to evaluate the harvester system as rectenna, a printed patch antenna making use of metasurface as ground plane, was designed, implemented, and then connected to the adaptive rectifier. The antenna achieved a gain of 3 dBi, a directivity of 5.3 dBi and a radiation efficiency of 57%.

5.2. Conclusions

With the aim of enhancing and overcoming the inability of conventional WPT rectifiers to operate over an extensive range of input powers while achieving relatively high PCE, the following points highlight the most important outcomes of this work:

- Dedicated RF energy source for energy transfer was retained and the ISM 915 MHz frequency selected due to the ease of accessibility, less attenuation, less sensitivity to circuit parasitics and ease of fabrication.
- The diode-based rectifier configuration has been selected as a result of its advantages of operating with low threshold voltage and high voltage breakdown.
- Based on the analysis performed, the diode parameters that allow to operate over wide range of input powers are a high voltage breakdown, $V_{br,}$ and a high saturation current, I_s. The diode parameters that maximize the PCE are low series resistance, $R_{s,}$ and low junction resistance, R_j. Therefore, trade-offs should be made between the above parameters to optimize the design of a rectifier that can operate over a wide range of input powers while maintaining relatively high PCE.
- Accordingly, an adaptive rectifier was designed and fabricated.
- To further increase the adaptive rectifier performance, an active load modulation block was designed to prevent the circuit to reach its voltage breakdown and expand the operation over range of input power.

- A harmonic trap block was then added and a dual-band configuration proposed to further increase the output DC and enhance the overall PCE.
- The designed configurations were demonstrated through successful comparison with existing published designs.
- An efficient low-cost metasurface-based printed patch antenna was designed to evaluate the system as a rectenna.

5.3. Future works

The work of this research can lead to further advances on both the system level and the component level. Therefore, the following recommendations can be considered to further expand the directions of research:

- Integrating the antenna to the adaptive rectifier with the aim to experimentally evaluate the harvester performance and thus, to (i) analyze the efficiency vs. the distance between the receiver and the transmitter, and (ii) to investigate the effect of the antenna alignment and polarization towards the PCE.
- Further investigating the impact of diode parameters on the rectifier PCE by considering different rectifier topologies. Thus proposing related configurations.
- Designing a multi-band system which can operate with over wide range of frequencies to collect and harvest more output DC power.
- With the aim of trapping harmonic, a differential configuration can be applied to enhance the PCE performance.
- Recycling and rectifying harmonics in order to further increase the output DC power.
- Integrating the harvester (antenna + rectifier) in a chip to operate at higher frequencies such as in the millimeter-wave band (e.g., in the objective of the future implementation of 5G wireless systems).

- Perform a full-wave analysis to investigate the effect of the metasurfaces as ground plane and the resulting radiation patterns.

References

[1] K. Niotaki, A. Georgiadis, A. Collado, and J. S. Vardakas, "Dual-band resistance compression networks for improved rectifier performance," *IEEE Trans. Microw. Theory Tech.*, vol. 62, no. 12, pp. 3512–3521, 2014.

[2] P. Nintanavongsa, U. Muncuk, D. R. Lewis, and and K. R. Chowdhury, "Design optimization and implementation for RF energy harvesting circuits," *IEEE J. Emerg. Sel. Top. Circuits Syst.*, vol. 2, no. 1, pp. 24–33, 2012.

[3] V. Marian, B. Allard, C. Vollaire, and J. Verdier, "Strategy for microwave energy harvesting from ambient field or a feeding source," *IEEE Trans. Power Electron.*, vol. 27, no. 11, pp. 4481–4491, 2012.

[4] A. M. Almohaimeed, M. C. E. Yagoub and R. E. Amaya, "A highly efficient power harvester with wide dynamic input power range for 900 MHz wireless power transfer applications," in *16th Mediterranean Microw. Symp. (MMS)*, Abu Dhabi, UAE, 2016, pp. 1–4.

[5] S. S. B. Hong, R. Ibrahim, M. H. M. Khir, H. Daud, and M. A. Zakariya, "Rectenna architecture based energy harvester for low power RFID application," in *4th Int.Conf. on Intelligent and Advanced Syst. (ICIAS)*, Kuala Lumpur, 2012, vol. 1, pp. 382–387.

[6] S. D. Deshmukh and S. N. Shilaskar, "wearable sensors and patient monitoring system : a review," in *Int.Conf. on Pervasive Computing (ICPC)*, Pune, 2015, pp. 1–3.

[7] G. Park, T. Rosing, M. D. Todd, C. R. Farrar, and W. Hodgkiss, "Energy harvesting for structural health monitoring sensor networks," *Los Alamos Natl. Lab.*, 2007.

[8] A. Costanzo and D. Masotti, "Wirelessly powering: an enabling technology for zero-power sensors, loT and D2D communication," in *IEEE MTT-S Int.Microw. Symp.*, Phoenix, AZ, 2015, pp. 1–4.

[9] D. Wang and R. Negra, "Design of a dual-band rectifier for wireless power

transmission," in *IEEE Wirel. Power Transfer (WPT),* Perugia, Italy, 2013, pp. 127–130.

[10] M. J. Nie, X. X. Yang, and G. N. Tan, "A broad band rectifier with wide input power range for electromagnetic energy harvesting," in *Proceedings of 3rd Asia-Pacific Conf. on Antennas and Propagation,* Harbin, China, 2014, pp. 1187–1189.

[11] . Han, O. Leitermann, D. A. Jackson, J. M. Rivas and D. J. Perreault, "Resistance compression networks for radio-frequency power conversion," *IEEE Trans. Power Electron.*, vol. 22, no. 1, pp. 41–53, 2007.

[12] K. K. A. and D. J. P. W. Inam, "High efficiency resonant DC / DC converter utilizing a resistance compression network," *IEEE Trans. Power Electron.*, vol. 29, no. 8, pp. 4126–4135, 2014.

[13] M. Del Prete, A. Costanzo, D. Masotti and A. Romani, "An alternative rectenna design approach for wirelessly powered energy autonomous systems," in *IEEE MTT-S Int.Microw. Symp. Digest (MTT)*, Seattle, WA, 2013, pp. 1–4.

[14] N. S. and T. M. Y. Huang, "A study on low power rectenna using DC-DC converter to track maximum power point," in *Asia-Pacific Microw. Conf. Proceedings (APMC)*, Seoul, South Korea, 2013, pp. 83–85.

[15] C. Liou, M. Lee, S. Huang and S. Mao, "High-power and high-efficiency RF rectifiers using series and parallel power-dividing networks and their applications to wirelessly powered devices," *IEEE Trans. Microw. Theory Tech.*, vol. 61, no. 1, pp. 616–624, 2013.

[16] H. C. Sun, Z. Zhong and Y. X. Guo, "Design of rectifier with extended operating input power range," *Electron. Lett.*, vol. 49, no. 18, pp. 1175–1176, 2013.

[17] X. Lu, P. Wang, D. Niyato, D. Kim, and Z. Han, "Wireless networks with RF energy harvesting: a contemporary survey," *IEEE Commun. Surv. Tutorials*, vol. 17, no. 2, pp. 1–33, 2014.

[18] O. McSpadden, Lu Fan and Kai Chang, "Design and experiments of a high-conversion-efficiency 5.8-GHz rectenna," *IEEE Trans. Microw. Theory Tech.*, vol. 46, no. 12, pp. 2053–2060, 1998.

[19] V. Marian, C. Vollaire, J. Verdier, and B. Allard, "Potentials of an adaptive rectenna circuit," *IEEE Antennas Wirel. Propag. Lett.*, vol. 10, pp. 1393–1396, 2011.

[20] M. K. Hosain and A. Z. Kouzani, "Design and analysis of efficient rectifiers for wireless power harvesting in DBS devices," in *8th IEEE Conf. on Industrial Electronics and Applications (ICIEA),* Melbourne, VIC, 2013, pp. 651–655.

[21] Z. Liu, Z. Zhong, and Y. Guo, "Enhanced dual-band ambient RF energy harvesting with ultra-wide power range," *IEEE Microw. Wirel. Components Lett.*, vol. 25, no. 9, pp. 630–632, 2015.

[22] A. M. Almohaimeed, M. C. E. Yagoub, and R. E. and Amaya, "A highly efficient power harvester with wide dynamic input power range for 900 MHz wireless power transfer applications," in *16th Mediterranean Microw. Symp. (MMS),* Abu Dhabi, UAE, 2016, pp. 1–4.

[23] A. M. Almohaimeed, R. E. Amaya, J. A. Lima, and M. C. E. Yagoub, "An adaptive power harvester with active load modulation for highly efficient short / long range RF," *Electron. J.*, vol. 7, no. RFID, WPT and Harvesting Energy, 2018.

[24] H. Sun, Z. Zhong, and Y. Guo, "An adaptive reconfigurable rectifier for wireless power transmission," *IEEE Microw. Wirel. Components Lett.*, vol. 23, no. 9, pp. 492–494, 2013.

[25] Y. Qin and D. H. Werner, "Rectenna with non-linear adaptive load capable of operating over a broad range of input power levels," in *IEEE Int.Symp. on Antennas and Propagation (APSURSI),* Fajardo,Puerto Rico, 2016, pp. 2155–2156.

[26] A. M. Almohaimeed, M. C. E. Yagoub, and R. E. and Amaya, "Efficient harvester with active load modulation and wide dynamic input power range for wireless power transfer applications," in *11th Annual IEEE Int.Systems Conf. (SysCon),* Montreal, QC, Canada, 2017, pp. 1–4.

[27] A. M. Almohaimeed, M. C. E. Yagoub, and R. E. and Amaya, "Efficient rectenna with wide dynamic input power range for 900 MHz wireless power transfer applications," in *IEEE Electrical Power and Energy Conf. (EPEC),* Ottawa, ON, Canada, 2016, pp. 1–4.

[28] A. M. Almohaimeed, M. C. E. Yagoub, J. A. Lima, and R. E. Amaya, "Dual-band harvester with wide range input power for WPT applications," in *IEEE PELS Workshop on Emerging Tech.: Wirel. Power (WoW)*, Montreal, Canada, 2018, no. 1, pp. 2–5.

[29] A. M. Almohaimeed, R. E. Amaya, and M. C. E. Yagoub, "UHF metasurface-based antenna for WPT RFID applications," in *IEEE Radio Frequency Identification (RFID 2018)*, Florida, USA, 2018, pp. 3–4.

[30] A. M. Almohaimeed, R. E. Amaya, and M. C. E. Yagoub, "Metasurface-based WPT rectenna with extensive input power range in the 900 mhz," in *31st Annual IEEE Canadian Conf. on Electrical and Computer Engineering (CCECE)*, Quebec, Canada, 2018, pp. 1–4.

[31] X. Wang, "*High Efficiency and High Sensitivity Wireless Power Transfer and Wireless Power Harvesting Systems*," PhD Thesis, Electrical Engineering, The University of Michigan, 2016.

[32] IndustryARC, "wireless-charging-market-report @ industryarc.com." [Online]. Available: http://industryarc.com/Report/7384/wireless-charging-market-report.html.

[33] Wireless Charging with Verizon Wireless @ www.verizonwireless.com." .

[34] RRC power solutions Inc, "@ www.rrc-wireless-power.com," 2017. .

[35] Plugless Charging Upgrade for Tesla Model S @ www.pluglesspower.com." .

[36] Witricity Cooperation @ witricity.com." .

[37] Energous Cooperation @ www.energous.com." .

[38] X. Lu, P. Wang, D. Niyato, D. I. Kim, and Z. Han, "Wireless networks with RF energy harvesting: a contemporary survey," *IEEE Commun. surveys & tutorials,* vol. 17, no. 2, pp. 757–789, 2014.

[39] X. Lu, P. Wang, D. Niyato, D. I. Kim, and and Z. Han, "Wirelss charger networking for mobile devices: fundamentals, standards, and applications," *IEEE Wirel. Commun.*, vol. 2, no. 5, pp. 559–565, 2015.

[40] "140804-25-most-interesting-medical-mems-sensors @ www.slideshare.net." [Online]. Available: https://www.slideshare.net/MikePinelisPhD/140804-25-most-interesting-medical-mems-sensors.

[41] L. Xie, Y. Shi, Y. T. Hou, and W. Lou, "Wireless power transfer and applications to sensor networks," *IEEE Wirel. Commun.*, vol. 20, no. 2, pp. 140–145, 2013.

[42] P. V. Nikitin, K. V. S. Rao, and S. Lazar, "An overview of near field UHF RFID," in *IEEE Int.Conf. on RFID*, Grapevine, TX, 2007, pp. 167–174.

[43] K. Fotopoulou and B. W. Flynn, "Optimum antenna coil structure for inductive powering of passive RFID tags," in *IEEE Int.Conf. on RFID*, Grapevine, TX, 2007, pp. 71–77.

[44] M. Budhia, G. A. Covic, and J. T. Boys, "Design and optimization of circular magnetic structures for lumped inductive power transfer systems," *IEEE Trans. Power Electron.*, vol. 26, no. 11, pp. 3096–3108, 2011.

[45] A. Karalis, J. D. Joannopoulos, and M. Soljacic, "Efficient wireless non-radiative mid-range energy transfer," *Ann. Physics, Elsevier*, vol. 323, no. 1, pp. 34–48, 2008.

[46] G. Abadal, J. Alda, and J. Agustí, "Electromagnetic radiation energy harvesting – the rectenna based approach," in *ICT Energy Concepts Towards Zero Power Information and Communication Tech.*, 2014, pp. 79–106.

[47] H. J. Visser and R. J. M. Vullers, "RF energy harvesting and transport for wireless sensor network applications: Principles and requirements," in the *Proc. of IEEE*, vol. 101, no. 6, pp. 1410–1423, 2013.

[48] W. C. Brown, "The history of power transmission radio waves," *IEEE Trans. Microw. Theory Tech.*, vol. 32, no. 9, pp. 1230–1242, 1984.

[49] N. Shinohara, "*History, Present and Future of WPT: Wireless Power Transfer via Radiowaves*, ISTE Ltd and John Wiley & Sons, Inc., 2014, pp. 1–20.

[50] B. Dessanti, N. Komerath, and S. Shah, "Design of a gigawatt space solar power satellite using optical concentrator system," in *IEEE Aerospace Conf.*, Big Sky, MT, 2013, pp. 1–9.

[51] S. Sasaki, K. Tanaka, and K. Maki, “Microwave power transmission technologies for solar power satellites,” *Proc. IEEE*, vol. 101, no. 6, pp. 1438–1447, 2013.

[52] A. Shameli, A. Safarian, A. Rofougaran, M. Rofougaran, and F. De Flaviis, “Power harvester design for passive UHF RFID tag using a voltage boosting technique,” *IEEE Trans. Microw. Theory Tech.*, vol. 55, no. 6, pp. 1089–1096, 2007.

[53] L. M. Borges et al., “Design and evaluation of multi-band RF energy harvesting circuits and antennas for WSNs,” in *21st Int.Conf. on Telecommunications (ICT)*, Lisbon, 2014, pp. 308–312.

[54] L. Hongqiang, Y. Xiaogang, and Miao Changyun, “Innovative wearable biomedical sensors for wireless ECG signs monitoring,” in *2nd Int.Conf. on Wirel., Mobile and Multimedia Networks (ICWMMN)*, Beijing, China, 2008, pp. 520–523.

[55] D. Boyle, M. Magno, B. O. Flynn, D. Brunelli, E. Popovici, and L. Benini, “Towards persistent structural health monitoring through sustainable wireless sensor networks,” in *Seventh Int.Conf. on Intelligent Sensors, Sensor Networks and Information Processing*, Adelaide, SA, 2011, pp. 323–328.

[56] A. Takacs, A. Okba, H. Aubert, S. Charlot, and P.-F. Calmon, “Recent advances in electromagnetic energy harvesting and wireless power transfer for IoT and SHM applications,” *in IEEE Int. Work. Electron. Control. Meas. Signals their Appl. to Mechatronics*, pp. 1–4, 2017.

[57] S. V. Nandury and B. A. Begum, “Smart WSN-based ubiquitous architecture for smart cities,” in *Int.Conf on Advances in Computing, Communications and Informatics (ICACCI)*, Kochi, 2015, pp. 2366–2373.

[58] F. Nasri, N. Moussa, and A. Mtibaa, “Internet of Things : Intelligent system for healthcare Based on WSN and android,” in *World Congress on Computer Applications and Information Systems (WCCAIS)*, Hammamet, 2014, pp. 1–6.

[59] R. A. Li, X. Sha, and K. Lin, “Smart Greenhouse : A Real-time mobile intelligent monitoring system based on WSN,” in *Int.Wirel. Communications and Mobile Computing Conf. (IWCMC)*, Nicosia, 2014, pp. 1152–1156.

[60] W. K. Lai, M.-T. Lin, and K.-T. Yang, “Intelligent monitor system based on WSN

to improve power utilization," in *9th Int.Conf. on Information, Communications & Signal Processing*, Tainan, 2013, pp. 1–5.

[61] N. Shinohara, "Recent wireless power transmission via microwave and millimeter-wave in Japan," in *42nd European Microw. Conf.*, Amsterdam, 2012, pp. 1347–1350.

[62] M. Arrawatia and G. Kumar, "RF energy harvesting system from cell towers in 900MHz band," in *National Conf. on Communications (NCC)*, Bengaluru, India, 2011, pp. 1–5.

[63] E. Falkenstein, M. Roberg, and Z. Popovic, "Low-power wireless power delivery," *IEEE Trans. Microw. Theory Tech.*, vol. 60, no. 7, pp. 2277–2286, 2012.

[64] A. Costanzo and D. Masotti, "Smart solutions in smart spaces," *IEEE Microw. Mag.*, vol. 17, no. 5, pp. 30–45, 2016.

[65] T. Soyata, L. Copeland, and W. Heinzelman, "RF energy harvesting for embedded systems: a survey of tradeoffs and methodology," *IEEE Circuits and Systems Magazine*, vol. 16, no. 1, pp. 22–57, 2016.

[66] R. A. Bercich, D. R. Duffy, and P. P. Irazoqui, "Far-field RF powering of implantable devices: Safety considerations," *IEEE Trans. Biomed. Eng.*, vol. 60, no. 8, pp. 2107–2112, 2013.

[67] C. Liu, Y. X. Guo, H. Sun, and S. Xiao, "Design and safety considerations of an implantable rectenna for far-field wirelesspower transfer," *IEEE Trans. Antennas Propag.*, vol. 62, no. 11, pp. 5798–5806, 2014.

[68] R. C. Johnson, *Antenna Engineering Handbook*, 3rd ed. McGraw Hill, 1993.

[69] "ELEC 5607 Antenna Engineering Course Notes Aldo Petosa," 2013.

[70] S. Bakogianni and S. Koulouridis, "Sub-1 GHz far-field powering of implantable medical devices: Design and safety considerations," in *IEEE Int.Symp. on Antennas and Propagation & USNC/URSI National Radio Science Meeting*, Vancouver, BC, 2015, pp. 942–943.

[71] C. Liu, Y.-X. Guo, and S. Xiao, "Compact dual-band antenna for implantable

devices," *IEEE Antennas Wirel. Propag. Lett.*, vol. 11, pp. 1508–1511, 2012.

[72] S. Stoecklin, A. Yousaf, T. Volk, and L. Reindl, "Efficient wireless powering of biomedical sensor systems for multichannel brain implants," *IEEE Trans. Instrum. Meas.*, vol. 65, no. 4, pp. 654–764, 2016.

[73] IARC classifies radiofrequency rlectromagnetic fields as possibly carcinogenic to humans," *Int.Agency for Research on Cancer*, pp. 1–6, 2011.

[74] Harald T. First, "A note on a simple transmission formula" in *Proceedings of the I.R.E and Wave and Electrons*, 1946, pp. 254–256.

[75] A. M. H. Almohaimeed, "Down-converter gilbert-cell mixer for wimax applications using 0 . 15μm GaAs HEMT technology," Master thesis, Ottawa University, 2014.

[76] M. Han, S. Jung, and H. Sohn, "High efficient rectenna using a harmonic rejection low pass filter for RF based wireless power transmission," in *11th Int.Symp. on Wireless Communications Systems (ISWCS)*, Barcelona, Spain, 2014, pp. 423–426.

[77] Y. Zhou, B. Froppier, and T. Razban, "Study of a matching circuit effect on a microwave rectifier," in *11th Mediterranean Microw. Symp. (MMS)*, Hammamet, 2011, pp. 29–33.

[78] Yu-Chun Liu, "RF energy harvesting for implantable ics with on-chip antenna," Master thesis, University of Central Florida Orlando, Florida, 2014.

[79] L.-G. Tran, H.-K. Cha, and W.-T. Park, "RF power harvesting: a review on designing methodologies and applications," *Micro Nano Syst. Lett.*, vol. 5, no. 1, p. 14, 2017.

[80] P. Kamalinejad, K. Keikhosravy, R. Molavi, S. Mirabbasi, and V. C. M. Leung, "Efficiency enhancement techniques and a dual-band approach in RF rectifiers for wireless power harvesting," in *IEEE Int.Symp. on Circuits and Systems (ISCAS)*, Melbourne VIC, 2014, pp. 2049–2052.

[81] S. Wong and C. Chen, "Power efficient multi-stage CMOS rectifier design for UHF RFID tags," *Integr. VLSI J.*, vol. 44, no. 3, pp. 242–255, 2011.

[82] Y. Kobayashi, M. Hori, H. Noji, G. Fukuda, and S. Kawasaki, "The S-band GaN-

based high power amplifier and rectenna for space energy transfer applications," in *IEEE MTT-S Int.Microw. Workshop Series on Innovative Wirel. Power Transmission: Technologies, Systems, and Applications*, Kyoto, 2012, pp. 271–274.

[83] S. Hemour, Y. Zhao, C. H. P. Lorenz, D. Houssameddine, Y. Gui, C. M. Hu, and K. Wu, "Towards low-power high-efficiency RF and microwave energy harvesting," *IEEE Trans. Microw. Theory Tech.*, vol. 62, no. 4, pp. 965–976, 2014.

[84] R. C. Jaeger and T. Blalock, *Microelectronic Circuit Design*, 4th Editio. The McGraw-Hill Companies, Inc., 2011.

[85] V. Marian, B. Allard, C. Vollaire, and J. Verdier, "Harvesting wireless power: Survey of energy-harvester conversion efficiency in far-field, wireless power transfer systems," *IEEE Microw. Mag.*, vol. 15, no. 4, pp. 108–120, 2014.

[86] B. L. Pham and A.-V. Pham, "Triple bands antenna and high efficiency rectifier design for RF energy harvesting at 900, 1900 and 2400 MHz," in *IEEE MTT-S Int.Microw. Symp. Digest (MTT)*, Seattle, WA, 2013, pp. 1–3.

[87] T. Oka, T. Ogata, K. Saito, and S. Tanaka, "Triple-band single-diode microwave rectifier using CRLH transmission line," in *Asia-Pacific Microw. Conf.*, Sendai, Japan, 2014, pp. 1013–1015.

[88] C. Song, Y. Huang, P. Carter, J. Zhou, S. D. Joseph, and G. Li, "Novel compact and broadband frequency-selectable rectennas for a wide input-power and load impedance range," *IEEE Trans. Antennas Propag.*, vol. 66, no. 7, pp. 3306–3316, 2018.

[89] T. W. Barton, J. M. Gordonson, and D. J. Perreault, "Transmission line resistance compression networks and applications to wireless power transfer," *EEE J. Emerg. Sel. Top. Power Electron.*, vol. 3, no. 1, pp. 252–260, 2015.

[90] K. Niotaki, A. Georgiadis, and A. Collado, "Dual-band rectifier based on resistance compression networks," in *IIEEE MTT-S Int.Microw. Symp. (IMS)*, Tampa, FL, 2014, pp. 1–3.

[91] A. Dolgov, R. Zane, and Z. Popovic, "Power management system for online low power RF energy harvesting optimization," *IEEE Trans. Circuits Syst. I Regul. Pap.*,

vol. 57, no. 7, pp. 1802–1811, 2010.

[92] A. N. Parks and J. R. Smith, “Sifting through the airwaves: Efficient and scalable multiband RF harvesting,” in *IEEE Int.Conf. on RFID (IEEE RFID)*, Orlando, FL, 2014, pp. 74–81.

[93] Y. Huang, N. Shinohara, and T. Mitani, “A constant efficiency of rectifying circuit in an extremely wide load range,” *IEEE Trans. Microw. Theory Tech.*, vol. 62, no. 4, pp. 986–993, 2014.

[94] M. Roberg, T. Reveyrand, I. Ramos, E. A. Falkenstein, and Z. Popovic, “High-efficiency harmonically terminated diode and transistor rectifiers,” *IEEE Trans. Microw. Theory Tech.*, vol. 60, no. 12, pp. 4043–4052, 2012.

[95] M. Roberg, E. Falkenstein, and Z. Popovic, “High-efficiency harmonically-terminated rectifier for wireless powering applications,” in *IEEE/MTT-S Int.Microw. Symp. Digest,* Montreal, QC, Canada, 2012, pp. 1–3.

[96] A. Ganti, J. Lin, R. A. Chinga, and S. Yoshida, “Harmonically terminated high-power rectifier for wireless power transfer,” *Wirel. Power Transf.*, vol. 3, no. 02, pp. 75–82, 2016.

[97] S. Ladan, S. Member, and K. Wu, “Nonlinear Modeling and Harmonic Recycling of Millimeter-Wave Rectifier Circuit,” *IEEE Trans. Microw. THEORY Tech.*, vol. 63, no. 3, pp. 1–8, 2015.

[98] J. Guo, H. Hong, and X. Zhu, “Automatic load control for highly efficient microwave rectifiers,” *in IEEE MTT-S Int. Microw. Work. Ser. Innov. Wirel. Power Transm. Technol. Syst. Appl. IMWS-IWPT 2012 - Proc.*, pp. 171–174, 2012.

[99] X. Wang, O. Abdelatty, and A. Mortazawi, “Design of a wide dynamic range rectifier array with an adaptive power distribution technique,” *46th European Microw. Conf. (EuMC)*, London, 2016, pp. 922-925.

[100] K. Hamano, R. Tanaka, S. Yoshida, H. Sakaki, K. Nishikawa, S. Kawasaki, K. Kawai, H. Okazaki, S. Narahashi, and N. Shinohara, “Wide dynamic range rectifier circuit with sequential power delivery technique,” *12th European Microw. Integrated Circuits Conf. (EuMIC)*, Nuremberg, 2017, pp. 415-418.

[101] "Avago Technologies, Schottky diode [online]@ www.avagotech.com." .

[102] www.skyworksinc.com, "Skyworks Solutions, Inc, Woburn, MA." [Online]. Available: www.skyworksinc.com.

[103] Matlab 2018, "Index @ www.Mathworks.Com." [Online]. Available: https://www.mathworks.com.

[104] K. S. Champlin and G. Eisenstein, "Cutoff frequency of submillimeter schottky-barrier diodes," *IEEE Trans. Microw. Theory Tech.*, vol. 26, no. 1, pp. 31–34, 1978.

[105] J. Guo, H. Zhang, S. Member, and X. Zhu, "Theoretical analysis of RF-DC conversion efficiency for class-f rectifiers," vol. 62, no. 1, pp. 1–9, 2014.

[106] T. W. Yoo and K. Chang, "Theoretical and experimental development of 10 and 35 GHz rectennas," *IEEE Trans. Microw. Theory Tech.*, vol. 40, no. 6, pp. 1259–1266, 1992.

[107] "Renesas Electronics America Inc." .

[108] "Keysight's Technology Advanced Design System (ADS), version 2016." .

[109] "Murata Manufacturing Co., Ltd.@ www.murata.com." .

[110] H. Sun, Y. Guo, M. He, and Z. Zhong, "Design of a high-hfficiency 2.45-GHz rectenna for low-input-power energy harvesting," *IEEE Antennas Wirel. Propag. Lett.*, vol. 11, pp. 929–932, 2012.

[111] U. Olgun, C. Chen, and J. L. Volakis, "Investigation of rectenna array configurations for enhanced RF power harvesting," *IEEE Antennas Wirel. Propag. Lett.*, vol. 10, pp. 262–265, 2011.

[112] C. Song, Y. Huang, J. Zhou, J. Zhang, S. Yuan, and P. Carter, "A high-efficiency broadband rectenna for ambient wireless energy harvesting," *IEEE Trans. Antennas Propag.*, vol. 63, no. 8, pp. 3486–3495, 2015.

[113] C. Song, Y. Huang, J. Zhou, and P. Carter, "Recent advances in broadband rectennas for wireless power transfer and ambient RF energy harvesting," in *11th European Conf. on Antennas and Propagation (EUCAP)*, Paris, 2017, pp. 341–345.

[114] A. A. Khalifa, "*Study of CMOS Rectifiers for Wirel. Energy Scavenging,*", PhD thesis, Linköpings university, 2010.

[115] B. Xiulong, Y. Kansheng, O. O'Conchubhair, and M. J. Ammann, "Differentially-fed omnidirectional circularly polarized patch antenna for RF energy harvesting," *2016 10th Eur. Conf. Antennas Propagation, EuCAP 2016*, 2016.

[116] Y. J. Ren and K. Chang, "New 5.8-GHz circularly polarized retrodirective rectenna arrays for wireless power transmission," *IEEE Trans. Microw. Theory Tech.*, vol. 54, no. 7, pp. 2970–2976, 2006.

[117] Y. Yang, L. Li, J. Li, Y. Liu, B. Zhang, H. Zhu, and K. Huang, "A Circularly polarized rectenna array based on substrate integrated waveguide structure with harmonic suppression," *IEEE Antennas Wirel. Propag. Lett.*, vol. 17, no. 4, pp. 684–688, 2018.

[118] A. Collado, S. Member, and A. Georgiadis, "A Compact dual-band rectenna using slot-loaded," vol. 12, pp. 1634–1637, 2013.

[119] H. Sun, Y. Guo, M. He, and Z. Zhong, "A Dual-band rectenna using broadband yagi antenna array for ambient RF power harvesting," *IEEE Antennas Wirel. Propag. Lett.*, vol. 12, pp. 918–921, 2013.

[120] Y. Yang, J. Li, L. Li, Y. Liu, B. Zhang, H. Zhu, and K. Huang, "A 5.8 GHz Circularly Polarized Rectenna with Harmonic Suppression and Rectenna Array for Wireless Power Transfer," *IEEE Antennas Wirel. Propag. Lett.*, vol. 17, no. 7, pp. 1276–1280, 2018.

[121] C. Wu, G. Pan, H. Hsu and J. Sun, "A 2 . 45-GHz planar array antenna with harmonic suppression for wireless power transmission applications," in *IEEE Wirel. Power Transfer Conf. (WPTC)*, Taipei, 2017, pp. 1–4.

[122] W. Lin and R. W. Ziolkowski, "Electrically-small, low-profile, dual-linear and circularly polarized huygens dipole antennas with broadside radiation patterns," in *2017 IEEE Int.Symp. on Antennas and Propagation & USNC/URSI National Radio Science Meeting*, San Diego, CA, 2017, pp. 547–548.

[123] H. Huang and T. Li, "A Spiral electrically small magnetic antenna with high

radiation efficiency for wireless power transfer," *IEEE Antennas Wirel. Propag. Lett.*, vol. 15, pp. 1495–1498, 2016.

[124] a. Ismahayati, P. J. Soh, R. Hadibah, and G. a E. Vandenbosch, "Design and analysis of a multiband koch fractal monopole antenna," *in IEEE Int. RF Microw. Conf.,* 2011, pp. 58–62.

[125] B. Taoufik, Z. Jamal, E. L. A. Larbi, B. Hamid, and T. Abdelali, "Fractal multiband planar antenna for wireless power transmission," in *2014 Int.Renewable and Sustainable Energy Conf. (IRSEC)*, Ouarzazate, 2014, pp. 1–3.

[126] C. L. Holloway, E. F. Kuester, J. A. Gordon, J. O'Hara, J. Booth, and D. R. Smith, "An overview of the theory and applications of metasurfaces: The two-dimensional equivalents of metamaterials," *IEEE Antennas Propag. Mag.*, vol. 54, no. 2, pp. 10–35, 2012.

[127] M. E. Badawe, T. Almoneef, and O. M. Ramahi, "A true metasurface antenna," in *IEEE Int.Symp. on Antennas and Propagation (APSURSI)*, Fajardo, 2016, pp. 1903–1904.

[128] M. Saad-Bin-Alam and S. Moury, "Multiple-band antenna coupled rectifier circuit for ambient RF energy harvesting for WSN," *2014 Int. Conf. Informatics, Electron. Vis.*,2014, pp. 1–4.

Appendix A

Rectifier Efficiency of Harmonic Balance (verified model)

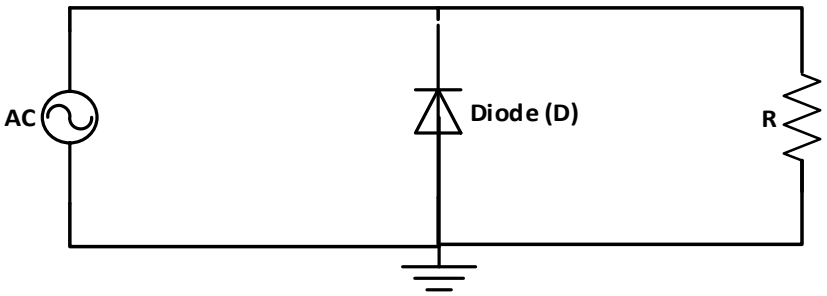

Figure A.1 Shunt half-wave rectifier configuration

A. Theoretical:

The input voltage in Figure A-2 can be represented as in the following:

$$V_{in} = V_p \sin \omega_0 t \tag{A.1}$$

In case of the $V_p < V_{th,}$ the diode is OFF, the output voltage is expressed as

$$Vout = V_p \sin \omega_0 t = V_{in} \qquad \Rightarrow \qquad V_{DC} = 0 \tag{A.2}$$

In case of the $V_p > V_{th}$ & $V_p < V_{br,}$

The diode is ON and the output voltage can be illustrated in Figure 3.4. In order to calculate the DC output voltage, the waveforms has been divided into four part (I_1, I_2, I_3, I_4) to do the area integral.

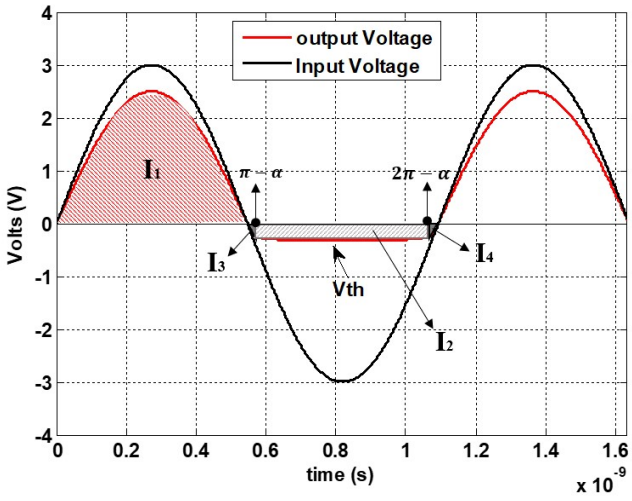

Figure A.2 Output voltage of half wave rectifier at V_p > V_{th} & V_p < V_{br}

Therefore,

$$I_1 = V_{dc} = \frac{1}{T}\int_0^{\pi} V_p \sin \omega_0 t \; dt \tag{A.3}$$

$$V_{dc1} = \frac{-V_p}{T}\cos \omega t\Big|_0^{\pi} = \frac{V_p}{\pi}$$

$$I_2 = V_{dc2} = V_{th}\left[(2\pi-\alpha)-(\pi+\alpha)\right] \tag{A.4}$$

$$V_{dc2} = V_{th}(\pi-2\alpha)$$

$$I_3 = I_4 = V_{dc,4} = \frac{1}{2\pi}\int_{\pi}^{\alpha} V_p \sin \omega_0 t \; dt \tag{A.5}$$

$$V_{dc3,4} = \frac{V_p}{2\pi}(1-\cos\alpha)$$

Where

$$\alpha = \sin^{-1}\left(\frac{-V_{th}}{V_{in}}\right)$$

The total output DC voltage as in the following,

$$V_{T_{dc}} = V_{dc1} + V_{dc2} + V_{dc3} + V_{dc4}$$

$$V_{T_{dc}} = \frac{V_p}{\pi} + V_{th}(\pi - 2\alpha) + \frac{V_p}{\pi}(1 - \cos\alpha) \tag{A.6}$$

In case of the $V_p > V_{th}$ & $V_p > V_{br,}$ the output voltage can be illustrated as in Figure 3.5

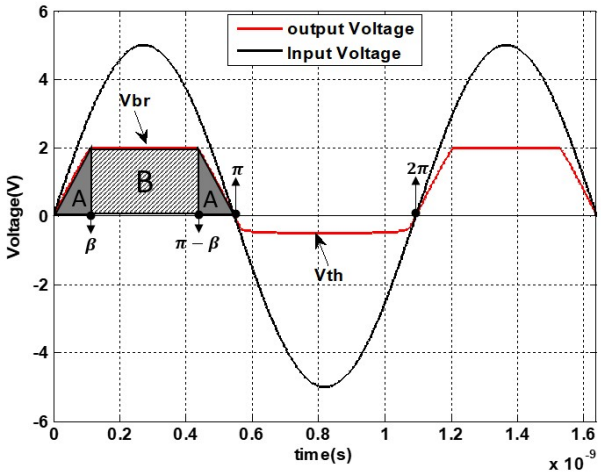

Figure A.3 Output voltage of half wave rectifier at $V_p > V_{th}$ & $V_p > V_{br,}$

$$A = V_{dc} = \frac{1}{T}\int_0^{\beta} V_p \sin\omega_0 t \; dt \tag{A.7}$$

$$V_{dc1} = \frac{1}{T}\int_0^{\beta} V_p \sin\omega_0 t dt$$

$$V_{dc1} = \frac{V_p}{2\pi}(1 - \cos\beta) = V_{dc3}$$

$$B = V_{dc2} = V_{br}(\pi - 2\beta) \tag{A.8}$$

where

$$\beta = \sin^{-1}\left(\frac{V_{br}}{V_{in}}\right)$$

$$V_{dc4} = V_{th}(\pi - 2\alpha) + \frac{V_p}{\pi}(1 - \cos\alpha)$$

$$V_{T_{dc}} = V_{dc_1} + V_{dc_2} + V_{dc_3} + V_{dc_4}$$

$$V_{T_{dc}} = \frac{V_p}{\pi}(1 - \cos\beta) + V_{br}(\pi - 2\beta) + V_{th}(\pi - 2\alpha) + \frac{V_p}{\pi}(1 - \cos\alpha) \tag{A.9}$$